MECHANISMS OF CLOSTRIDIAL NEUROTOXIN BINDING AND ENTRY

A Dissertation

presented to

the Faculty of the Graduate School

at the University of Missouri-Columbia

In Partial Fulfillment

of the Requirements for the Degree

Doctor of Philosophy

---

by

JOSHUA R BURNS

Dr. Michael Baldwin, Dissertation Supervisor

MAY 2016

The undersigned, appointed by the dean of the Graduate School, have examined the dissertation entitled

MECHANISMS OF CLOSTRIDIAL NEUROTOXIN

BINDING AND ENTRY

presented by Joshua R. Burns, a candidate for the degree of doctor of philosophy,

and hereby certify that, in their opinion, it is worthy of acceptance.

Professor Michael Baldwin

Professor Mark McIntosh

Professor Donald Burke

Professor Deborah Anderson

Professor Lesa Beamer

DEDICATION

This work is dedicated to my wife, Jennifer.
She has stood by me, supported, nourished, sustained, and adventured with me.

Her patience, love, and kindness has kept me moving forward.

ACKNOWLEDGEMENTS

I would like to acknowledge, and thank, Michael Baldwin for the time, effort, persistence, and patience he invested in my training over the course of the last 6 years. He has taught me the technical skills required to be a competent scientist, how to critically evaluate manuscripts, become a better writer, how to interact with scientific community, and how to communicate my ideas more effectively. Mike has been confident in my ability when I was uncertain, and encouraged me to pursue ideas I would have otherwise not considered. While in the Baldwin lab, Mike has taught me to see myself as a scientist.

I would like to acknowledge my doctoral thesis committee, Mark McIntosh, Donald Burke, Deb Anderson, and Lesa Beamer. I appreciate the guidance they have provided during the course of my graduate education.

I would like to acknowledge the MMI staff, specifically Jana Clark and Shelly Crawford for scheduling assistance and help with administrative issues.

I would like to thank Manijeh Heidari for helping with reagents, thoughtfulness, and kindness. I appreciate everything you do.

Current and previous members of the Baldwin lab have been influential teachers. Each have taught me important lessons. I have found my interactions with the undergraduate students to be the most influential. I thank Mike for giving me the opportunity to work with them. The undergraduates have taught me time management skills, improved how I communicate my science, and allowed me the opportunity to develop and coordinate individual research plans. As a group they have helped me grow as a manager and a teacher more than they will ever know.

I would like to acknowledge my previous employer, St. John's Mercy Medical Center, and my previous lab manager, the late Lynda Bohn. We worked together for 7 years. She gave me the opportunity to learn clinical microbiology by offering me the opportunity to work as a lab tech beginning in 2003. I was the first person to hold the position of lab tech in her department and I was the only person in her department that had not yet earned a degree, as I was still completing mine. She taught me how to interact with hospital administration, physicians, and nursing staff. She taught me how to relay results quickly, efficiently and correctly. She taught me how to handle numerous specimen types, how to handle high volume situations, and how to set up and culture a wide array of specimens under different

conditions. My time at St. John's and the people I interacted with were a huge reason I considered pursing a Ph.D.

Finally, my undergraduate advisor, Jennifer Firestine saw my dedication to finishing an education that I had started earlier in life. She knew I worked full time and coordinated with me as much as possible so I could complete my bachelor's degree while meeting the demands of my job. She was patient, rigorous, and demanding. She taught me the essentials of analytical biochemistry which I have tried to incorporate into my graduate studies.

TABLE OF CONTENTS

LIST OF FIGURES

LIST OF TABLES

ABSTRACT

The botulinum neurotoxins (BoNTs) and tetanus neurotoxin (TeNT) make up the clostridial neurotoxin (CNT) family. The CNTs are produced by *Clostridium botulinum* and *Clostridum tetani* respectively, and are the most potent human protein toxins. Eight CNT family members have been identified: seven botulinum neurotoxins (A-G) and tetanus neurotoxin (TeNT). Intoxication with BoNT is largely restricted to peripheral motor neurons, and results in flaccid paralysis. TeNT is sorted into a retrograde axonal trafficking pathway, transported to the central nervous system, and causes spastic paralysis.

The CNTs are typical AB toxins. They are secreted as ~150 kDa single chain proteins that undergo processing to produce a disulfide linked, dichain active form. The "A" or active domain is ~50 kDa zinc dependent protease, also known as the light chain (LC), that inhibits synaptic vesicle fusion with the plasma membrane through cleavage of soluble N-ethylmaleimide sensitive factor attachment protein receptor (SNARE) proteins. LCs cleave one of three neuronal SNARE proteins, preventing synaptic vesicle exocytosis. The "B" subunit is ~100 kDa, and contains a heavy chain translocation domain (HCT) and heavy chain receptor binding domain (HCR). Through an unclear mechanism,

the HCT undergoes a conformational change upon acidification and forms pH dependent channels, facilitating transport of the LC into the neuronal cytosol.

The HCR binds neuronal receptors on the presynaptic membrane of α-motor neurons. In order to explain the neuronal specificity of the CNTs, a dual receptor model was put forward. One co-receptor is ganglioside, a glycosphingolipid with a carbohydrate backbone decorated with sialic acids and a sphingolipid anchor. To satisfy the co-receptor model, the CNTs bind either a resident synaptic vesicle protein or a second ganglioside.

The focus of this work was to examine mechanisms of CNT binding and translocation to better understand CNT pathogenesis. Special emphasis was placed on understanding the ganglioside binding interactions in retrograde axonal trafficking, BoNT/A1 and A2 subtype specific ganglioside interactions, and the role of receptor contributions in CNT translocation.

Improving our understanding of basic mechanisms of CNT pathogenesis, including binding, entry, and translocation we can improve inhibitor designs, vaccine development, and further CNT platforms for pharmaceutical development.

CHAPTER 1: INTRODUCTION

1.1 Clostridial toxins

Bacteria have had a broad impact on humanity and affect our lives in both positive and negative ways. One genus, *Clostridium,* has significantly impacted the health of many animals including humans. *Clostridia* are primarily environmental, anaerobic spore-forming bacteria capable of using almost unlimited nutrient sources [1]. Of the ~150 known clostridial species, 10% are pathogenic and produce about 20% of known bacterial toxins [2]. Of particular relevance to humans are *Clostridium perfringens* and *Clostridium sordellii* which produce multiple toxins including hemolysin, collagenase, fibrinolysin, and β-pore forming, cholesterol dependent cytolysins that contribute to the condition of *Clostidia* gas gangrene in humans and animals and have caused numerouse deaths world-wide [3, 4]. Other species of note are: *Clostridium difficile* which produces large glucosylating toxins [5]; *Clostridium tetani* that produces tetanus neurotoxin (TeNT); and *Clostridium botulinum*, *C. baratii, C. argentinense*, and *C. butyricum* that produce botulinum neurotoxins (BoNTs). Together, BoNTs and TeNT are known as the clostridial neurotoxins (CNTs) (**Table 1**).

Table 1. Principal diseases of toxigenic clostridia

Table 1.
Phylogenetic heterogeneity, number of toxins, and subsequent main diseases of toxigenic *Clostridium* species.

Clostridium species	Toxin number	Main disease
C. argentinense	1	Botulism
C. baratii	2	Botulism
C. botulinum	3	Botulism
C. butyricum	1	Botulism
C. bifermentans	3	Gangrene
C. chauvoei	4	Gangrene
C. difficile	3	Colitis
C. haemolyticum	3	Hemoglobinuria
C. histolyticum	5	Gangrene
C. novyi	8	Gangrene
C. perfringens	14	Gangrene, enteritis
C. septicum	4	Gangrene, enterotoxemia
C. sordellii	4	Gangrene
C. spiroforme	1	Enteritis
C. tetani	2	Tetanus

They are neuro specific with an estimated LD_{50} of 1-3ng/kg, and considered the most lethal proteins known to man [2]. TeNT, a protein neurotoxin, is the causative agent of tetanus, a disease diagnosed by general rigidity and convulsive spasms, first described by Hippocrates in the 5^{th} century BC In 1884 Carle and Rattone successfully transmitted tetanus to animals through infected human pus [6]. Follow up experiments identified tetanus neurotoxin (TeNT), as the causative agent of tetanus. The closely related botulinum neurotoxins (BoNTs) and TeNT comprise the clostridial neurotoxin (CNT) family. CNTs are considered the most potent naturally produced protein toxins. An estimated lethal dose of BoNT/A for humans is ~1ng/kg [7].

1.2 Clostridial neurotoxins

The clostridial neurotoxin (CNT) family includes eight family members: seven serotypes of botulinum neurotoxin (BoNTs A-G) and tetanus neurotoxin [8, 9]. Intoxication with TeNT occurs occasionally as a complication of deep wound infections with *Clostridium tetani*. Infection is initiated by contamination of open wounds or abrasions in the skin with endospores, commonly found in the soil environment. Upon germination, vegetative cells rapidly replicate within the tissue releasing enzymes and exotoxins including TeNT into the lymph and

blood system. The toxin is then transported to the neuromuscular junctions where intoxication occurs.

Botulism, the condition that results from intoxication with BoNT, was recognized in the 1820s with the onset of industrial scale manufacturing of foods after routinely causing food poisoning in sausages or "botulus" [10]. There are six phylogenetically distinct groups of clostridia that produce seven antigenically distinct BoNTs: *Clostridium botulinum* (group I-III); *Clostridium argentinense*; *Clostridium butyricum*; and *Clostridium baratii* (**Table 2**) [11-14]. Seven BoNT serotypes are identified by letter (A-G), where antiserum specific for one BoNT serotype cannot neutralize intoxication by a different serotype. In general, genes encoding BoNTs A, B, E, and F are located on the bacterial chromosome, BoNT serotypes C and D are transcribed from bacteriophage, and BoNT G and TeNT are located on a plasmid [11]. The seven BoNT serotypes are further divided into subtypes if they vary by more than 2.5% amino acid identity [2, 15]. Humans are likely sensitive to all CNTs, but only a subset: BoNTs A, B, E, F, and TeNT have been associated with natural human intoxications [16]. The natural variation observed with the BoNTs has not been observed with TeNT [17].

Table 2: BoNT phylogeny

Botulinum						
	Proteolytic *C. botulinum* Group I	Non-Proteolytic *C. botulinum* Group II	*C. botulinum* Group III	*C. argentinense*	*C. butyricum*	*C. baratii*
Serotype	A, B, F	B, E, F	C, D	G	E	F
Subtype	A1, A2, A3, A4, A5, B1, B2, B3, A(B) Ab, Ba, Bf, F1, F2, F3, F4, F5	E1, E2, E3, E6, E7, E8 No proteolytic B, F6	C, D, C/D, D/C		E4, E5	F7

In 2014, data from the Centers for Disease Control and Prevention (CDC) indicated 9% of laboratory confirmed cases of botulism originated from foodborne contamination, 80% were associated with infant botulism, 10% were from a wound source, and 1% of cases were from an unknown origin (http://www.cdc.gov/nationalsurveillance/botulism-surveillance.html). Infant botulism is a unique condition that occurs when contaminated spores are ingested, transmitting BoNT from the GI tract into the bloodstream [18, 19]. Specifically, spores that have been introduced into the body and survive the low pH environment of the stomach are able to germinate in the anaerobic environment of the gut. Once in the gut, toxin transcytoses the intestinal barrier and enters general circulation. *In vitro* data supports the role of CNT transcytosis. However, efficiency varies with serotype [20, 21]. Although not represented in the CDC study, aerosol delivery of BoNTs results in botulism, as detected in animal models. These data suggest developing weaponized BoNTs are possible [22, 23].

1.2.1 Disruption of neuronal signaling

BoNT and TeNT have similar mechanisms of pathogenesis. BoNT is largely retained in the peripheral nervous system, preventing the release of acetylcholine, resulting in flaccid muscle paralysis. TeNT

undergoes retrograde axonal trafficking to reach the central nervous system where it prevents the release of inhibitory neurotransmitters such as γ-aminobutyric acid (GABA) and glycine, causing spastic muscle paralysis [24, 25]. In either case, patients usually die from asphyxiation, as the muscles that control breathing become paralyzed.

The CNTs are typical AB toxins and share common structural organization [24, 26]. They are initially synthesized as ~150 kDa single-chain molecules that must undergo proteolytic cleavage in order to convert to active di-chain molecules. CNTs are composed of an N-terminal zinc metalloprotease domain (~50 kDa) termed light chain and a C-terminal domain (~100 kDa) termed heavy chain involved in neuronal entry linked through a single disulfide bond [9, 26, 27]. The light chain (LC, active, or protease domain) is specific for neuronal SNARE (soluble N-ethylmaleimide attachment protein receptor) proteins [28, 29]. The heavy chain (HC) has two functional domains: an N-terminal heavy chain translocation domain (HCT) and a C-terminal heavy chain receptor binding domain (HCR) domain with sub-domains HCR_N and HCR_C.

CNT intoxication is a three step process: binding and internalization, translocation, and cleavage of substrate. In step one, HCRs bind the presynaptic membrane of α-motor neurons via co-receptor interactions. All CNTs bind gangliosides, complex

glycosphingolipids decorated with one or more sialic acid sugars. A subset also bind synaptic vesicle proteins. With the exception of BoNT/C, BoNT/D, and mosaic toxins like BoNT C/D and D-SA, ganglioside binding occurs through a conserved ganglioside binding motif (GBM) [30, 31]. BoNT/C and /D lack the conserved GBM but still coordinate gangliosides for binding and entry [31].

After binding to motor neurons, BoNTs undergo receptor mediated endocytosis and uptake into acidified endosomal compartments. By comparison, TeNT is rapidly sorted into the retrograde axonal pathway for transport to the central nervous system (CNS) [9, 32]. The mechanism by which TeNT is delivered to the CNS is unclear. However, the heavy chain receptor binding domain of TeNT (HCR/T) has been shown to co-localize with Rab5 type endosomes prior to retrograde trafficking in Rab7 positive structures suggesting this is a dynamic process [33]. Once TeNT reaches the CNS, it is released from motor neurons to intoxicate inhibitory interneurons via a similar mechanism to the BoNTs.

In step 2, the HCT presumably undergoes a structural change forming a protein conducting channel within the endosomal membrane facilitating LC translocation from the endosome lumen into the neuronal cytosol [8, 34, 35]. The thioredoxin/thioredoxin reductase-redox system subsequently reduces the disulfide bond between HCT

and LC, releasing LC into the neuronal cytosol [36]. In step 3, LC cleaves one or more neuronal SNARE proteins preventing the formation of functional SNARE complexes, and thereby abrogating synaptic vesicle exocytosis [36].

1.3 Clostridial neurotoxin structure

The CNTs are extremely complex nanomachines that have developed high specificity for neuronal membranes and protein substrates. The CNTs share between 36.5% and 51.6% overall amino acid sequence identity and common structural characteristics [37]. However, individual domains within the CNTs typically contain higher amino acid sequence conservation as compared to overall amino acid identity [26, 37]. Crystal structures of BoNT/A (PDB: 3BTA, solved at 3.3 Å), BoNT/B (PDB: 2NPO, solved at 2.6 Å) and BoNT/E (PDB: 3FFZ, solved at 2.6 Å) show similar trimodular domain organization. However, in the crystal structure of BoNT/E the LC and HCR domain were found on the same side of the HCT domain where as in BoNT/A, the HCT was between the LC and HCR (**Figure 1**) [27, 38, 39]. Aspects of CNT structure are important to CNT function. The CNTs contain a protease sensitive loop

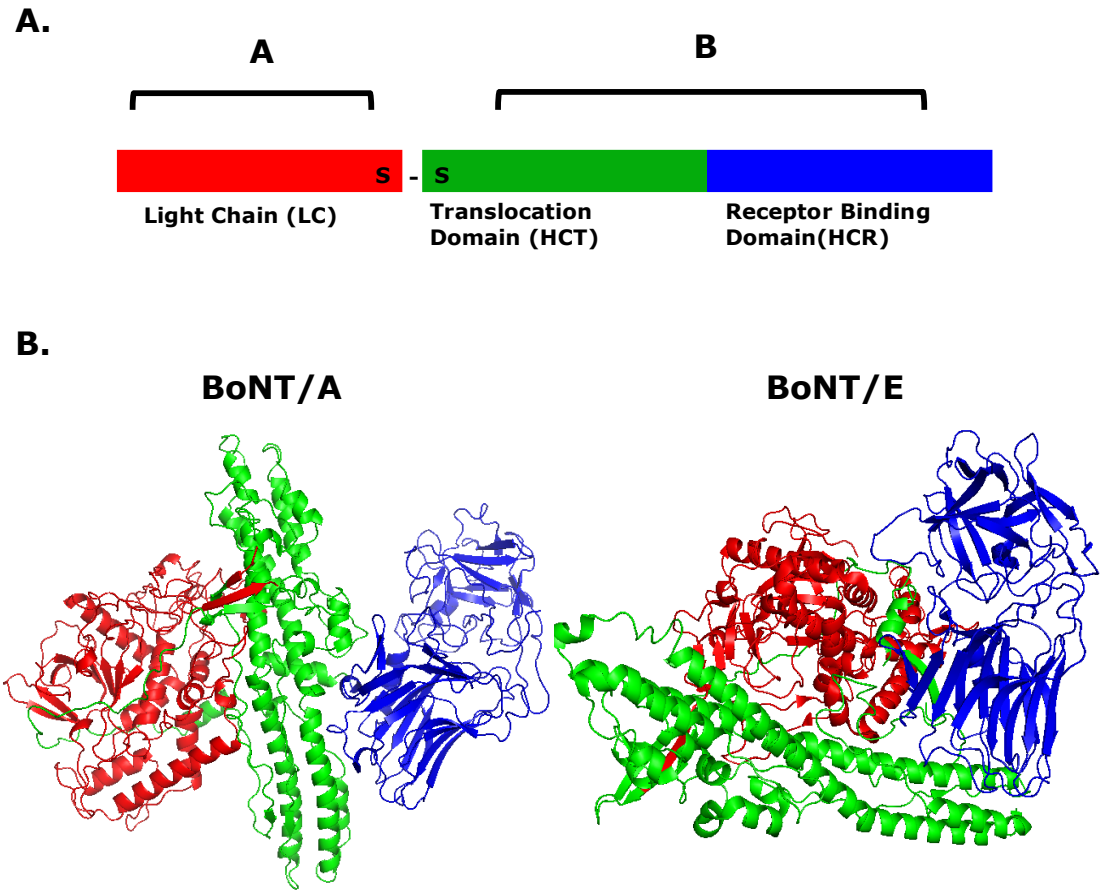

Figure 1. Organization of the clostridial neurotoxins. Active CNTs are disulfide AB toxins that contain 3 domains. (A) The light chain (LC) is shown in red, the heavy chain translocation domain (HCT) is shown in green, and the heavy chain receptor binding domain (HCR) is shown in blue. (B) Crystal structures of BoNT/A (PDB: 3BTA) and BoNT/E (PDB: 3FFZ) showing LC, HCT, and HCR in red, green, and blue respectively.

located between the LC and HC, that is cleaved either by bacterial or host proteases, forming a di-chain active toxin [24, 40, 41]. The HCT domain is primarily alpha helical containing two large (~100 Å) alpha helices and several smaller alpha-helices linked by variable loop regions and a "belt" region that wraps around the LC [26, 27, 42, 43]. The HCT translocation belt wraps LC in a manner similar to how LC bind SNAREs, suggesting the belt may chaperone LCs while in the holotoxin complex. These data suggest the HCT belt may help prevent autocatalysis or off target activity [44, 45].

The HCR consists of an HCR_N subdomain of unknown function that adopts a jelly roll fold and an HCR_C subdomain that adopts a modified β-trefoil fold that facilitates toxin binding [27, 46]. Additionally, individual recombinant LC and HCR domains from all known CNT serotypes have been purified in *Escherichia coli* (*E. coli)*, undergone X-ray structure determination, and found to retain relevant domain activity: LCs cleave substrate and HCRs bind receptors and enter neurons [31, 47-51].

1.3.1 Clostridial neurotoxin binding and entry

In 1986 Montecucco proposed a "dual receptor" model in which toxins necessarily bind ganglioside and protein co-receptors as an explanation for the high specificity of CNTs for α-motor neurons [52].

In this model, gangliosides act as the point of initial contact with the neuronal membrane while the protein mediates toxin entry [52]. Ganglioside binding is mediated through a shallow pocket located at the distal tip of the HCR domain that is formed by a conserved ganglioside binding motif (GBM) defined by E/D…H…SXWY…G [51]. Gangliosides involved in neurotoxin binding generally contain a GA1 oligosaccharide core (Gal4-GalNAc3-Gal2-Glc1-Cer) to which one or more sialic acids (in humans specifically, *N*-acetylneuraminic acid) are bound [53]. A second receptor for many of the BoNTs has been identified as a synaptic vesicle resident protein, specifically: synaptic vesicle protein 2 for BoNTs A, D, E, and F [54-56]; and synaptotagmins I and II for BoNTs B and G [57-59]. Additional comments on binding and entry are continued in Chapter 2-Introduction.

1.3.2 Clostridial neurotoxin translocation

In order to access the neuronal cytosol, LCs must cross the endosomal membrane and the disulfide bond linking the HC and LC must be reduced. Two BoNT/A variants lacking the HCR domain were able to create ion conducting channels in Neuro2a membranes: LC-HCT was able to create ion conducting channels at low pH while HCT alone formed channels in a pH independent manner [35, 60, 61].

The effect of pH on the HCT is not entirely clear. Although pH was not required for channel formation, the HCT may have neutral and low pH states as discussed in this thesis. Far UV spectroscopy of isolated LC/A at pH 5.0 and 7.4 showed a correlation between decreased alpha helical content at pH 5.0 and an increase in the presence of channel and protease activities [34]. The role of HCR in translocation is not clear. The HCR has been proposed to restrict HCT from membrane insertion until HCT was within the acidified interior of the endosome [35, 43, 60]. One proposed model suggests HCR is an intramolecular chaperone for HCT, regulating when HCT can insert into the lipid membrane in order to create a channel in the lipid bilayer and allowing LC to translocate [35]. Accordingly, BoNT/A was able to form 15-20 Å diameter channels in lipid membranes at low pH [62].

Many aspects of CNT translocation are not well understood. Work in this dissertation supports the idea that HCR contributes to, but is not required for, translocation [63, 64]. Similarly, the mechanism of HCT channel formation prior to productive LC translocation is not fully understood. Additional comments on CNT translocation can be found in Chapter 4 Tetanus neurotoxin utilizes two sequential membrane interactions for channel formation.

1.3.3 Clostridial neurotoxin protease domain

All CNT LCs are zinc metalloproteases characterized by a conserved zinc binding motif (HEXXH) and belong to peptidase family M4 of which Thermolysin is the representative enzyme [65, 66]. All LCs bind one zinc atom in the active site but BoNT/C coordinates an additional zinc atom that is believed to contribute to LC structure [24, 67]. Individual LCs cleave one or more of three SNARE protein substrates: SNAP-25 (synaptosomal associated protein of 25 kDa), VAMP2 (vesicle associated membrane protein 2 also referred to synaptobrevin 2), or syntaxin 1 (**Table 3**). BoNTs A and E recognize unique sites on SNAP-25; BoNTs B, D, F, G, and TeNT cleave VAMP2; BoNT C is able to cleave both SNAP-25 and syntaxin 1 [9, 49, 50, 66, 68-75]. Intracellular localization of LC also varies among the CNTs with LC/A localizing to the plasma membrane and the remaining LCs appearing to be cytosolic [76, 77]. The mechanism(s) by which LC/A localizes to the plasma membrane is not fully resolved, but the N-terminal 8 amino acids of play an essential role [76].

Table 3: Tetanus and botulinum neurotoxins: substrate cleavage sites

Toxin	*Substrate*	*Peptide Bond Cleaved: P4-P3-P2-P1-P1'-P2'-P3'-P4'*
BoNT/A	SNAP-25	Glu-Ala-Asn-Gln^{197}-Arg-Ala-Thr-Lys
BoNT/B	VAMP2 (synaptobrevin)	Gly-Ala-Ser-Gln^{76}-Phe-Glu-Thr-Ser
BoNT/C	SNAP-25 and Syntaxin 1	Ala-Asn-Gln-Arg^{198}-Ala-Thr-Lys-Met Asp-Thr-Lys-Lys^{254}-Ala-Val-Lys-Phe
BoNT/D	VAMP2	Arg-Asp-Gln-Lys^{61}-Leu-Ser-Glu-Leu
BoNT/E	SNAP-25	Gln-Ile-Asp-Arg^{180}-Ile-Met-Glu-Lys
BoNT/F	VAMP2	Glu-Arg-Asp-Gln^{60}-Lys-Leu-Ser-Glu
BoNT/G	VAMP2	Glu-Thr-Ser-Ala^{81}-Ala-Lys-Leu-Lys
TeNT	VAMP2	Gly-Ala-Ser-Gln^{76}-Phe-Glu-Thr-Ser

The interactions between individual LCs and their cognate SNARE protein targets has been extensively studied. Unlike other zinc proteases, CNTs recognize extended regions of their substrates for cleavage. In the case of BoNTs A and E, two sub-sites have been identified within SNAP-25 which contribute to substrate recognition. The recognition or active site (AS) region contains the site of cleavage. The binding (B) domain, contributes to substrate affinity [45, 78, 79], While LC/T and LC/B recognize and cleave VAMP2 at the same site, [66] the substrate recognition sequences between the two LCs are very different [80]. One result of this knowledge is a variant of LC/E capable of cleaving SNAP-23, not SNAP-25 [81]. Duration of disease has been correlated to stability of SNARE complexes. LC/A shortens SNAP-25 by nine amino acids. Shortened SNAP-25 peptides may be retained within SNARE complexes, contributing to extended disease state and longer synaptic blockade [44, 82]. In contrast, LC/E cleaves a 26 amino acid product from SNAP-25, releasing SNAP-25 into the cytosol and correlating to a shorter duration of synaptic blockade [83, 84].

1.4 Treatment and vaccine strategies

If an individual comes in contact with BoNT or spores that have germinated and are expressing toxin, treatment options are limited.

Primary therapies consist of supportive respiratory care and early delivery of antitoxin therapy [85, 86]. Antitoxin therapy neutralizes serotype specific intoxication, but only neutralizes unbound toxin [87]. Treatment for TeNT intoxication can be more complicated. Constant spasms associated with tetanus require administration of paralytic drugs to control muscle spasms in addition to gastric tube feeding and tracheostomy for breathing assistance [88-90]. There has been a significant decline in total reported tetanus cases since the development of a tetanus toxoid vaccine in 1924 [91]. However, in areas without access to the vaccine, deaths can be high. Development of a botulism vaccine has been more difficult. Using an approach similar to the creation of the tetanus vaccine, formalin treated *C. botulinum* extracts were alum precipitated to increase purity [92] and tested for serotype specificity [93, 94]. Reaction to the initial toxoid injection was mild, but more than one injection resulted in systemic reactions [94]. Additional vaccine efforts included development of a pentavalent vaccine in 1976 that included BoNTs A, B, C, D, and E [95]. The pentavalent BoNT toxoid was ethanol precipitated after formalin inactivation, creating a better tolerated vaccine candidate. The pentavalent vaccine was discontinued in 2011 because of short half-life, poor supply, and poor efficacy [96]. Recent vaccine development has utilized recombinant technology. An HCR derived

vaccine candidate derived from all seven BoNT serotypes was found to be protective [97-99]. Full length, catalytic inactive vaccine candidates are also under investigation.

1.5 Summary

TeNT and BoNT are highly potent neurotoxins. They are not cytotoxic, but, have exquisite specificity for the pre-synaptic neuronal membrane and have capacity to inhibit synaptic vesicle exocytosis. Outward disease presentation is the result of differences in the intracellular transport mechanisms of BoNTs and TeNT. Current research aims to understand fundamental aspects of CNT intoxication, shared and unique, among CNT members. This body of work focuses on understanding mechanisms of binding and entry and mechanisms of channel formation and translocation using TeNT and BoNT/A variants.

CHAPTER 2: INVESTIGATING THE ROLE OF GANGLIOSIDES IN RETROGRADE AXONAL TRANSPORT OF TETANUS NEUROTOXIN

2.1 Abstract

Botulinum neurotoxin (BoNTs) and tetanus neurotoxin (TeNT) together constitute the clostridial neurotoxin family (CNT). The CNTs are the most potent toxins known to man in part due to high specificity for the neuronal membrane and specific cleavage of SNARE proteins. The CNTs all bind at least one molecule of ganglioside to facilitate neuronal entry. Unlike the other CNT family members, TeNT is sorted into the retrograde axonal transport pathway after binding and entry. The mechanisms behind TeNT retrograde axonal trafficking are not completely understood. We propose a model whereby TeNT retrograde axonal trafficking is dependent on the unique ability to bind the ganglioside GM1a. Using structure-based mutagenesis in conjunction with a solid-phase ganglioside binding assay a TeNT variant, HCR/T^{ARTS}-A_{Loop}, was created. Binding of HCR/T^{ARTS}-A_{Loop} to GM1a was reduced by at least three orders of magnitude, while binding to gangliosides containing a Sia5 sugar was unaffected. Biochemical data suggested that replacement of threonine 1270 with a phenylalanine that is highly conserved among the BoNTs was critical for conferring

the dependence on the Sia5 sugar. Unexpectedly, restoration of the second ganglioside binding site in HCR/T^{ARTS}-A_{Loop}, restored binding to ganglioside GM1a through an unknown mechanism. This novel protein variant, HCR/T^{MO}, is able to bind and enter neuronal cells but appears to localize to unique microdomains within the plasma membrane.

2.2 Introduction

CNTs (BoNTs A-G and TeNT) are considered the most lethal protein toxins known to man. Among the CNT serotypes, humans are more sensitive to BoNTs A, B, E, and F and TeNT than other serotypes [16]. The extreme potency of these toxins is due in part to high specificity for the neuromuscular junction and specificity to inhibit synaptic vesicle exocytosis through cleavage of "S"oluble "*N*"-ethylmaleimide sensitive factor "A"ttachment protein "RE"ceptor (SNARE) substrate proteins [8, 9, 16]. CNT binding to the neuromuscular junction is a key first step in the intoxication process. A C-terminal receptor binding domain simultaneously recognizes synaptic vesicle proteins and complex glycosphingolipid, or more specifically ganglioside, co-receptors [100, 101]. **Table 4** lists the current protein co-receptors identified for each BoNT serotype. [47, 51, 102, 103].

Table 4. Tetanus and botulinum neurotoxin receptors

Toxin type	Protein receptor	Non protein receptors
BoNT/A	SV2A, SV2B, SV2C	Ganglioside
BoNT/B	Syt-I/II (synaptotagmin II)	Ganglioside
BoNT/C		Dual Ganglioside
BoNT/D	SV2	Ganglioside
BoNT/E	Glycosylated SV2A and B	Ganglioside
BoNT/F	Glycosylated SV2	Ganglioside
BoNT/G	Syt-I/II (synaptotagmin II)	Ganglioside
TeNT	SV2 and Nidogen*	Dual Ganglioside

SV2: synaptic vesicle protein 2, isoforms A-C; SytI/II: synaptotagmins I and II.
*Multiple protein receptors have been proposed for TeNT. The most recent are SV2 and Nidogen. Additional characterization is required to verify if these, or any other proposed protein receptors for TeNT play a biological role.

Although basic mechanisms of co-receptor recognition are understood, complex mechanisms of co-receptor recognition have not been completely characterized for all serotypes. In addition, the role of ganglioside co-receptor recognition in TeNT retrograde axonal trafficking is not understood. Complex gangliosides are located in the outer leaflet of the neuronal membrane and contain a common Ceramide-Glc1-Gal2-GalNAc3-Gal4 core (hereafter referred to as GA1) and at least one *N*- acetylneuraminic acid (sialic acid) creating "a" and "b" series gangliosides (**Figure 2**) [104-106]. A wealth of evidence supports the role of gangliosides as CNT co-receptors. For example, the binding affinity of BoNT/A for b series gangliosides was determined to be $\sim 10^{-8}$ M and in the presence of a monoclonal antibody to ganglioside GT1b (K_d 0.33 nM), BoNT/A entry into neurons was less efficient [107]. Similarly, BoNT/A was insensitive to murine neuroblastoma (Neuro2A) cells chemically inhibited in ganglioside biosynthesis and to neurons from mice lacking both a and b series ganglioside synthase genes: β1,4-*N*-acetylgalactosaminyltransferase (G_{M2}/G_{D2} synthase; EC 2.4.1.92) and α2,8 sialyltransferase (GD3 synthase genes) [108-110].

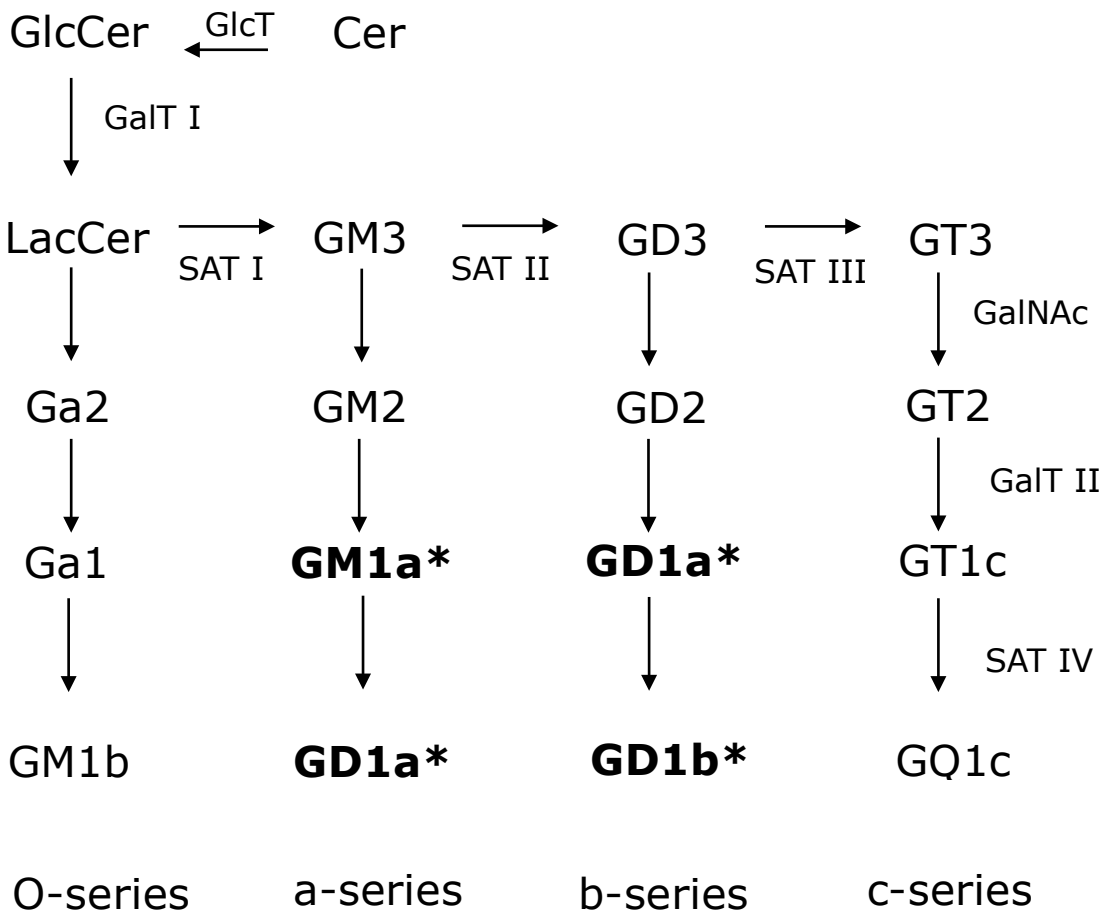

Figure 2. Ganglioside biosynthesis. Major gangliosides found in mammalian brain are in bold and annotated with an asterisk (*). GlcT: ceramide glucosyltransferase; GalT I/II: galactosyltransferase I/II; GalNAcT: N-acetylgalactosaminyltransferase; SAT I/II/III/IV: sialyltransferase I/II/III/IV. This research was originally published in The Journal of biological chemistry. Kolter, T, Proia, R. L, and Sandhoff, K. Combinatorial ganglioside biosynthesis. *J Biol Chem*. 2002; 277: 29 :25859-62 © the American Society for Biochemistry and Molecular Biology and used with permission.

Together, these data suggest gangliosides are necessary for binding and entry of BoNT/A BoNTs A, B, E, and F and TeNT contain a conserved ganglioside binding motif (GBM) E/D…H…SXWY…G (**Figure 3**) [47, 102, 111] which forms a shallow cleft in the surface of the HCR to which the oligosaccharide moiety of GA1 binds (**Figure 4**). The hydrophobic faces of the GalNac3-Gal4 sugars pack against the indole ring of the conserved tryptophan, whereas the polar faces are hydrogen bonded to the protein (**Figure 4**) [47, 51, 102, 112]. However, binding interactions with the GBM alone are not sufficient to bind ganglioside [47]. CNTs utilize non-conserved amino acids located outside the GBM to stabilize ganglioside binding (**Figure 4**). BoNTs A, B, E, and F stabilize the interaction between toxin and ganglioside by forming hydrogen bonds, in conjunction with additional hydrophobic interactions to a specific *N*-acetylneuraminic acid linked to Gal4 on the GA1 core (**Figure 5**) (indicated as Sia5).

Unlike the BoNTs, binding of TeNT to gangliosides is not dependent on Sia5. TeNT stabilizes binding to gangliosides through a unique asparagine residue (N1219) that hydrogen bonds to GalNAc3 (**Figure 5**) [47, 51, 102]. The interaction of N1219 with GalNAc3, rather than Sia5, confers upon TeNT the unique ability to bind gangliosides such as GM1a.

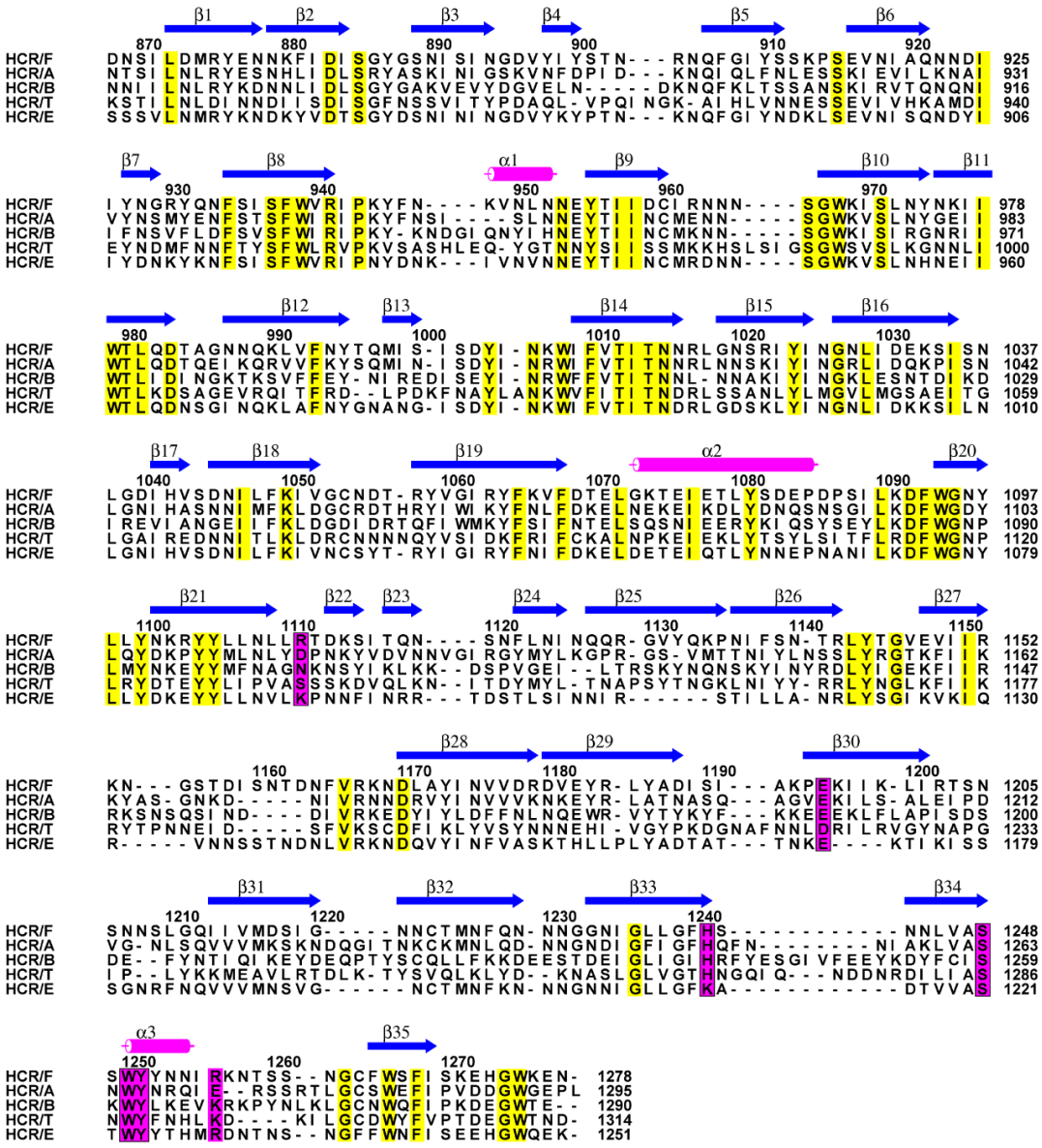

Figure 3. Structure based sequence alignment of BoNT and TeNT HCRs. Conserved amino acids in BoNT serotypes A,B,E, and F and TeNT HCRs are highlighted in yellow. Amino acids that form the conserved ganglioside binding motif (GBM) are highlighted in purple. This figure was originally published in The Journal of Biological Chemistry. Benson,M.A., Fu,Z., Kim J.J., Baldwin,M.R. Unique Ganglioside Recognition Strategies for Clostridial Neurotoxins. *Journal of Biological Chemistry* September 30, 2011; 286:34015-34022. © the American Society for Biochemistry and Molecular Biology and used with permission.

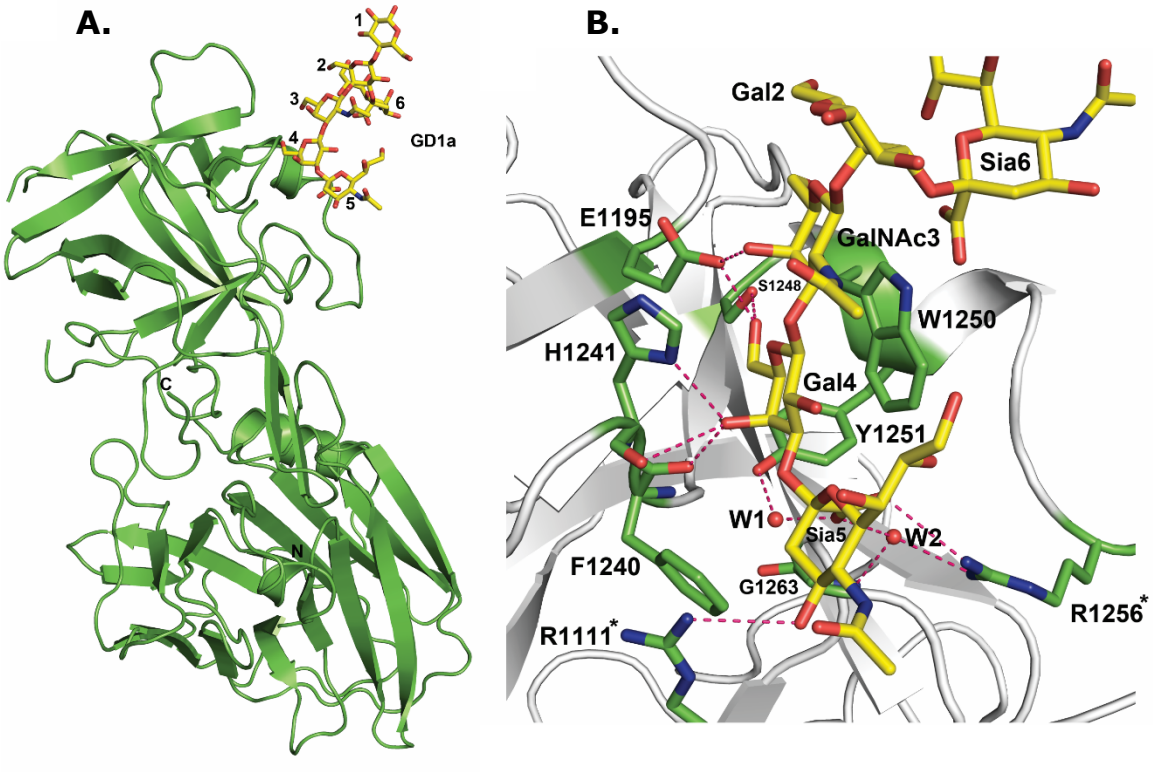

Figure 4. Structure of HCR/F in complex with GD1a- oligosaccharide (OS). (A) Ribbon representation of HCR/F (green) with GD1a-OS (atomic color sticks). (B) Ribbon representation illustrating position of GD1a-OS (atomic color sticks) in the HCR/F ganglioside binding motif (GBM). Amino acids that directly interact with GD1a-OS shown as green sticks with hydrogen bond interactions. This figure was adapted from an original research article published in The Journal of Biological Chemistry. Benson,M.A., Fu,Z., Kim J.J., Baldwin,M.R. Unique Ganglioside Recognition Strategies for Clostridial Neurotoxins. *Journal of Biological Chemistry* September 30, 2011; 286:34015-34022. © the American Society for Biochemistry and Molecular Biology and used with permission.

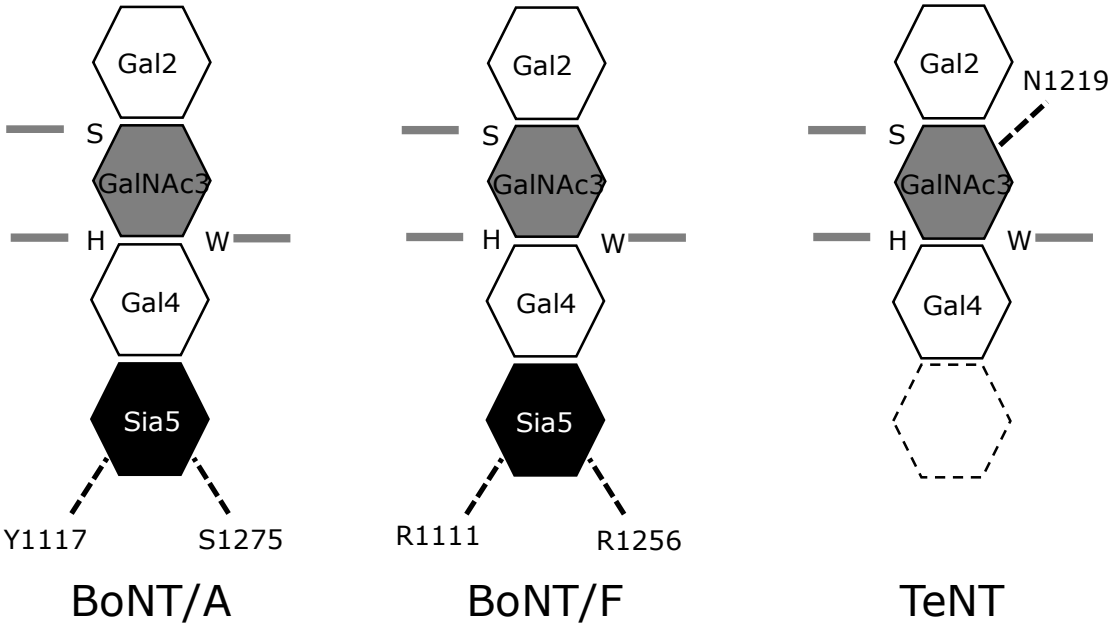

Fig 5. Model of HCR dependent ganglioside binding. Monosaccharides are represented by hexagons: Gal2 and Gal4 are colored white, GalNAc3 is colored light gray, and Sia5 is colored dark gray. Amino acids involved in binding to ganglioside are indicated by single letter codes. Hydrogen bonds are indicated by dashed lines.

Therefore, N1219 fulfills a function in TeNT analogous to the role of residues that hydrogen bond to Sia5 in the BoNTs.

Previous reports by Rummel *et al*. and Chen *et al*. established TeNT can simultaneously bind two gangliosides at physically separate binding sites [51, 102, 103, 111]. The conserved GBM forms the "W" site, so named because of the conserved tryptophan, W1289 in TeNT which interacts with the GA1 carbohydrate core. The second binding site (hereafter referred to as the "R" site) is centered around a unique arginine, R1226, which coordinates sialic acid moieties attached to the Gal2 sugar of the GA1 core [51]. The location of the R site in TeNT overlaps with the known protein co-receptor binding sites of BoNTs B and G suggesting it may play an important role in binding and entry [113]. This is supported by the observation that mutation of R1226 abrogates ganglioside binding and results in an atoxic protein [114]. Importantly, mutation of R1226 does not impact ganglioside binding to the GA1 core, implying the two binding sites are functionally independent of one another [102]. **Figure 6** validates the previously characterized variant HCR/T^{R1226L} [102, 111]. In addition to a dual ganglioside model described for TeNT, co-receptor models describing TeNT binding to protein receptors have also been proposed [115, 116].

	HCR/T	R1266L
GD1a	1.6 ± 0.18	60.1 ± 5.2
GM1a	56.6 ± 4.7	25.8 ± 4.1

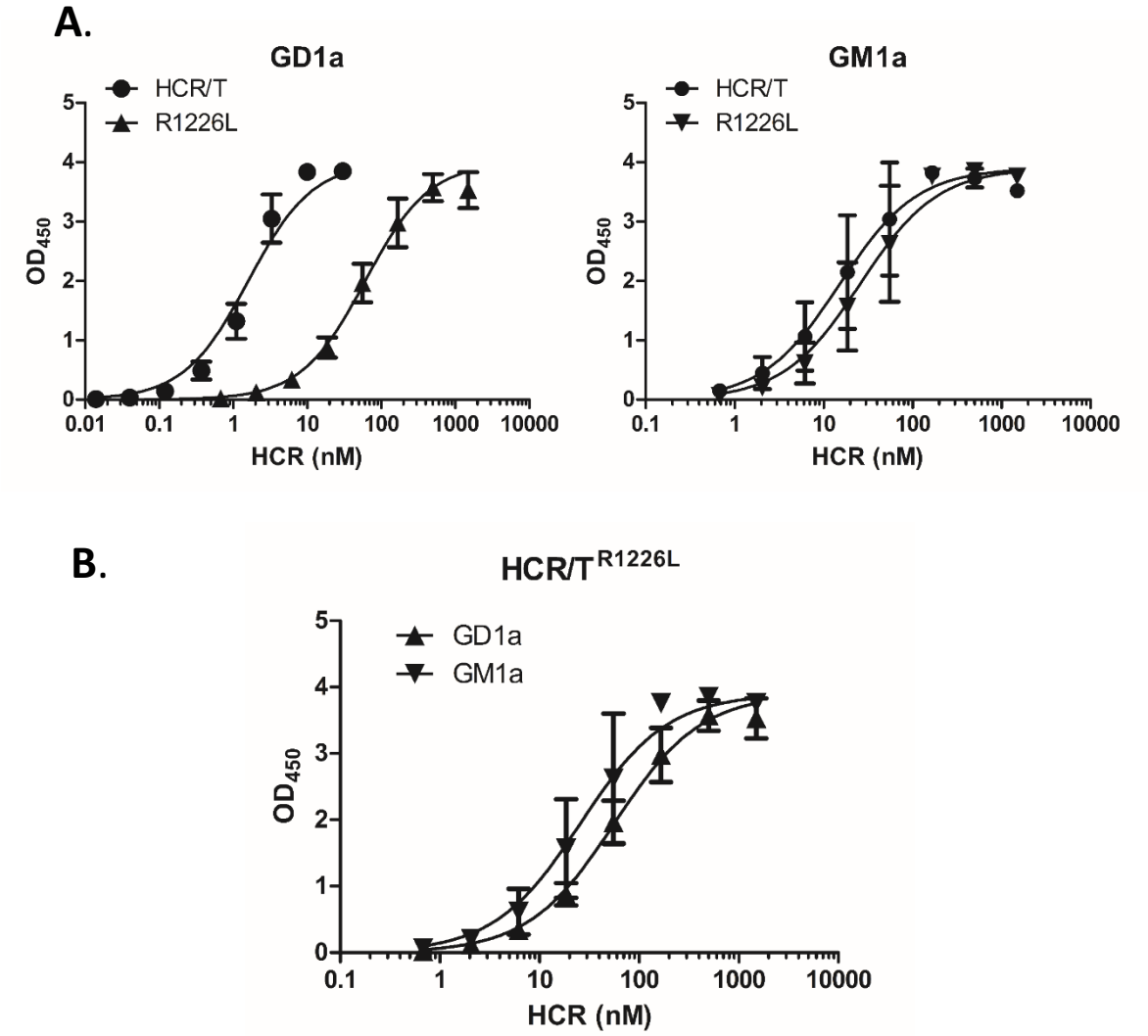

Figure 6. HCR/T and HCR/T^{R1226L} binding to GD1a and GM1a. (A) Binding of HCR/T (●) to immobilized GD1a or GM1a or HCR/T^{R1226L} to 5 µg GD1a (▲) (*left panel*) or GM1a (▼) (*right panel*) to microtiter plates (B) Binding of HCR/T^{R1226L} to 5 µg GD1a (▲) or GM1a (▼). Experiments were performed in phosphate buffered saline with 1% BSA (w/v) and 0.04% (v/v) Tween-20 at 4ºC for 2hrs. Bound HCR complexes were detected by anti-FLAG M2 monoclonal antibody (1:10,000), goat anti-mouse poly HRP (1:12,000) and ultra TMB. The plates were read at 450 nM after quenching with 0.1M H_2SO_4. All values represent the arithmetic mean ± SD of 3 independent experiments performed in triplicate. Data were plotted using GraphPad Prism version 5 (GraphPad Software Inc.).

Upon binding to the presynaptic membrane of α-motor neurons (MNs) BoNTs are rapidly internalized into acidifying compartments ultimately leading to SNARE protein cleavage and disruption of signal transmission. In contrast, TeNT is rapidly sorted into distinct vesicular carriers which undergo fast retrograde axonal transport to the spinal cord. Importantly, these vesicular compartments fail to acidify during transport, likely explaining the failure of TeNT to translocate the LC within MNs [117]. Upon reaching the dendritic bodies, TeNT is released into the adjacent synaptic clefts, allowing binding to the inhibitory interneurons present within the spinal column [32, 65]. TeNT is subsequently internalized into an acidified compartment resulting in the translocation of LC into the cytosol, where it cleaves the SNARE protein synaptobrevin-2, preventing release of the neurotransmitters γ-aminobutyric acid (GABA) and glycine [66]. The resultant reduction in the strength of inhibitory inputs on MNs results in a hyper-excited state, which in turn causes the characteristic violent and persistent spasms associated with tetanus. While the ability of TeNT to shuttle from the periphery to the central nervous system is universally accepted, the mechanistic basis for this process remains unknown.

One proposed mechanism suggests after binding and entering MNs, TeNT is rapidly sorted to an alternate pathway to BoNTs where it co-localizes with $p75^{NTR}$ neurotrophin receptor and Tropomyosin

receptor kinase B (TrkB), facilitating retrograde axonal trafficking [33, 118]. Additional data suggest that TeNT binding to the neuronal membrane can directly activate intracellular signaling cascades initiated by $p75^{NTR}$ neurotrophin receptor and Tropomyosin receptor kinase A (TrkA) among others [119], and that this may also contribute to the retrograde transport of TeNT.

Interestingly, the unrelated alpha toxin from *Clostridium perfringens* also induces TrkA signaling, through a mechanism that is dependent on toxin binding to ganglioside GM1a [120]. This raises the possibility that TeNT binding to GM1a could be significant among the CNTs, as it may induce signaling required for productive retrograde axonal transport.

In addition to the clostridial neurotoxins, ganglioside dependent retrograde trafficking is a mechanism of pathogenesis utilized by cholera toxin and the *Escherichia coli* (*E. coli*) heat labile family of toxins. Cholera toxin (CT) and the *E. coli* heat labile family of toxins (LT) utilize gangliosides as receptors and then undergo retrograde transport through the trans-Golgi network to the endoplasmic reticulum (ER). CT, LTI and LTIIc bind GM1a; LTIIa bind b series gangliosides such as GD1b, and LTIIb binds GD1a [121, 122]. In human intestinal epithelial cells, CT has been reported to bind GM1a and undergo retrograde transport. In similar experiments, LTIIb was

not able to undergo retrograde transport although it bound to the surface of human epithelial cells via GD1a receptor [122]. Later reports established the ceramide moiety of GM1a may play a significant role in the retrograde transport properties of GM1a and ultimately of CT bound to GM1a [123]. Recently, a beta lactamase reporter construct (βLac-LTIIc) was able to translocate β-lactamase when bound to b series gangliosides exogenously added to Neuro2a cells [124]. Together, these data suggest binding to specific gangliosides can lead to retrograde transport of expressed cargo protein. Additionally, these data suggest that the ability of TeNT to bind GM1a may be a necessary component in the ability of TeNT to undergo retrograde axonal trafficking.

In the following study, we have investigated the potential role of ganglioside recognition in the retrograde transport of TeNT. Our model was: binding to ganglioside GM1a is required to sort TeNT into the retrograde axonal pathway. To test our model, we created a variant of TeNT that was dependent on the presence of the Sia5 sugar for binding and entry. In addition, we eliminated the dependence of GM1a in order to test the ability of TeNT to undergo GM1a dependent retrograde axonal trafficking.

2.3 Experimental procedures

2.3.1 Site-directed mutagenesis of TeNT HCR

A previously described, modified, pET28a expression vector (Novagen) – hereafter referred to as pET28-3×FLAG – containing a 3×FLAG epitope immediately downstream of the hexahistidine epitope tag was used as the expression vector for all TeNT HCR constructs [125]. *E. coli* optimized TeNT HCR DNA (aa 865-1315) was previously synthesized and subcloned into the modified pET28-3×FLAG expression vector via unique 5' *Kpn*I and 3' *Pst*I restriction sites [111]. Point mutations were introduced into the TeNT HCR gene by site directed mutagenesis using Quikchange® or Quikchange® II Site-Directed Mutagenesis Kits (Agilent) and confirmed by DNA sequencing.

See **Appendix 6.1, Chapter 2 primers**, for a complete list of primers used in this study.

2.3.2 Generation of TeNT – BoNT HCR loop chimeras using Splicing by Overlap Extension (SOE)-PCR

Chimeric HCR/T proteins containing short sequences of amino acids derived from BoNT A, E, or F were generated by Splicing by Overlap Extension (SOE)-PCR. For each PCR fragment, the primer at the end to be joined is constructed such that it has a 5' overhang of 30 nucleotides encoding BoNT amino acids which is complementary to the

5’ end of the second PCR fragment. In the first round of PCR, two fragments of approximately 1300 and 300 base pairs were amplified and subsequently gel purified. Once purified, a second round of PCR was carried out by mixing equimolar amounts of the two purified products with only primers from the two far ends. The overlapping complementary sequences introduced in round 1 served as primers and the two sequences containing the BoNT insertion were fused (**Figure 7**). DNA was digested using *Kpn*I and *Pst*I restriction enzymes, ligated into pET28-3×FLAG and verified by DNA sequencing.

2.3.3 Expression and purification of wild-type and mutated TeNT HCRs

E. coli BL-21(DE3) was transformed with pET28-3×FLAG HCR and grown in Lysogeny broth (LB) in the presence of 50 μg/ml kanamycin (LB_{Kan}) at 37ºC overnight. Transformants were stored in 12% (v/v) glycerol at -80ºC [125]. For purification of HCR, *E. coli* with pET28-3×FLAG HCR were plated onto LB_{Kan} agar plates and grown overnight at 37ºC. A single colony was isolated into 3 ml LB_{Kan} and grown for 3 hours at 37ºC.

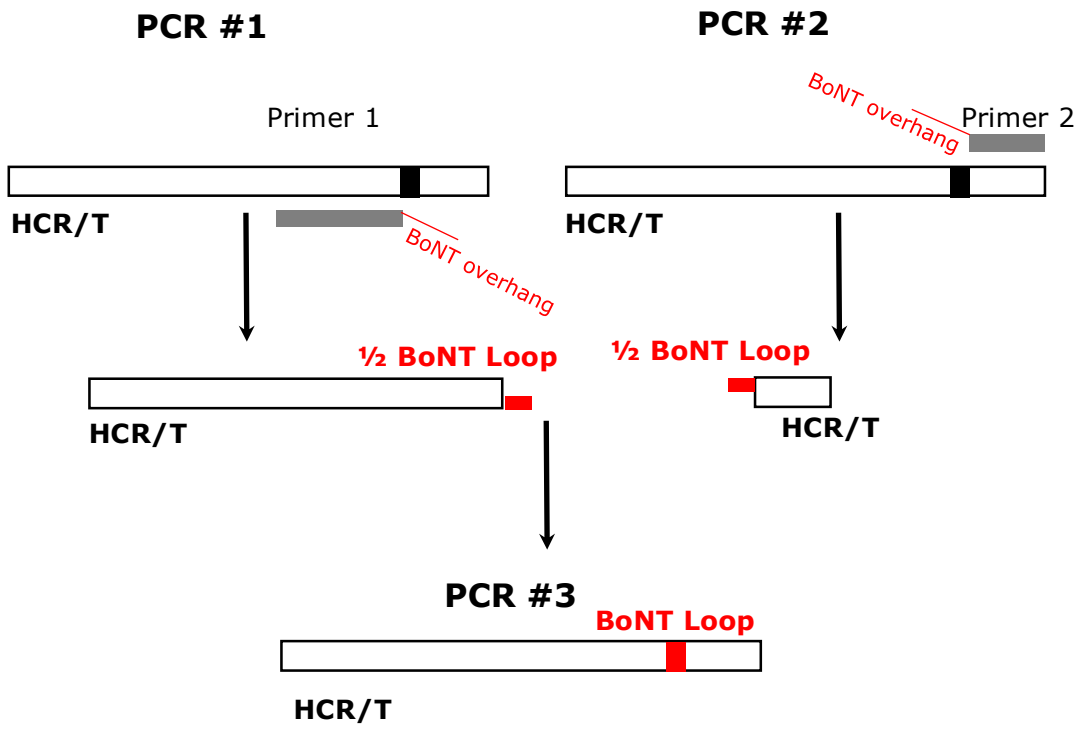

Figure 7. Splicing by overlap extension PCR. Schematic of splicing by overlap PCR strategy. Unique PCR primers (#1 and #2) were designed to delete a segment of HCR/T DNA (*E. coli* optimized) and replace deleted DNA with similar sequence from BoNT A, E or F (*E. coli* optimized DNA). In step 2, PCR products from reactions #1 and #2 were used as PCR templates for step #3 to create TeNT-BoNT chimeras.

Subsequently, 250 µl of culture was spread onto fresh LB_{Kan} agar plates and grown overnight at 37ºC The lawn of bacteria was suspended in 8 ml LB and inoculated into 400 ml LB_{Kan} for 3 hours at 37ºC at 250 r.p.m. (an OD_{600} of ~0.6). Isopropyl β-D-1-thiogalactopyranoside (IPTG) was added to a final concentration of 1 mM. Incubation continued overnight following temperature reduction to 16ºC [111]. Bacterial cells were harvested by centrifugation at 5000 ×*g* for 20 min at 4ºC, lysed by French press, and clarified by centrifugation at 15000 ×*g* for 20 min at 4ºC. Lysates were filtered through a 0.22 µm cellulose acetate syringe type filter prior to sequential column chromatography: Ni^{2+}-nitrilotriacetic acid (NTA) agarose (Qiagen) affinity chromatography followed by size exclusion chromatography using a S200-HR gel filtration column (GE Biosciences). Column fractions containing purified 3×FLAG-HCR were pooled, concentrated using an Amicon type centrifugal filtration device, and dialyzed into 500 mM NaCl 30 mM HEPES (pH 7.6) overnight at 4ºC. Purified 3×FLAG-HCRs were stored undiluted at -80ºC.

2.3.4 Solid phase ganglioside binding assay

A solid phase ganglioside binding assay was carried out as described previously [47]. Briefly, purified bovine brain gangliosides (GT1b, GD1b, GD1a, GM1a, GD3) (Matreya, LLC) were dissolved in

methanol (MeOH) at 2.5 or 5 mg/ml, diluted to 50 µg/ml in MeOH, and 100 µl per well was applied to non-protein binding 96 well plates (Corning Costar #3591). MeOH was allowed to evaporate overnight at room temperature in order to immobilize the ganglioside onto the plate surface. Nonspecific binding sites were blocked by a 30 minute incubation in carbonate solution (50 mM Na_2CO_3 containing 2% BSA, pH 9.6). Various concentrations of HCRs were added to the plates and incubated at 4ºC for 90 minutes. Post incubation, 96 well plates were washed three times in PBS with 0.04% (v/v) Tween 20.

An antibody solution containing anti-FLAG M2 monoclonal antibody (1:10,000) and goat anti-mouse poly HRP (1:12,000; Pierce) in PBS with 1% BSA and 0.04% Tween20 was applied and incubated for 20 min at 4ºC. Following incubation, the plate was washed three times in PBS with 0.04% Tween 20. Bound HCR complexes were detected using Ultra TMB (Pierce) as the HRP substrate. The reaction was terminated by the addition of an equal volume of 0.1 M H_2S0_4. The absorbance at 450 nm was determined using a plate reader (BioTek). Based on detection methodology it was not possible to directly determine the equilibrium dissociation constant (K_d). Rather, the concentration of HCR required to give 50% of maximum binding (B_{50}) was estimated by fitting the data to a one-site binding model where $Y = B_{\max} \cdot X \,/\, (\mathrm{B}_{50}+\mathrm{X})$ using GraphPad Prism. The goodness of fit

was estimated by calculating R^2, with values <0.9 indicating the model was not appropriate.

2.3.5 Crystallization of HCR/T^{MO}

HCR/T^{MO} was crystallized by Zhuji Fu in the laboratory of Dr. Jung Ja Kim at the Medical College of Wisconsin. Purified HCR/T^{MO} was purified by Joshua Burns (as described) dialyzed against 20 mM Tris-HCl (pH 7.9) containing 100 mM NaCl and concentrated to a final concentration of 10 mg/ml. Crystals were obtained by vapor diffusion using hanging drop techniques. Hanging drops containing 2 µl of 10 mg/ml HCR/T^{MO} and 2 µl of well solution (100 mM bis(trispropane)) buffer, pH 7.0, 25% polyethylene glycol 2000 and 300 mM ammonium sulfate) were equilibrated against 0.5 ml of the well solution at 19°C. The HCR/T^{MO} crystals belong to the triclinic space group P1, with cell dimensions *a* = 65.5, *b* = 84.3, and *c* = 117.6 Å and α = 72.6°, β = 67.1°, and γ = 84.1°. There are four molecules in an asymmetric unit with a Matthews coefficient of 2.8 $Å^3$/Da. The 2.4 Å data used in the initial molecular replacement were obtained at −175°C using an in-house R-AXIS IV++ detector. HKL2000 [126] was used in the data processing. The 1.9 Å data used for the later stages of refinement were collected at Advanced Photon Source beamline SBC 19ID.

Statistics for data collection and processing are summarized in **Table 5**.The structure of HCR/T^{MO} was solved by the molecular replacement method with MOLREP within the CCP4 program suite [127] in the resolution range of 20–4.0 Å. The monomer structure of HCR/T complexed with GT2 (Protein Data Bank code 3HMY) was used as the search model. The initial structure obtained from molecular replacement was refined using the program CNS [128]. The refinement protocol, as carried out by the Jung Ja Kim lab consisted of rigid body minimization, positional and temperature factor refinement, and simulated annealing. The structure was further refined with alternating manual adjustments using the TURBO-FRODO program package. The current model was completed with $R_{crystal}/R_{free}$ values of 0.212/0.243. The statistics of structural refinement are given in **Table 5**.

2.3.6 TeNT HCR binding to rat cortical neurons

12 mm acid etched coverslips were coated with 50 µg/mL poly-D-lysine overnight. Coverslips were washed twice with cell culture grade water before neurons were plated. Rat embryonic day 18 (E18) cortical neurons (Brainbits) were disassociated per Brainbits protocol and cultured in Neurobasal medium supplemented with 0.5 mM

Table 5. Data collection and refinement statistics (molecular replacement)

	HCR/T^{MO}
Data collection	
Space group	P1
Cell dimensions	
a, *b*, *c* (Å)	65.5, 84.3, 117.6
α, β, γ (°)	72.6, 67.1, 84.1
Resolution (Å)	30-1.9 (1.97-1.90) *
R_{sym}	0.059/0.409
$I / \sigma I$	16.2 (2.1)
Completeness (%)	95.2 (68.5)
Redundancy	2.5 (2.2)
No. of Molecules/asymmetric unit	4
Refinement	
Resolution (Å)	30-1.9
No. reflections	357,226
$R_{crystal}$ / R_{free}	0.212/0.243
No. atoms	
Protein	13,272
Water	424
B-factors(Å^2)	
Protein	41.1
Water	39.3
R.m.s. deviations	
Bond lengths (Å)	0.007
Bond angles (°)	1.4
Ramachandran plot	
Most favored (%)	86.7
Additional allowed (%)	12.5
Generously allowed (%)	0.8
Disallowed (%)	0.0

*Values in parentheses are for highest-resolution shell.

Glutamax, B27 supplement, and Primocin 10-14 days prior to use. Cells were treated with 20 nM HCR overnight at 37°C, washed three times in cold Hank's Balanced Salt Solution (HBSS) and fixed with 4% (w/v) paraformaldehyde solution/(w/o) sucrose in PBS for 30 min at 4°C. Bound HCR was detected by immunofluorescence using mouse anti-FLAG (clone M2 1:1000) and goat anti-mouse IgG Alexa 488 or 633 (1:500). Endogenous proteins were detected by rabbit anti-synaptophysin (1:200) and anti-rabbit IgG Alexa 488 or 633. A recombinant cholera toxin B subunit conjugate (Alexa 555) was used to detect ganglioside GM1a in lipid raft fractions. Cells were processed using standard immunofluorescence procedures, mounted in ProLong Gold Antifade reagent, and acquired using a Leica SPE-2 in confocal scanning mode.

2.4 Results

2.4.1 Optimizing HCR/T to bind Sia5 dependent gangliosides

TeNT is unique among the CNTs because it is sorted into the retrograde axonal pathway and because it binds with high affinity to GM1a - a ganglioside that does not contain the Sia5 sugar [33, 103, 111, 118]. Our hypothesis was: binding to ganglioside GM1a is required to sort TeNT into the retrograde axonal pathway. In order to

test whether GM1a plays a role in TeNT retrograde axonal trafficking, a variant of HCR/T dependent on the Sia5 sugar for binding at the W site was designed. Our strategy was to modify the conserved binding pocket of TeNT and incorporate structural features that confer Sia5 binding as occurs in the evolutionarily related BoNTs.

As described in the Introduction, HCR/T contains two physically separate binding sites: the sialic acid binding site, or R site, and the W or tryptophan site. Therefore, to investigate binding solely at the W site it is necessary to inactivate the R site. This was achieved through generation of a previously described mutated variant HCR/T-R1226L [102, 111] (**Figure 6**). Amino acids that contribute to Sia5 binding in the BoNTs were identified using the crystal structure of HCR/F in complex with the oligosaccharide moiety of GD1a (PDB: 3RSJ) in conjunction with a sequence alignment of HCRs A, E, F, and T [47]. F1240 (BoNT/F numbering) was selected due to: (i) conservation with other BoNT serotypes and (ii) the deleterious effect of F1240 mutation on ganglioside binding (**Figure 4 and Figure 8**, Baldwin lab, personal communication). R1111 was selected because it creates a bond to Sia5 in HCR/F and L1110 was selected because it may support the positioning of R1111 [71].

HCR/B	HCR/B_I1239F	HCR/B_I1239A
3217 ± 193.5	119.4 ± 7.6	940742 ± 1.7e+006

HCR/F	HCR/F_F1240I	HCR/F_F1240A
40.84 ± 2.9	357.5 ± 25.12	465731 ± 1.4e+006

A.

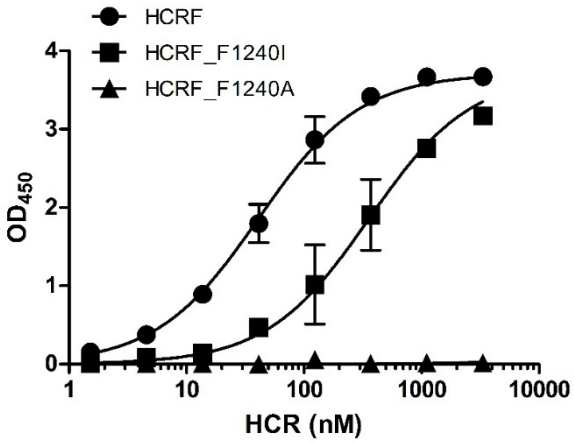

B.

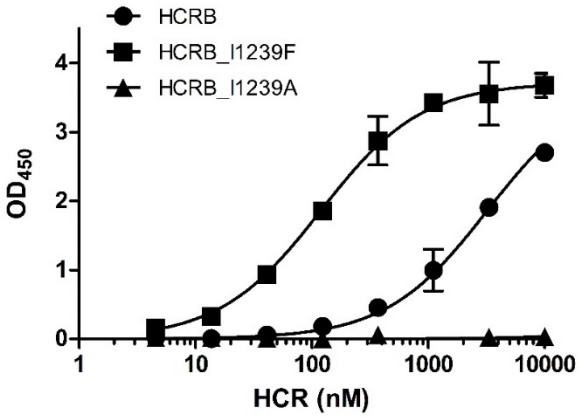

Figure 8. Binding of wild type and mutated HCRs to ganglioside GT1b. (A) HCR/F (●), HCR/F^{F1240I} (■) (corresponding amino acid in HCR/B), and HCR/F^{F1240A} (▲) were incubated with 5µg GT1b (B) HCR/B (●), HCR/B^{I1239F} (■), (corresponding amino acid in HCR/F), and HCR/B^{I1239A} (▲) were incubated with 5µg GT1b. Wild type HCRs and variants were incubated with indicated concentration of GT1b and assayed for binding as described in Chapter 2 Methods. All values represent the arithmetic mean± SD of 3 independent experiments performed in triplicate. Data were plotted using GraphPad Prism.

The reciprocal point mutations in HCR/T: T1270F, A1134L, and S1135R were generated on the HCR/T^{R1226L} background using site directed mutagenesis, creating the variant HCR/T $^{A1134L, R1226L, T1270F, S1135R}$ (hereafter referred to as HCR/T^{ARTS}). After verifying the correct mutations were introduced as described in Methods, HCR/T^{ARTS} was expressed, purified, and screened using the solid phase binding assay to determine half maximal binding affinity (B_{50}) on ganglioside containing Sia5 (GD1a) and ganglioside lacking Sia5 (GM1a). The binding affinities of HCR/T^{ARTS} for GD1a and GM1a were ~30 nM and ~60 nM which are similar to the previously reported B_{50} values of ~75 nM for HCR/T^{R1226L} for both GD1a and GM1a. These data suggest (i) additional interactions with Sia5, if present, do not enhance HCR/T^{ARTS} binding to Sia5 containing gangliosides or (ii) existing GA1 core interactions have higher affinity compared to new interactions with Sia5. In order to determine if core GA1 affinity was masking interactions with Sia5, unique interactions between HCR/T and the GA1 core were identified. (**Figure 5 and Figure 9**).

HCR/T contains a, N1219, unique amino acid that coordinates binding to GA1 through GalNAc3. When previously characterized, HCR/$T^{R1226L/N1219A}$ abrogated ganglioside binding [47].

	ARTS
GD1a	16.51 ± 2.978
GM1a	80.34 ± 14.63

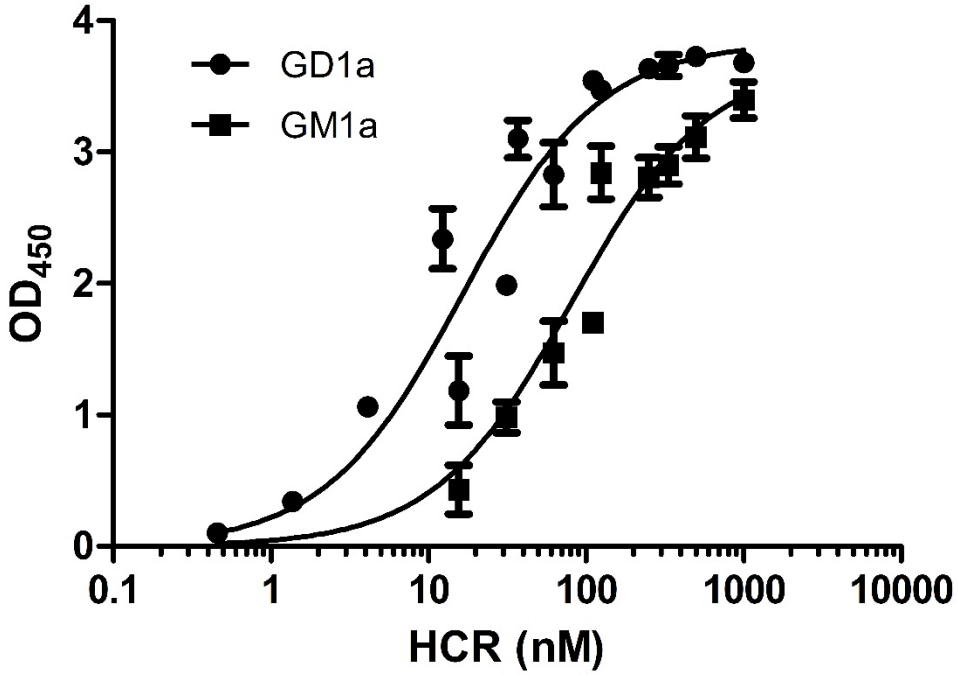

Figure 9. Binding of HCR/T^{ARTS} to gangliosides GD1a and GM1a. Immobilized gangliosides (5µg) GD1a (●) or GM1a (■) were incubated with indicated concentrations of HCR/T^{ARTS} and assayed for binding as described in Chapter 2 Methods. All values represent the arithmetic mean ± SD of 2 independent experiments performed in duplicate. Data were plotted using GraphPad Prism version 5 (GraphPad Software Inc.)

Similarly, HCR/T$^{ARTS/N1219A}$ inhibited all ganglioside binding. Additional point mutations were tested (N1219S, N1219V) and both point mutations were equally inhibitory to ganglioside binding, creating affinities below the limit of detection of our assay for both GD1a and GM1a. Further mutation of HCR/T-N1219 was not pursued

2.4.2 HCR/T-BoNT loop chimeras display altered ganglioside binding properties

Based on the observation that HCR/T^{ARTS} was not significantly altered in ganglioside binding, additional mutations designed to increase binding to Sia5 were considered. BoNT/A (S1275) and BoNT/F (R1256) both contain additional amino acids that could provide potential interactions with the Sia5 sugar. However, direct substitution of these residues with the corresponding positions in HCR/T was not possible due to differences in the orientation of the main chain backbone in these regions. Therefore, it was decided to attempt to swap the entire loop region of HCR/T with the equivalent regions from BoNTs A, E, and F. The initial exchange was performed with BoNT/F to maintain consistency with the previously introduced substitutions.

Using SOE-PCR, the corresponding amino acids in HCR/T (1293 through 1300) were replaced with the BoNT/F amino acids (1254-1263) in the HCR/T^{ARTS} background, creating HCR/T^{ARTS}-F_{Loop} HCR/T-BoNT loop chimeras were purified as described in Methods and analyzed for relative binding affinity to GD1a and GM1a using the solid phase binding assay. Further testing suggested HCR/T^{ARTS}-F_{Loop} and HCR/T^{R1226L} do not have significantly different affinity for GD1a or GM1a (**Figure 10**). Based on these data, two additional loop chimeras were generated containing BoNT/A residues 1270-1279 and BoNT/E residues 1228-1237. In comparison, HCR/T^{ARTS}-A_{Loop} was stably expressed and preliminary screening indicated HCR/T^{ARTS}-A_{Loop} bound ganglioside GD1a with similar affinity to HCR/T^{R1226L}, while binding to GM1a was not evident (**Figure 11**). Based on these observations the binding properties of HCR/T^{ARTS}-A_{Loop} were characterized further. The HCR/T^{ARTS}-E_{Loop} protein was successfully cloned but not pursued further.

2.4.3 Crystal structure of the variant HCR/$T^{A1134L, T1270F, S1135R}$-$A_{Loop}$ (HCR/T^{MO})

While HCR/T^{ARTS}-A_{Loop} appeared to bind ganglioside in a Sia5 dependent manner,

R1226L/GD1a	ARTS-FLoop/GD1a	R1226L/GM1a	ARTS-FLoop/GM1a
49.0 ± 6.3	6.213 ± 0.8	11.53 ± 2.4	12.9 ± 3.5

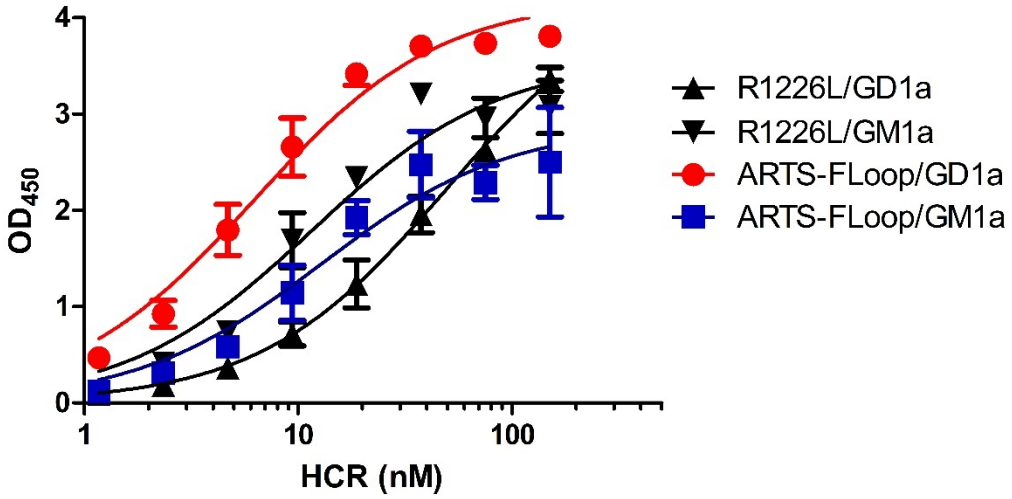

Figure 10. Binding of HCR/T^{ARTS} F$_{Loop}$ to gangliosides GD1a and GM1a. Gangliosides GD1a and GM1a were incubated with HCR/T^{R1226L} (▼/▲) and HCR/T^{ARTS} F$_{Loop}$ (△/▽). Gangliosides were incubated with indicated concentrations of HCR/T variants and assayed for binding as described in Chapter 2 Methods. All values represent the arithmetic mean ± SD of at least 3 independent experiments performed in triplicate. Data were plotted using GraphPad Prism version 5 (GraphPad Software Inc.)

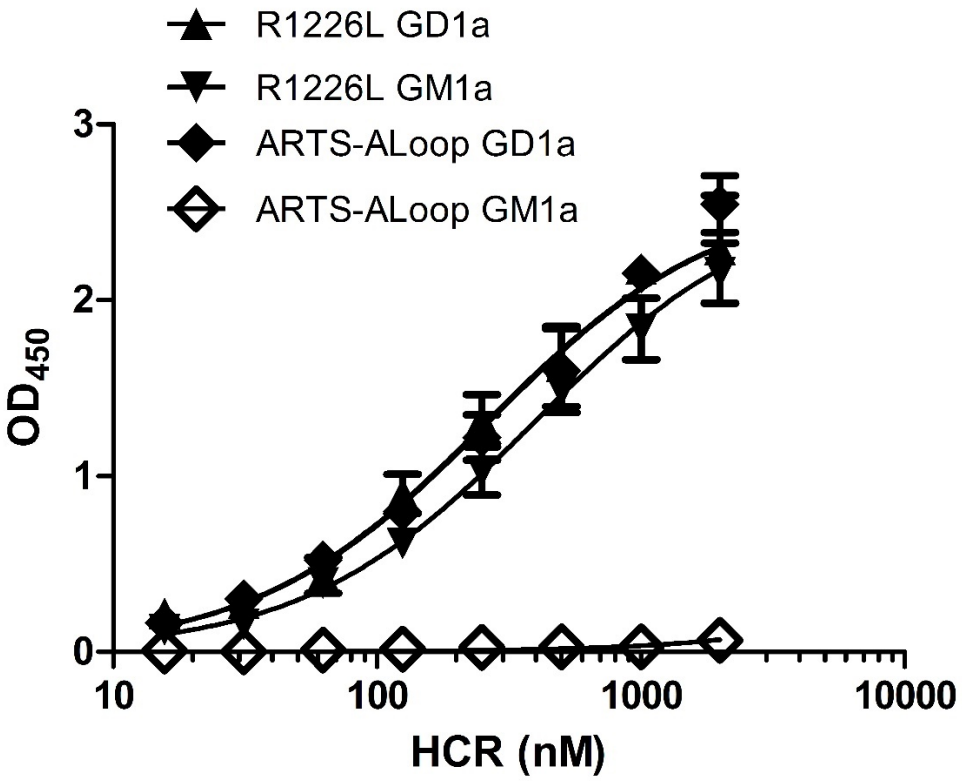

Figure 11. Binding of HCR/T^{ARTS} A$_{Loop}$ to gangliosides GD1a and GM1a. Gangliosides GD1a and GM1a were incubated with HCR/T variants HCR/T^{R1226L} (▼/▲) and HCR/T^{ARTS} A$_{Loop}$ (◇/◆). Gangliosides GD1a or GM1a were incubated with indicated concentrations of HCR/T variants and assayed for binding as described in Chapter 2 Methods. All values represent the arithmetic mean ± SD of at least 3 independent experiments performed in triplicate. Data were plotted using GraphPad Prism version 5 (GraphPad Software Inc).

it is important to emphasize that restoration of the sialic acid, or "R", binding site (R1226) is essential to determine the consequences of these alterations in the context of *in vivo* binding. Therefore, to further characterize the binding properties of HCR/T^{ARTS}-A_{Loop}, (lacking the R site, R-) three further variants were created: HCR/$T^{A1134L,\ T1270F,\ S1135R}$-$A_{Loop}$ (HCR/T^{ARTS}-A_{Loop} with restored R site, hereafter dubbed HCR/T^{MO}); HCR/T-$^{\mathbf{W1289A},\ A1134L,\ T1270F,\ S1135R}$-$A_{Loop}$ (R site only, no W site or W-); and HCR/T-$^{\mathbf{W1289A},\ A1134L,\ \mathbf{R1226L},\ T1270F,\ S1135R}$-$A_{Loop}$ (R-/W-). The inclusion of the W1289A mutation acts to inhibit all binding at the GA1 core binding site, thereby allowing direct investigation of binding to the restored R site. Using the solid phase binding assay, the binding profile of the HCR/T variants at 1 μM was determined using a range of gangliosides capable of interacting with either the R or W sites or both. In **Figure 12,** the comparison of HCR/T and HCR/T^{MO} indicates restoration of R1226 in the HCR/T^{ARTS}-A_{Loop} background reconstituted binding to GM1a. Additionally, ganglioside GD3, a ganglioside previously shown to specifically bind to the R site of HCR/T [103] had higher affinity for HCR/$T^{MO/W1298A}$ as compared to HCR/T ^{W1298A}. These data suggest ganglioside affinity at the R site may be increased in HCR/T^{MO} relative to HCR/T.

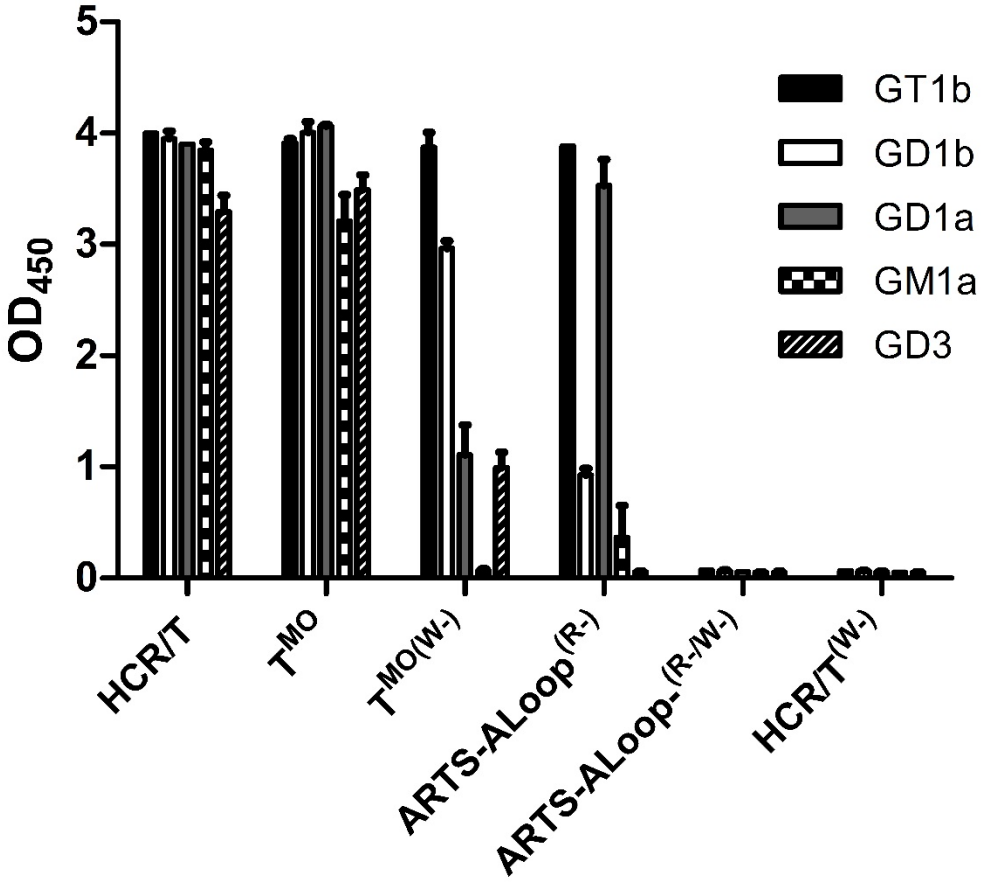

Figure 12. Binding of HCR/T and mutated HCRs to multiple gangliosides. 1 μM: HCR/T, HCR/T^{TMO}, HCR/$T^{TMO(W-)}$, HCR/$T^{ARTS}A_{Loop}{}^{(R-)}$, HCR/$T^{ARTS}A_{Loop}{}^{(R-/W-)}$, and HCR/$T^{(W-)}$ were incubated with gangliosides GT1b (dark gray*),* GD1b (white), GD1a (light gray), GM1a (white with dark gray squares) and GD3 (white with dark gray stripes). Gangliosides were incubated with HCR/T or indicated variants and assayed for binding as described in Chapter 2 Methods. All values represent the arithmetic mean ± SD of at least 2 independent experiments performed in duplicate. Data were plotted using GraphPad Prism version 5 (GraphPad Software Inc.)

In order to gain further insight into the role of the HCR/T^{ARTS}-A_{Loop} mutations in ganglioside binding, HCR/T^{MO} was crystallized by Zhuji Fu in the lab of Dr. Jung Ja Kim at the Medical College of Wisconsin. The structure of recombinant HCR/T^{MO} was determined to a resolution of 1.9 Å by the molecular replacement method using the monomer structure of HCR/T complexed with GT2 (PDB: 3HMY) as the search probe. The overall structure of HCR/T^{MO} was highly similar to HCR/T, with an overall root mean square deviation of 0.3 Å (398 Cα atoms), with the notable exception of loop residues 1293-1300 which adopt an alternate conformation as compared to HCR/T (**Figure 13**). Using the structure provided by the Jung Ja Kim lab, a superposition of HCR/T^{MO} and HCR/T in complex with GT1b oligosaccharide (PDB: 1FV2) was created. Molecular docking of the oligosaccharide moiety of GT1b into HCR/T^{MO} suggests that the overall binding mode is similar to HCR/T with additional hydrogen bonds between HCR/T^{MO} and Sia5 formed by R1135 and R1299 and one bridging water molecule.

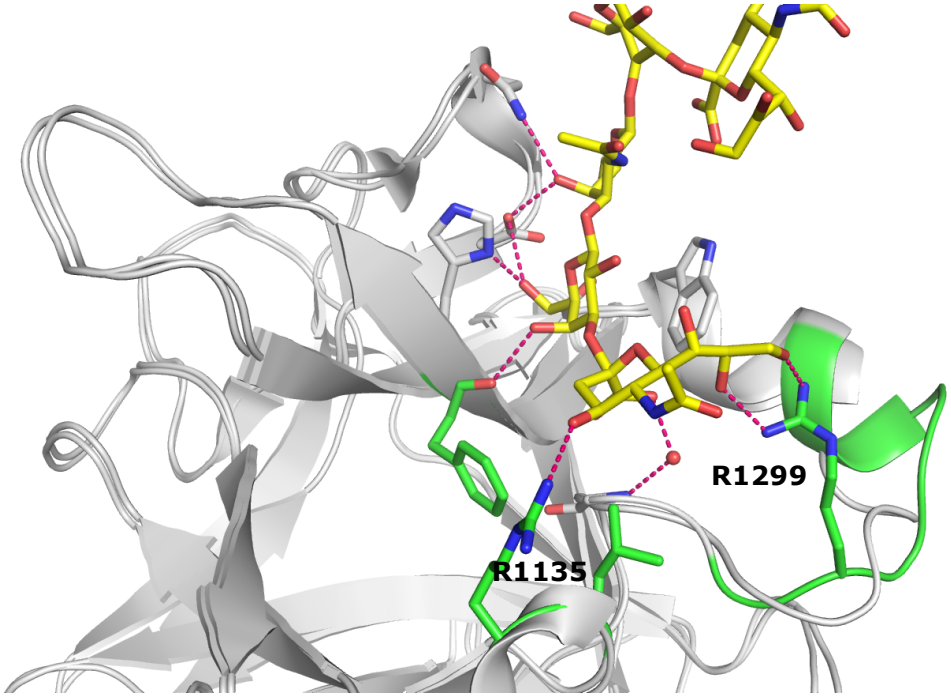

Figure 13. Superposition of HCR/T and HCR/T^{MO} binding pockets.
A ribbon representation of HCR/T^{MO} and the GT1b oligosaccharide from HCR/T (PDB 1FV2) (*stick representation*) are shown. HCR/T^{MO} residues able to bind the GT1b oligosaccharide are colored in atomic color. Potential interactions with Arg1135 and Arg1299 are indicated. Superposition created from HCR/T^{MO} provided by Jung Ja Kim Lab, Medical College of Wisconsin. Superposition created by Joshua Burns.

2.5 Discussion

TeNT is unique among the CNTs because it is sorted into the retrograde axonal pathway and because it binds with high affinity to GM1a - a ganglioside that does not contain the Sia5 sugar [33, 103, 111, 118]. In order to test whether GM1a plays a role in TeNT retrograde axonal trafficking, a variant of HCR/T dependent on the Sia5 sugar for binding at the W site was designed. Our strategy was to modify the binding pocket to incorporate structural features that confer Sia5 binding to the evolutionarily related BoNTs. Amino acid substitutions were initially introduced into HCR/T based on residues previously demonstrated to be important for ganglioside binding in BoNT/F. HCR/T^{ARTS} contained three mutations (T1270F, A1134L, and S1135R) designed to promote interactions with Sia5; yet initial screening suggested the introduced changes did not significantly alter binding to gangliosides GD1a or GM1a (**Figure 9**). However, mutation of HCR/T T1270F alone resulted in a dramatic decrease in binding to GD1a (**Figure 14**), suggesting that mutations A1134L and/or S1135R may interact with T1270F to restore binding. Although the exact role of the phenylalanine is unclear, previous studies in

.

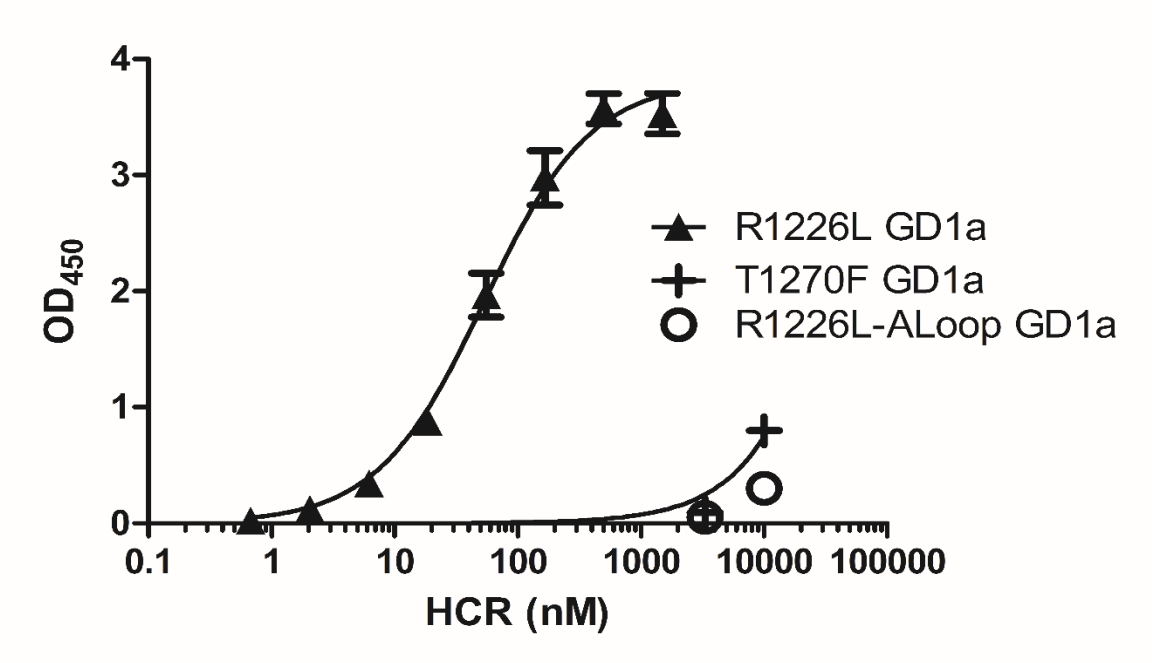

Figure 14. Binding of HCR/T variants to GD1a ganglioside. GD1a ganglioside was incubated with HCR/T variants HCR/T^{R1226L} (▲), HCR/$T^{R1226L/T1270F}$ (+) and HCR/$T^{R1226L}A_{Loop}$ (O). Ganglioside was incubated with indicated concentrations of HCR/T variants and assayed for binding as described in Chapter 2, Methods. All values represent the arithmetic mean ± SD of 2 independent experiments performed in duplicate. Data were plotted using GraphPad Prism version 5 (GraphPad Software Inc.)

BoNTs A, B, and F demonstrate this residue plays an important role in recognition of Sia5 (**Figure 8**), possibly by forming a stacking interaction with the hydrophobic face of the sugar ring. It was therefore hypothesized that more global changes in the Sia5 binding pocket between BoNTs and TeNT may also indirectly regulate ganglioside binding. In support of this model, replacement of a structurally divergent loop region within HCR/T (residues 1293-1300) with the corresponding sequences of BoNT/F and BoNT/A caused significant reductions in GM1a binding (**Figures 10 and 11**). Indeed, insertion of the A loop sequence alone was sufficient to abolish binding to both GD1a and GM1a (**Figure 11**). These data argue that recognition of Sia5 is a multifaceted process that regulates binding of the GA1 core sequence to the GBM. Previous structural and biochemical data suggest GM1a does not bind the R site of TeNT, presumably because the affinity for the Gal2-linked sialic acid is not sufficient [102, 103, 111]. Unexpectedly, restoration of the R site in HCR/T^{ARTS}-A_{Loop} background, generating HCR/T^{MO}, restored GM1a binding to near wild-type levels (**Figures 12 and 15**). Binding of HCR/T^{MO} to ganglioside was further probed using GD3 which was previously shown to bind exclusively to the R site [103, 111, 129] (**Figure 16)**.

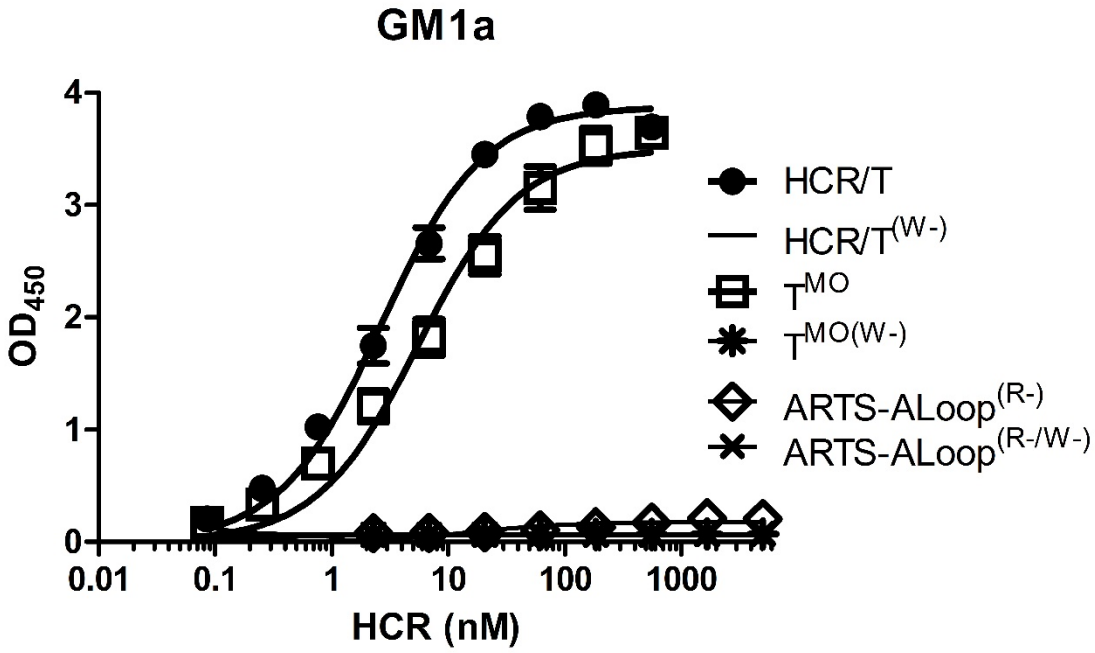

Figure 15. Binding of HCR/T variants to GM1a ganglioside. GM1a ganglioside was incubated with HCR/T (●), HCR/T($^{W-}$) (-), HCR/T^{TMO} (□), HCR/T$^{TMO(W-)}$ (✶), HCR/T^{ARTS}A$_{Loop}$$^{(R-)}$ (◇) and HCR/T^{ARTS}A$_{Loop}$$^{(R-/W-)}$(x). Ganglioside was incubated with indicated concentrations of HCR/T or variant and assayed for binding as described in Chapter 2, Methods. All values represent the arithmetic mean ± SD of at least 3 independent experiments performed in triplicate. Data were plotted using GraphPad Prism version 5 (GraphPad Software Inc.)

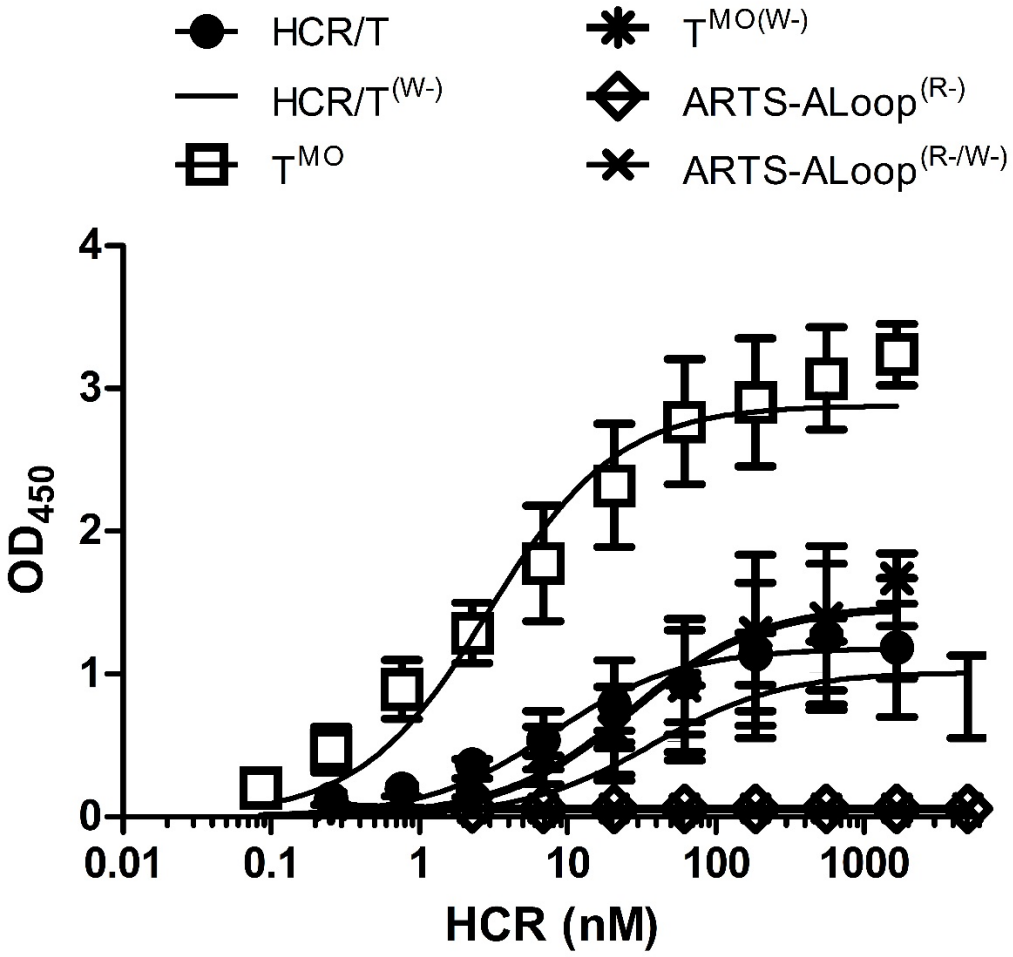

Figure 16. Binding of HCR/T variants to GD3 ganglioside. GD3 ganglioside was incubated with HCR/T (●), HCR/T$^{(W-)}$ (-), HCR/T^{TMO} (□), HCR/T$^{TMO(W-)}$ (✶), HCR/T^{ARTS}A$_{Loop}^{(R-)}$ (◇) and HCR/T^{ARTS}A$_{Loop}^{(R-/W-)}$(x). Ganglioside was incubated with indicated concentrations of HCR/T or variant and assayed for binding as described in Chapter 2, Methods. All values represent the arithmetic mean ± SD of at least 4 independent experiments performed in triplicate. Data were plotted using GraphPad Prism version 5 (GraphPad Software Inc.)

Contrary to expectations, HCR/T^{MO} has an elevated affinity for GD3 as compared with wild type HCR/T. In addition, mutation of the conserved GBM Trp residue confirmed GD3 binding was to the R site alone. These data imply that mutations at the W pocket have altered the affinity of the R site for ganglioside. However, the mechanistic basis for this claim is unclear given that the HCR/T^{MO} crystal structure does not reveal any significant changes in the R site. Although binding of HCR/T^{MO} was clearly observed in the solid phase binding assay, previous studies suggest ganglioside interactions occurring on cellular membranes are less promiscuous. To determine if the observed affinity for GM1a was an artifact of the plate assay, binding and entry into Neuro2a cells exogenously loaded with GM1a was determined under the conditions described by Chen *et al.* [103]. In agreement with previous observations, loading cells with GM1a alone was not sufficient to induce binding and entry of HCR/T^{MO}, suggesting the R site was not able to bind GM1a [102, 103]. When Neuro2a cells were similarly loaded with GT1b or an equimolar mixture of GD3/GM1a (gangliosides binding to the R and W sites of TeNT respectively) HCR/T^{MO} was able to bind and internalize efficiently (**Figure 17A**). Moreover, when HCR/T^{ARTS}-A_{Loop} was added to Neuro2a

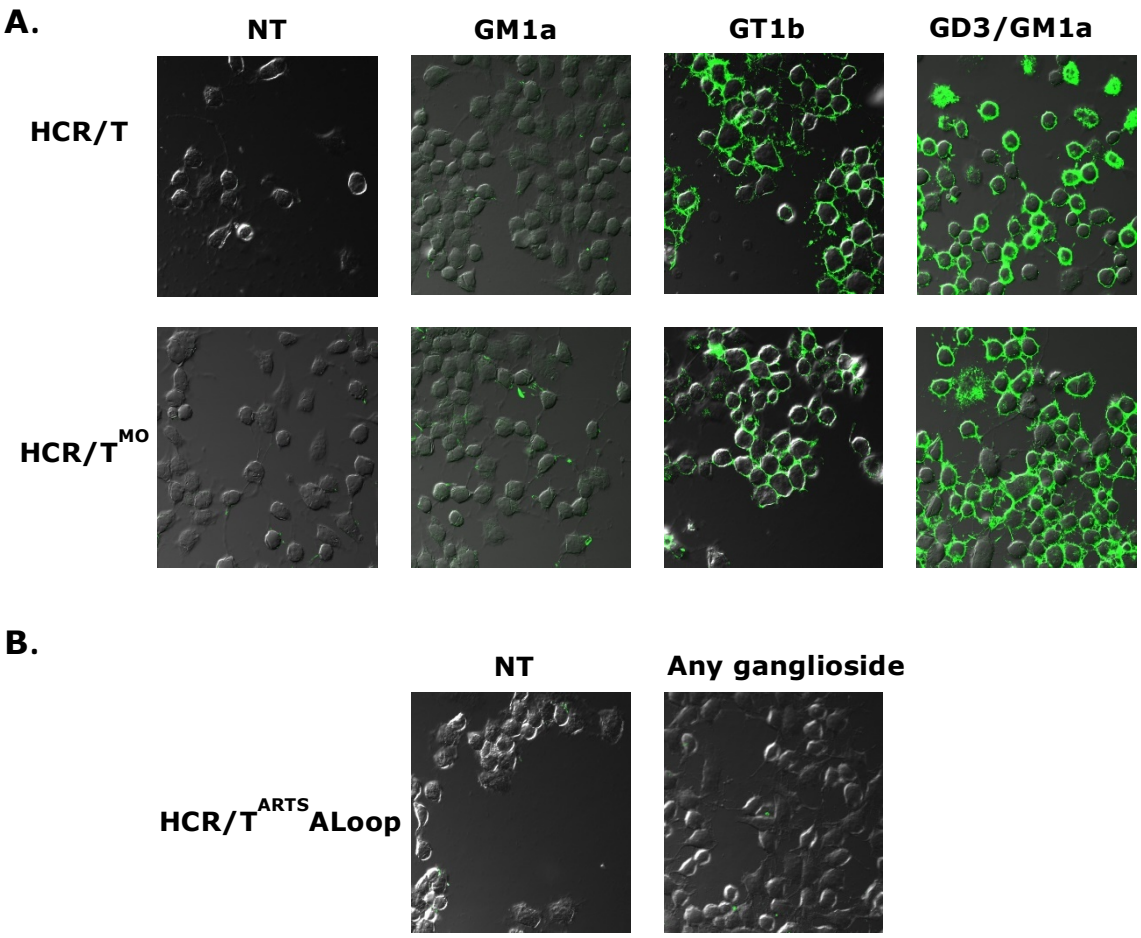

Figure 17(A-B). HCR/T^{MO} enters cells similar to HCR/T. (A) Exogenous gangliosides GM1a, GT1b, or combination of GD3 and GM1a were added to Neuro2A cells prior to exposure to, HCR/T or HCR/T^{MO}. HCRs were detected by FLAG epitope sequence and processed for immunofluorescence. (B) HCR/T^{ARTS} ALoop was similarly added to Neuro2A cells previously treated with GM1a, GT1b, or GD3 and GM1a, detected by FLAG epitope sequence and processed for immunofluorescence. No binding was detected under any conditions. Representative of images from 5 images.

cells similarly loaded with gangliosides no binding above untreated control cells was observed (**17B**). These data suggest that recognition of GM1a by HCR/T^{MO} in the solid phase binding assay does not extend to GM1a in the context of a biological membrane. Rather, the data argue that similar to wild type HCR/T, the R site of HCR/T^{MO} preferentially recognizes disialic acid moieties on the cell surface.

2.6 Future Directions

At present the precise mechanism(s) by which HCR/T^{MO} recognizes gangliosides remains unresolved. Future studies designed to shed more light on the binding mechanism include using mass spectroscopy to determine the molar ratios of ganglioside to protein in the bound complexes (similar to the procedure of Rummel *et al*.) [102]. If successful, the approach could independently confirm the ability of HCR/T^{MO} to bind GM1a in solution and verify if binding was to the R site specifically. Similarly, a co-crystal of HCR/T^{MO} bound to either GD1a or GT1b would provide direct evidence for interactions between the Sia5 sugar and HCR/T^{MO}. In order to determine if the R site has higher binding affinity as compared to HCR/T, we could use a more sensitive technique to measure binding, such as surface plasmon resonance, to determine if there is difference in R site affinity.

The major unanswered question however, is if there is a difference in retrograde trafficking as compared to HCR/T. Preliminary experiments using *ex vivo* cultures of rat cortical neurons suggest that HCR/T^{MO} binds differently to cells than HCR/T. Colocalization experiments demonstrate that HCR/T^{MO} segregates more efficiently with the cholera toxin B subunit (a marker of lipid rafts) than does HCR/T (**Figure 17 C-E**). However, this still does not directly address the issue of retrograde axonal trafficking. An attempt to look at retrograde axonal trafficking directly in cultured motor neurons in collaboration with Dr. Gipi Schiavo's laboratory was initiated [33, 130]. However, the only response received thus far was that overall binding of HCR/T^{MO} to motor neurons was reduced by ~20% as compared to wild type. We could evaluate the ability of HCR/T^{MO} to undergo retrograde axonal trafficking using a live rat model by looking for a difference in hind limb pathology [131]. Based on the summation of our data, it is not clear that investing in animals and a pathologist is best at this time because we are not able to describe a definite binding mechanism to HCR/T^{MO}, or define how the binding mechanism is different from HCR/T.

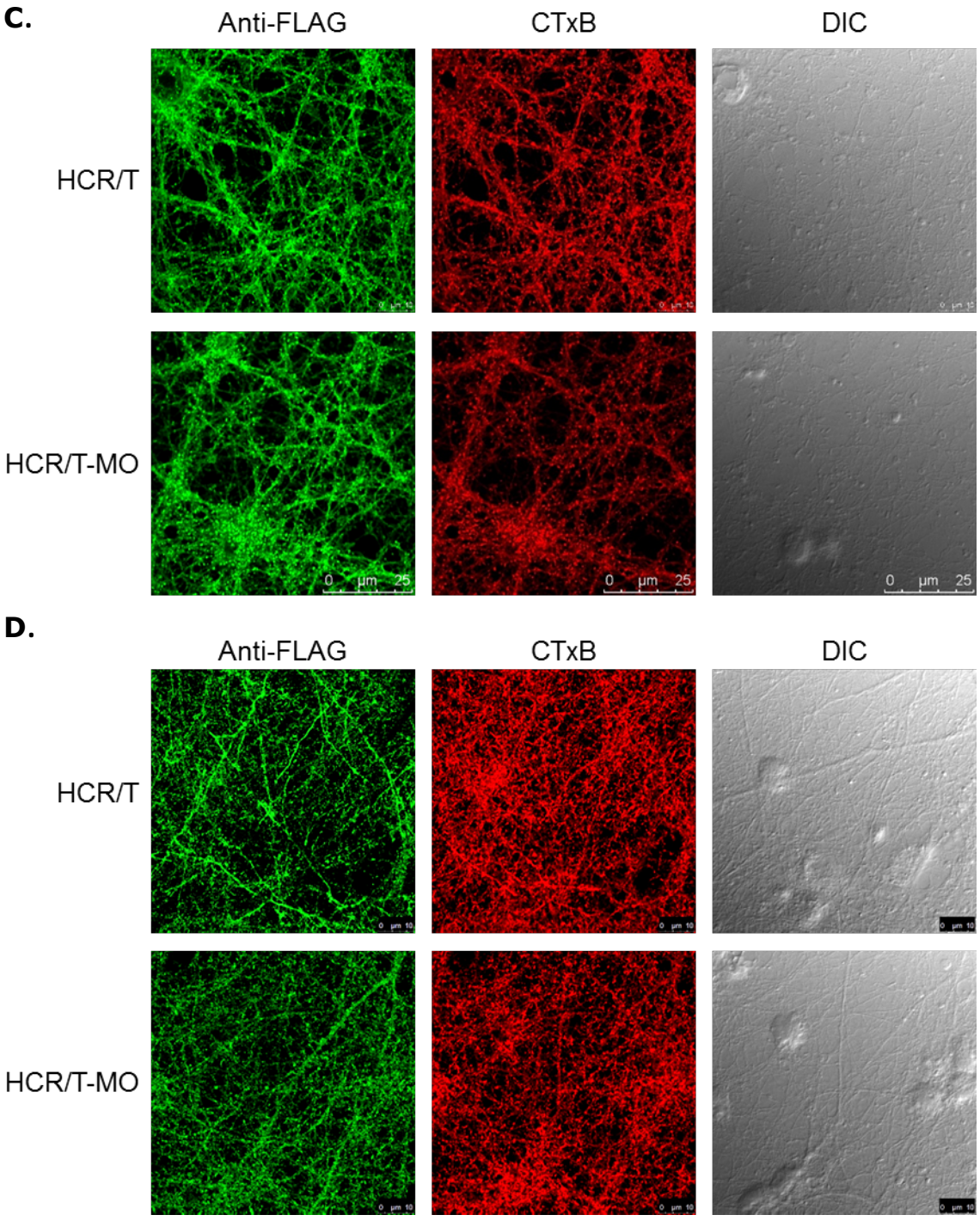
C.
Anti-FLAG
CTxB
DIC
HCR/T
HCR/T-MO
0 µm 25
D.
Anti-FLAG
CTxB
DIC
HCR/T
HCR/T-MO

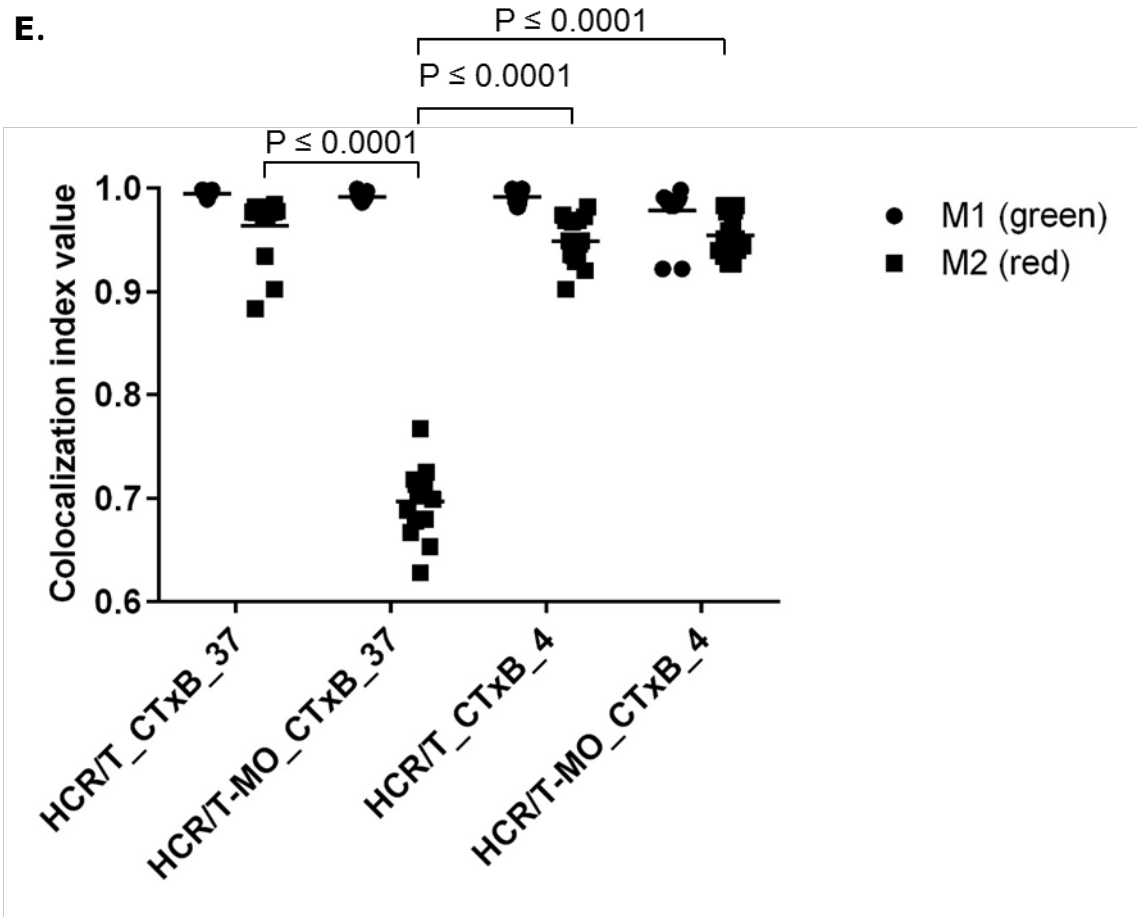

Figure 17 (C-E). Colocalization of tetanus toxin HCR domains with cholera toxin b subunit at 37°C and 4°C. (A) Rat primary cortical neurons were exposed to either 10 nM HCR/T (upper panels) or 10 nM HCR/T-MO (lower panels) in the presence of 10 nM cholera toxin b subunit (CTxB) for 15 minutes at 37°C. Cells were subsequently fixed and HCR detected by indirect immunofluorescence as described in the Methods section. (B) Neurons were treated exactly as described in (A), except that the temperature was shifted to 4°C. (C) Colocalization of TeNT HCRs with cholera toxin b subunit (CTxB) was determined by the method of Manders et al.[132]. Data was analyzed by two-way ANOVA and Holm-Sidak's multiple comparisons test with an alpha value of 0.01. Colocalization indexes M1 and M2 are defined by: ∑S1i,coloc / ∑S1i and ∑S2i,coloc / ∑S2i respectively. ∑S1i and ∑S2i represent signal intensities in the green (S1) and red (S2) channels. ∑S1i, coloc and ∑S2i,coloc represent those pixels that display non-random fluorescence in the opposite channel, n=15 random fields. Data are an average of 2 biological repeats.

Additionally, recent data suggest TeNT holotoxin may undergo retrograde axonal trafficking more efficiently than HCR/T alone, suggesting regions of the molecule outside the HCR contribute to cellular sorting [133]., If appropriate technologies become available studies designed to test the role of GM1a in retrograde axonal trafficking may be undertaken with HCR/T^{MO} holotoxin or HCR/T^{MO}.

CHAPTER 3: UNIQUE GANGLIOSIDE RECOGNITION STRATEGIES FOR BOTULINUM A1 and A2

3.1 Abstract

Botulinum neurotoxins (BoNTs) have been identified as Tier 1 category "A" Select Agents by the Centers for Disease Control and Prevention. Currently, seven BoNT serotypes (A-G) and ~40 subtypes have been identified. Sequencing of BoNT/A genes from multiple isolates of *Clostridium botulinum* have revealed a high degree of sequence variability, and so far, eight BoNT/A subtypes (BoNT/A1-8) have been identified. Two subtypes, BoNT/A1 and BoNT/A2, share a high degree of amino acid sequence identity (~89%), yet BoNT/A2 has significantly enhanced toxicity compared to BoNT/A1. While available data suggests the enhanced toxicity of BoNT/A2 may result from increased efficiency of binding and entry, the mechanistic basis for this remains unclear. Paradoxically, structural predications suggest ganglioside interactions, and specific interactions with the Sia5 sugar, may be present in BoNT/A1 that may not exist in BoNT/A2. This implied that BoNT/A2 would bind ganglioside with lower affinity than BoNT/A1. However, a solid-phase binding assay demonstrated that the affinity of A1 and A2 for gangliosides was similar. Further biochemical characterization revealed that two previously proposed protein-carbohydrate

interactions [Tyr1117 (OH): Sia5 and Ser1264 (OG): Sia5] do not significantly contribute to ganglioside binding. Indeed, it appears that the presence of the tyrosyl side chain in A1 or the phenyl side chain in A2 (Phe1117) reduce binding to Sia5 containing gangliosides. Cellular binding assays demonstrate that HCR/A1^{Y1117A} and HCR/A2^{F1117A} enter cells faster than parental domains and suggest a strategy for improving the toxicity and hence therapeutic benefits of botulinum neurotoxins.

3.2 Introduction

Recognition of botulism in the 1820s lead to the discovery and early characterization of botulinum neurotoxin (BoNT) in the 1890s. Increasing outbreaks established that unique, antigen specific BoNT toxins were capable of causing disease [134]. Modern sequencing technology and access to bacterial strains has provided a platform to begin comprehensive study of BoNT diversity. Currently, seven serotypes and over 40 BoNT subtypes have been identified. Overall amino acid composition of a subtype must differ by at least 2.5% to be unique, but can be up to 30% different in some cases [135, 136]. Botulinum neurotoxin type A1 (BoNT/A) is produced by *C. botulinum* group I isolates and is considered the parental toxin for all clostridial neurotoxins including tetanus toxin. There are currently 8 described

subtypes for BoNT/A (A1-A8). BoNT/A1 (parental), BoNT/A2 originally isolated from a patient in Kyoto, Japan [137, 138], BoNT/A3 was responsible for a famous outbreak at a hotel in Loch Maree, Scotland in 1926 [139, 140], BoNT/A4 was isolated from a strain of *C. botulinum* that produces both A and B toxins [141], BoNT/A5 was recently isolated in 2010 from a patient in Wisconsin [142], BoNTs A6 and A7 were recently described from patients in France [143, 144], and BoNT/A8 has also been recently described [145]. Vaccine studies confirm CNT subtypes are neutralized by vaccination with corresponding subtypes but levels of cross-protection and neutralizing epitopes are different [97, 140, 146].

Functional characterization of BoNT/A subtypes has been undertaken. The gold standard for determining BoNT toxicity has been the mouse bioassay (MBA) [147, 148]. Using mouse LD_{50}s, specific activities of individual BoNTs can be compared. MBA results indicated the specific activity (U/mg) for BoNT A1(1.25×10^8) = A2(1.24×10^8) ~ A5(1.4×10^8) > A3(5.8×10^7) >A4(1.25×10^5) [148]. Analysis using cultured primary neurons, rodent twitch tension, and grip strength assays suggested BoNT/A2 was more potent than BoNT/A1 [149, 150]. In accord, data collected using rodent primary neurons and neurons derived from human induced pluripotent stem cells, suggested the effective concentration of BoNT/A2 resulting in 50%

cleavage of SNAP-25 (EC_{50}) was tenfold lower than the EC_{50} for BoNT/A1 [148]. Moreover, BoNT/A2 intoxicated mice were noted to have experienced a more rapid onset of death than BoNT/A1 intoxicated mice with paralysis similar to BoNT/A3 intoxicated mice. [148]. These data suggest BoNTs A2 and A1 may target unique subsets of neurons after neuronal entry.

The molecular basis for the apparent increased potency of BoNT/A2 as compared with the remaining A subtypes is not currently understood. Analysis of catalytic efficiency determined BoNTs A1 and A2 cleaved SNAP-25 *in vitro* with similar kinetic efficiency, BoNT/A3 had half the activity of BoNT/A1, and BoNT/A4 was tenfold less active than BoNT/A1 [151, 152]. Thus the activity of the LC does not appear to be responsible for the increased toxicity of A2. Interestingly, when recombinant HCR derivatives (HCR/A1 and HCR/A2) were applied to rat primary spinal cord neurons and mouse Neuro2A cells, HCR/A2 entered cells more rapidly than HCR/A1 [149]. Moreover, studies with an inhibitor of BoNT LC translocation (toosendanin), suggested that the enhanced neurotoxicity of BoNT/A2 compared to A1 is due to more rapid translocation of LC/A2 or to a step in the intoxication process preceding translocation [149]. Thus it appears that differences in cellular binding and entry may account for the increased toxicity of A2 *in vivo*.

A global alignment of BoNT/A1 with BoNT/A2 shows a high degree of amino acid sequence conservation (89%), with greater variability observed when comparing the four major structural domains of the toxins to each other (LC, 95%; HCT, 87%; HCR_N, 83%; and HCR_C, 90%) [151]. The structural elements involved in ganglioside recognition in BoNT/A1 have been well-characterized. BoNT/A1 contains a conserved ganglioside binding motif (GBM; E…H…SXWY…G) which coordinates the GA1 carbohydrate core of gangliosides containing Sia5. Mutation of the central tryptophan residue (W1266L) increased paralytic halftime and reduced binding to rat brain synaptosomes and immobilized ganglioside similar to $TeNT^{W1289A}$ [102, 153]. Predictably, mutation of the remaining GBM residues also increased paralytic halftimes and decreased overall toxicity. More recently, a co-crystal of HCR/A with the oligosaccharide moiety of GT1b suggested that ganglioside binding was further stabilized by hydrogen bonds formed between Y1117, S1275, R1276, and Sia5 [112]. However, biochemical confirmation of these interactions was not reported. Similar interactions were reported in a co-crystal of HCR/F with the oligosaccharide moiety of GD1a [47, 112], suggesting interactions with Sia5 may be essential for BoNT ganglioside recognition. Our hypothesis is that interactions between BoNT/A2 and

the Sia5 sugar are required for efficient binding and entry and contribute to increased toxicity.

Development of BoNT/A2 will expand current BoNT utility in pharmaceutical applications, broaden our insight into inhibitor design, and expand our knowledge of BoNT entry mechanisms. However, the current lack of understanding of BoNT/A2 entry and toxicity mechanisms is preventing full development of the BoNT/A2 platform. This research in conjunction with other ongoing programs will shed light on the entry and toxicity mechanisms of the BoNT/A serotype specifically and more generally the clostridial neurotoxins.

3.3 Experimental procedures

3.3.1 Cloning and mutagenesis of HCR and TEM-Bla_BoNT/A fusion proteins

A previously described, modified, pET28a expression vector (Novagen) – hereafter referred to as pET28-3×FLAG – containing a 3×FLAG epitope immediately downstream of the hexahistidine epitope tag was used as the expression vector for all HCR constructs [125]. Briefly, *E. coli* optimized HCR DNA (aa 873-1295) was chemically synthesized (Genscript, Inc) and subcloned into pET28-3×FLAG via unique 5' *KpnI* and 3' *XhoI* restriction sites. Point mutations were

introduced into the HCR/A1 and A2 genes by site directed mutagenesis using Quikchange® II Site-Directed Mutagenesis Kits (Agilent) and confirmed by DNA sequencing.

TEM-Bla reporter proteins: the TEM-Bla gene from pUC57 was amplified by PCR, ligated into the *Nco*I and *Nde*I sites of pET28a, and confirmed by DNA sequencing. Subsequently, synthetic DNA fragments encoding BoNT/A1 residues 1-846 and 845-1295 were sequentially cloned into pET28a harboring the TEM-Bla gene using *Nde*I, *Sca*I, and *Xho*I restriction sites. The BoNT/A2 construct was generated in a similar manner. In both cases, the toxin gene contained three point mutations (E224A, R363A, and Y366F) which inactivate the enzymatic activity of LC resulting in non-toxic proteins.

3.3.2 Expression and purification of HCR and TEM-Bla_BoNT/A fusion proteins

WT and mutated HCRs were expressed and purified as previously described in Chapter 2 methods, section 2.2.3. In addition to an N-terminal hexahistadine tag, TEM-Bla_BoNT/A1 and A2 contain C-terminal Strep-Tag II® epitopes. pET28a-TEM-Bla_BoNT/A1 or A2 DNA was transformed into BL-21 (DE3) Ai cells and cultured on LB-Kan plates overnight. Expression and purification of pET28a-TEM-Bla_BoNT/A1 was performed under similar conditions to those

described in Chapter 2 methods, section 2.2.3. After 3 hours at 37ºC at 250 r.p.m bacteria were induced with a final concentration of 1 mM IPTG and 5% L-Arabinose. Incubation continued overnight following temperature reduction to 16ºC. Following overnight culture, TEM-Bla_BoNT/A1 was isolated by sequential chromatography using Streptactin-sepharose and Ni-NTA-agarose and subsequently dialyzed into PBS.

3.3.3 Solid phase ganglioside binding assay

The solid phase binding assay was carried out as described in Chapter 2 Methods, section 2.2.4. WT and mutated HCRs were added to 96 well plates containing previously immobilized ganglioside GT1b. Post incubation, an antibody solution containing anti-FLAG M2 monoclonal antibody (1:8,000) and goat anti-mouse poly HRP (1:10,000; Pierce) was prepared to detect bound HCR complexes. Bound HCR complexes were detected using Ultra TMB (Pierce) as the HRP substrate. The reaction was terminated by addition of an equal volume of 0.1 M H_2S0_4. The absorbance at 450 nm was determined using a plate reader (BioTek). The concentration of HCR required to give 50% of maximum binding (B_{50}) was estimated.

3.3.4 HCR binding to rat cortical neurons

As described in Chapter 2 Methods, section 2.2.6, rat embryonic day 18 (E18) cortical neurons (Brainbits) were mechanically dissociated per the Brainbits, llc protocol and cultured in supplemented Neurobasal medium on poly-D-lysine coated cover slips 10-14 days prior to use. Cells were treated with 10, 50, and 250 nM HCRs for 5 min. in neuron stimulation buffer (15 mM HEPES, 95 mM NaCl, 56 mM KCl, 2.2 mM CaCl2, 0.5 mM MgCl2, pH 7.4), washed three times in cold Hank's Balanced Salt Solution (HBSS), and fixed in 4% (w/v) paraformaldehyde/4% (w/v) sucrose solution in PBS for 30 min at room temperature. Cells were subsequently quenched with 0.1M glycine, permeabilized with 0.25% (v/v) Triton X-100, and blocked using Image-IT reagent. Bound HCR was detected by immunofluorescence using mouse anti-FLAG (clone M2 1:1000) and goat anti-mouse IgG Alexa 488 (1:200). Endogenous synaptophysin was detected using rabbit anti-synaptophysin (1:100) and anti-rabbit IgG Alexa 568 (1:200). Cells were processed using standard immunofluorescence procedures, mounted in ProLong Gold Antifade reagent, and acquired using a Leica SPE-2 in confocal scanning mode. Colocalization was analyzed using Li's Intensity Correlation Quotient (ICQ) equation within the JaCoP plugin module for ImageJ [154]. An average of 15 random fields and at least biological repeats were performed. Data were analyzed using unpaired student t-test.

3.3.5 LC translocation assay

TEM-Bla_BoNT/A1 was incubated with rat primary cortical neurons for a minimum of three hours at 37ºC. Cells were washed twice with HBSS and then loaded with the fluorescent TEM-Bla substrate CCF4-AM (ThermoFisher Scientific) for 90 min at room temperature. Cells were washed with HBSS, trypsinized, filtered to remove large cell aggregates, and analyzed by flow cytometry. Cells were excited at 405 nm, side scatter emission was set at 450/50 and forward scatter emission was set at 515/20 using a BD LSR Fortessa X-20 instrument.

3.4 Results

3.4.1 HCR/A2 enters neurons by way of recycling secretory vesicles

Previous studies have demonstrated that the uptake of BoNT/A2 into neurons is stimulated by conditions which promote synaptic vesicle exocytosis. Therefore, to further characterize the entry of BoNT/A2, a recombinant HCR domain containing the FLAG epitope was generated. In agreement with previous observations, little or no binding of HCR/A2 to rat primary cortical neurons was observed either

at 4°C or when cells were exposed to protein under non-depolarizing conditions (low K^+ buffer) (**data not shown**). However, when cells were exposed to HCR/A2 under depolarizing conditions (high K^+ buffer) a significant increase in binding and uptake was observed (**Figure 18**, panel A, green channel). Co-staining for the synaptic vesicle protein synaptophysin (**Figure 18**, panel B, red channel) suggested a qualitative relationship between the two proteins visualized in the merged image (**Figure 18**, panel C) as yellow pixels.

The degree of colocalization was evaluated more quantitatively by performing Intensity Correlation Analysis. This is a method in which the intensities of the pixels in the green and red channels are compared statistically by calculating the PDM (Produce of the Differences of the Means) value for each pixel. When pixel intensities for either green or red channels are plotted as a function of the PDM values (**Figure 18**, panel D), it is clear that they are skewed towards positive values, consistent with a dependent staining pattern. Averaging of the calculated Intensity Correlation Quotient (ICQ) values for multiple fields gave a value of 0.263±0.04 which strongly supports this idea. By comparison, HCR/A2 was strongly segregated from the dendritic marker MAP2 (**Figure 18**, panel E) supporting the specificity of the HCR/A2–Synaptophysin colocalization.

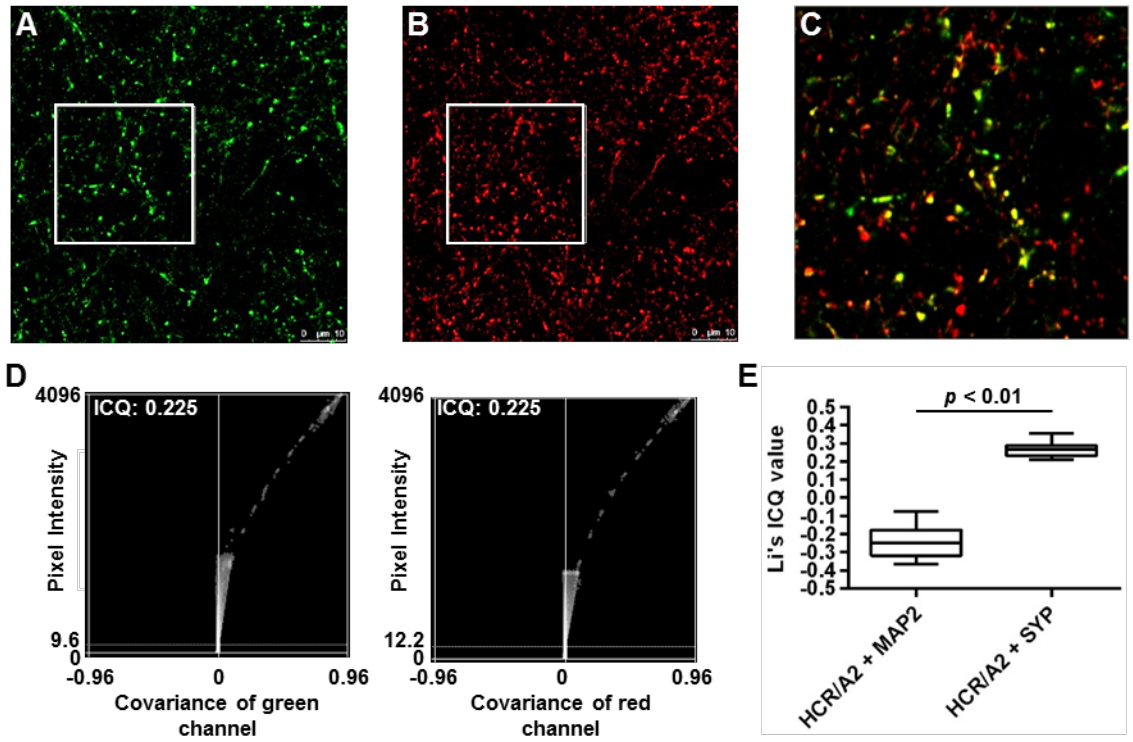

Figure 18. HCR/A2 enters neurons by way of recycling secretory vesicles. (A) Rat cortical neurons were incubated for 5 min at 37°C in high K+ buffer to stimulate vesicle recycling. Cells were then washed, fixed, and permeabilized as described in the Methods section. Internalized HCR/A2 was stained using a mouse anti-FLAG antibody and an Alexa Fluor 488-conjugated goat anti-mouse secondary antibody. (B) The integral synaptic vesicle membrane protein Synaptophysin (SYP) was stained using a rabbit anti-SYP antibody and an Alexa Fluor 568-conjugated goat anti-rabbit secondary antibody. (C) An enlarged optical section of the region highlighted by the white box in panels A and B showing a high degree of co-localization between the two proteins. (D) An intensity correlation plot for panels A and B showing dependent staining among the two variables in the study: HCR/A2 and SYP [155]. (E) Quantification of Intensity correlation quotient (ICQ) values for HCR/A2 and SYP and HCR/A2 and Microtubule-associated protein 2 (MAP2), n=15 random fields and ≥ 2 biological repeats. Data analyzed using unpaired t-test.

These data argue that similar to BoNT/A1, entry of BoNT/A2 is through recycling synaptic vesicles likely mediated by interactions with ganglioside and SV2 co-receptors.

3.4.2 Sequence diversity in residues forming the ganglioside binding pocket of BoNT/A1 and BoNT/A2

As outlined in the introduction, accumulating evidence suggests that differences in cellular binding and/or entry may account for the increased toxicity of BoNT/A2 relative to BoNT/A1 *in vivo* One possible mechanism by which the entry of BoNT/A2 could differ is through unique interactions with ganglioside co-receptors. To begin to address this possibility, a homology model of HCR/A2 was generated using SWISS-Model (http://swissmodel.expasy.org/interactive) [156]. The co-crystal of HCR/A1 with GT1b oligosaccharide (PDB: 2VU9) was used as the template to generate the HCR/A2 model. Next, the HCR/A2 model was overlaid with the co-crystal structure of HCR/A1 bound to GT1b (**Figure 19**). As expected, residues forming the GBM were conserved between A1 and A2, while residues predicted to make hydrogen bonds (S1275 and R1276) with Sia5 were similarly conserved

Adapted from PDB: 2VU9. PLoS Pathog. 2008 Aug 15;4(8):e1000129. PMID: 18704164

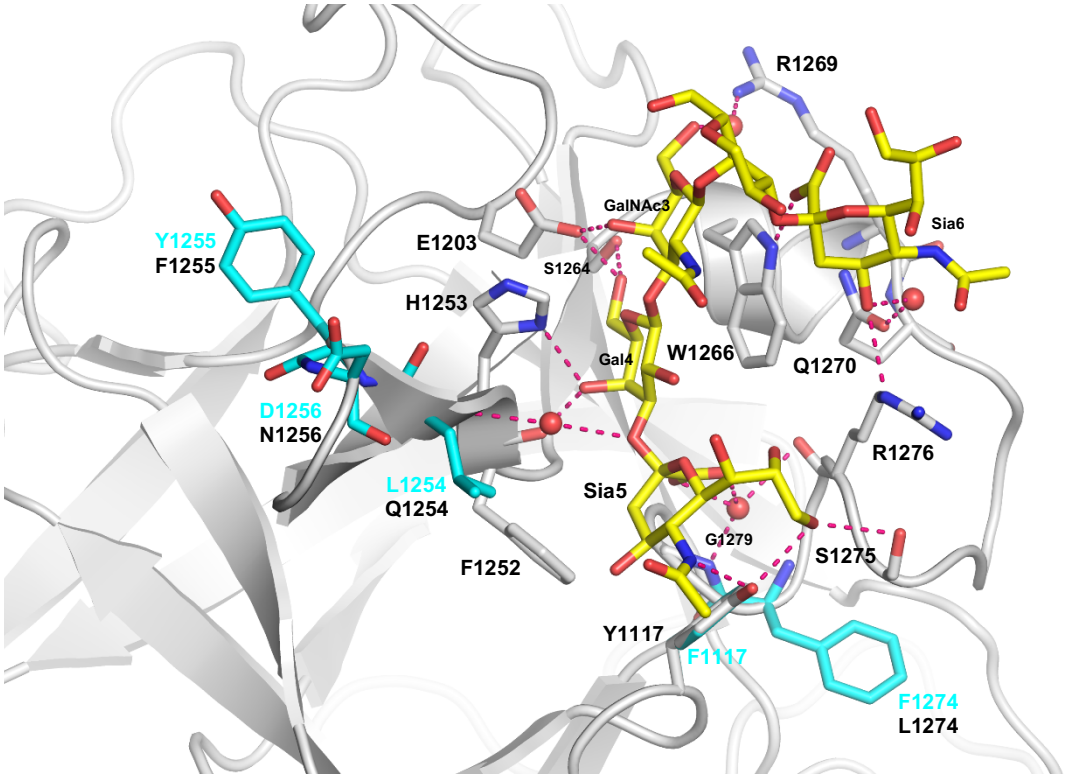

Figure 19. Superposition of HCR/A1 in complex with GT1b and a 3D homology model of HCR/A2. Overall structure of HCR/A1 is displayed as ribbon diagram with grey Cα. GT1b represented as sticks with yellow carbons. The GT1b coordinating residues are shown as sticks with grey carbons. The HCR/A2 residues which vary with HCR/A1 are shown as sticks with cyan carbons.

However, HCR/A1 Y1117 – which is predicted to form two hydrogen bonds to Sia5 – was replaced by phenylalanine in HCR/A2. In addition, several other residues which contribute to the overall structure of the ganglioside binding pocket were also not conserved between the A subtypes.

3.4.3 HCR/A1 and HCR/A2 bind ganglioside GT1b with similar affinity

To determine what effect amino acid differences in the ganglioside binding pocket may have on ganglioside binding, wild-type and variant proteins were compared directly using a solid-phase binding assay (Solid phase binding assays were carried out with assistance from Greg Lambert). HCR/A1 and HCR/A2 bound GT1b with similar affinity (~150 nM for A2 and ~250 nM A1) **(Figure 20A** and **Table 6)**. HCR/A1^{S1275} and HCR/A2^{S1275} variants were created and were similarly unaffected in the ability to bind ganglioside (**Table 6**). The co-crystal structure of HCR/A1 bound to GT1b suggested that Y1117 forms two hydrogen bonds to Sia5. Consequently, the equivalent position in HCR/A2 with phenylalanine (F1117) was expected to have reduced ganglioside binding. However, both increased affinity to GT1b when mutated to alanine (**Figure 20B)**.

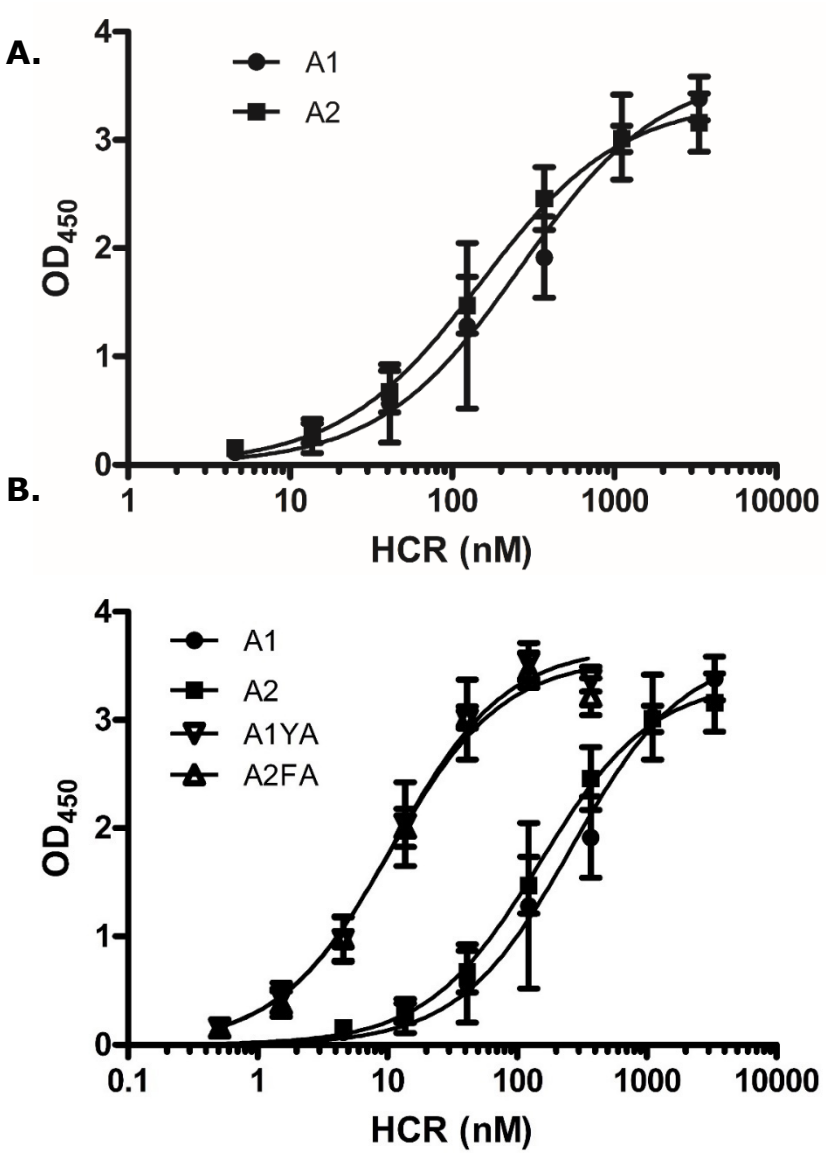

Figure 20. Binding of HCR/A variants to ganglioside. (A) GT1b ganglioside was incubated with HCR/A1 (●), HCR/A2. (■) or (B) HCR/A1^{Y1117A} or HCRA2^{F1117A}. Ganglioside was incubated with indicated HCRs and assayed for binding as described in Chapter 2, Methods. All values represent the arithmetic mean ± SD of ≥4 independent experiments performed in duplicate. Data were plotted using GraphPad Prism version 5 (GraphPad Software Inc.)

Table 6. Binding affinities of BoNT/A HCRs

HCR	B_{50}
HCR/A1	263.5
HCR/A2	150.3
$HCR/A1^{S1275A}$	193.6
$HCR/A1^{Y1117F}$	243.7
$HCR/A1^{Y1117A}$	11.04*
$HCR/A2^{S1275A}$	243.4
$HCR/A2^{F1117Y}$	103.6
$HCR/A2^{F1117A}$	10.51*

Only values with a difference greater than 5 fold are considered significant. Significant values are marked with an asterisk (*).

It was decided to more fully address the role of Y1117 in binding to ganglioside. Mutational analysis revealed that ganglioside binding of HCR/A1^{Y1117F} and HCR/A2^{F1117Y} were largely unchanged, arguing against a major role for the tyrosine hydroxyl group in binding to Sia5 (**Table 6**). Indeed, replacement of tyrosine or phenylalanine with alanine resulted in a significant increase in affinity of HCR/A1 and HCR/A2 respectively for GT1b (**Figure 20B** and **Table 6**.).Similarly, replacement of S1275 – another residue predicted to form a hydrogen bond to GT1b – with alanine did not cause a significant change in affinity (**Table 6**).

3.4.4 HCR/A1^{Y1117A} and HCR/A2^{F1117A} increase efficiency of entry into cortical neurons

In order to determine if increased ganglioside binding efficiency *in vitro* resulted in more efficient cellular uptake, cortical neurons were treated with HCR/A1, HCR/A2, HCR/A1^{Y1117A}, and HCR/A2^{F1117A} under depolarizing conditions. Cells were subsequently fixed and internalized HCR was visualized by immunofluorescence microscopy. In agreement with previously published observations, uptake of HCR/A2 was more efficient than HCR/A1 at equivalent concentrations (**Figure 21B**).

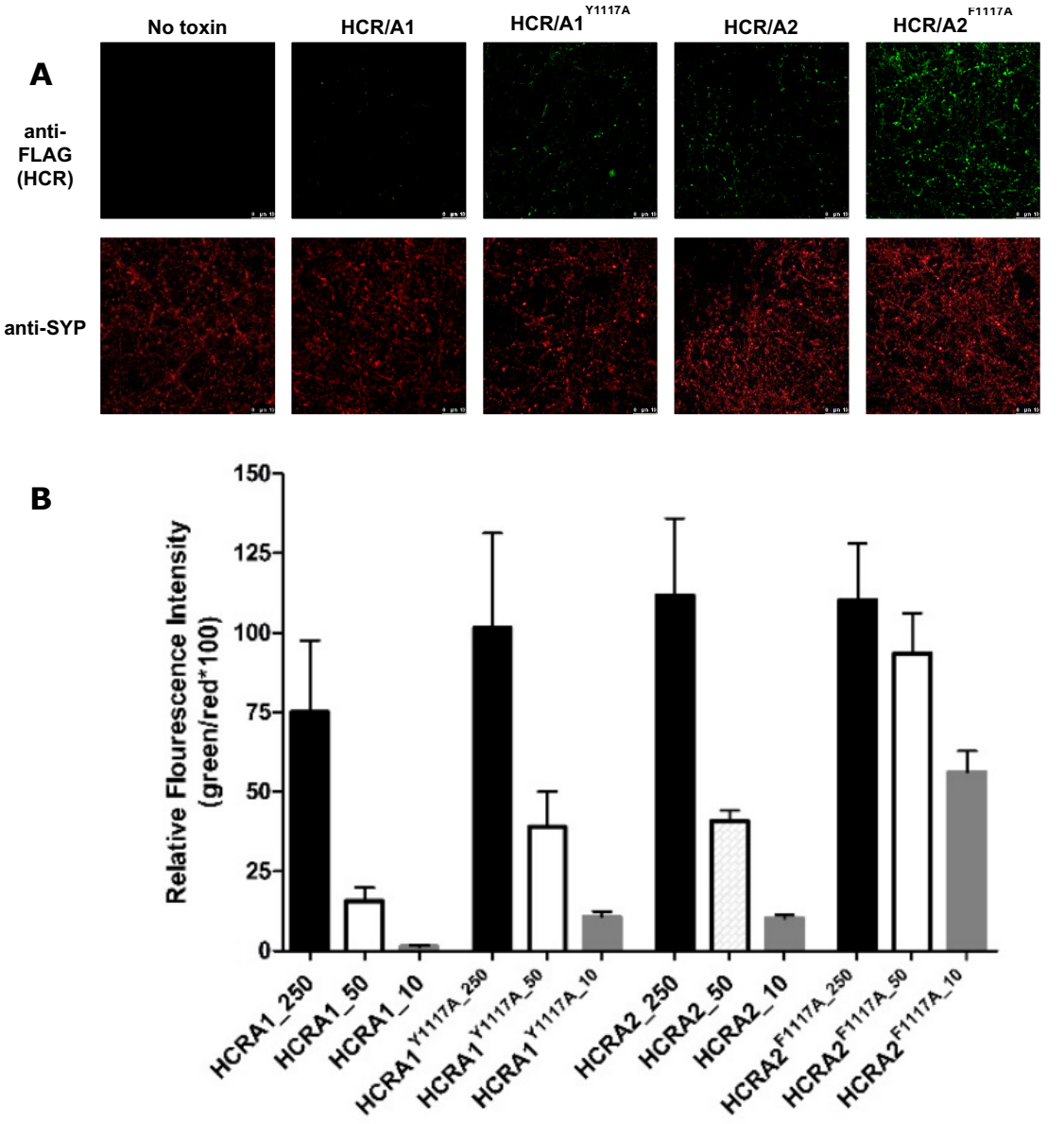

Figure 21. HCR/A1^{Y1117A} and HCR/A2^{F1117A} bind and enter neurons with higher efficiency. (A) Rat cortical neurons were incubated for 5 min at 37°C in high K+ buffer to stimulate vesicle recycling. Cells were then washed, fixed, and permeabilized as described in the Methods section. Internalized HCRs were stained using a mouse anti-FLAG antibody and an Alexa Fluor 488-conjugated goat anti-mouse secondary antibody and the integral synaptic vesicle membrane protein Synaptophysin (SYP) was stained using a rabbit anti-SYP antibody and an Alexa Fluor 568-conjugated goat anti-rabbit secondary antibody for determination of ICQ values (B) n=15 random fields, 2 biological repeats. Statistical analysis using one way ANOVA. P ≤0.001. See analysis (see Table 7).

Table 7. ANOVA Analysis and multiple comparisons for Figure 21B.

Number of families	1					
Number of comparisons per family	66					
Alpha	0.05					
Tukey's multiple comparisons test	Mean Diff.	95% CI of diff.	Significant?	Summary	Adjusted P Value	
HCRA1_250 vs. HCRA1_50	59.4	41.43 to 77.37	Yes	****	< 0.0001	A-B
HCRA1_250 vs. HCRA1_10	73.74	55.78 to 91.71	Yes	****	< 0.0001	A-C
HCRA1_250 vs. HCRA1Y1117A_250	-26.66	-44.63 to -8.695	Yes	***	0.0001	A-D
HCRA1_250 vs. HCRA1Y1117A_50	36.04	18.07 to 54.01	Yes	****	< 0.0001	A-E
HCRA1_250 vs. HCRA1Y1117A_10	64.37	46.41 to 82.34	Yes	****	< 0.0001	A-F
HCRA1_250 vs. HCRA2_250	-36.6	-54.57 to -18.64	Yes	****	< 0.0001	A-G
HCRA1_250 vs. HCRA2_50	34.36	16.40 to 52.33	Yes	****	< 0.0001	A-H
HCRA1_250 vs. HCRA2_10	64.95	46.98 to 82.92	Yes	****	< 0.0001	A-I
HCRA1_250 vs. HCRA2F1117A_250	-35.14	-53.10 to -17.17	Yes	****	< 0.0001	A-J
HCRA1_250 vs. HCRA2F1117A_50	-18.37	-36.33 to -0.4000	Yes	*	0.0402	A-K
HCRA1_250 vs. HCRA2F1117A_10	18.91	0.9440 to 36.88	Yes	*	0.0295	A-L
HCRA1_50 vs. HCRA1_10	14.34	-3.625 to 32.31	No	ns	0.2633	B-C
HCRA1_50 vs. HCRA1Y1117A_250	-86.06	-104.0 to -68.10	Yes	****	< 0.0001	B-D
HCRA1_50 vs. HCRA1Y1117A_50	-23.36	-41.33 to -5.395	Yes	**	0.0016	B-E
HCRA1_50 vs. HCRA1Y1117A_10	4.973	-12.99 to 22.94	No	ns	0.9989	B-F
HCRA1_50 vs. HCRA2_250	-96	-114.0 to -78.04	Yes	****	< 0.0001	B-G
HCRA1_50 vs. HCRA2_50	-25.04	-43.00 to -7.071	Yes	***	0.0005	B-H
HCRA1_50 vs. HCRA2_10	5.55	-12.42 to 23.52	No	ns	0.997	B-I
HCRA1_50 vs. HCRA2F1117A_250	-94.54	-112.5 to -76.57	Yes	****	< 0.0001	B-J
HCRA1_50 vs. HCRA2F1117A_50	-77.77	-95.73 to -59.80	Yes	****	< 0.0001	B-K
HCRA1_50 vs. HCRA2F1117A_10	-40.49	-58.46 to -22.52	Yes	****	< 0.0001	B-L
HCRA1_10 vs. HCRA1Y1117A_250	-100.4	-118.4 to -82.44	Yes	****	< 0.0001	C-D
HCRA1_10 vs. HCRA1Y1117A_50	-37.7	-55.67 to -19.74	Yes	****	< 0.0001	C-E

HCRA1_10 vs. HCRA1Y1117A_10	-9.368	-27.33 to 8.599	No	ns	0.8526	C-F
HCRA1_10 vs. HCRA2_250	-110.3	-128.3 to -92.38	Yes	****	< 0.0001	C-G
HCRA1_10 vs. HCRA2_50	-39.38	-57.35 to -21.41	Yes	****	< 0.0001	C-H
HCRA1_10 vs. HCRA2_10	-8.791	-26.76 to 9.175	No	ns	0.8987	C-I
HCRA1_10 vs. HCRA2F1117A_250	-108.9	-126.8 to -90.91	Yes	****	< 0.0001	C-J
HCRA1_10 vs. HCRA2F1117A_50	-92.11	-110.1 to -74.14	Yes	****	< 0.0001	C-K
HCRA1_10 vs. HCRA2F1117A_10	-54.83	-72.80 to -36.86	Yes	****	< 0.0001	C-L
HCRA1Y1117A_250 vs. HCRA1Y1117A_50	62.7	44.73 to 80.67	Yes	****	< 0.0001	D-E
HCRA1Y1117A_250 vs. HCRA1Y1117A_10	91.04	73.07 to 109.0	Yes	****	< 0.0001	D-F
HCRA1Y1117A_250 vs. HCRA2_250	-9.94	-27.91 to 8.027	No	ns	0.797	D-G
HCRA1Y1117A_250 vs. HCRA2_50	61.02	43.06 to 78.99	Yes	****	< 0.0001	D-H
HCRA1Y1117A_250 vs. HCRA2_10	91.61	73.65 to 109.6	Yes	****	< 0.0001	D-I
HCRA1Y1117A_250 vs. HCRA2F1117A_250	-8.475	-26.44 to 9.491	No	ns	0.9195	D-J
HCRA1Y1117A_250 vs. HCRA2F1117A_50	8.295	-9.671 to 26.26	No	ns	0.93	D-K
HCRA1Y1117A_250 vs. HCRA2F1117A_10	45.57	27.61 to 63.54	Yes	****	< 0.0001	D-L
HCRA1Y1117A_50 vs. HCRA1Y1117A_10	28.33	10.37 to 46.30	Yes	****	< 0.0001	E-F
HCRA1Y1117A_50 vs. HCRA2_250	-72.64	-90.61 to -54.67	Yes	****	< 0.0001	E-G
HCRA1Y1117A_50 vs. HCRA2_50	-1.677	-19.64 to 16.29	No	ns	> 0.9999	E-H
HCRA1Y1117A_50 vs. HCRA2_10	28.91	10.94 to 46.88	Yes	****	< 0.0001	E-I
HCRA1Y1117A_50 vs. HCRA2F1117A_250	-71.18	-89.14 to -53.21	Yes	****	< 0.0001	E-J
HCRA1Y1117A_50 vs. HCRA2F1117A_50	-54.41	-72.37 to -36.44	Yes	****	< 0.0001	E-K
HCRA1Y1117A_50 vs. HCRA2F1117A_10	-17.13	-35.10 to 0.8380	No	ns	0.0774	E-L
HCRA1Y1117A_10 vs. HCRA2_250	-101	-118.9 to -83.01	Yes	****	< 0.0001	F-G
HCRA1Y1117A_10 vs. HCRA2_50	-30.01	-47.98 to -12.04	Yes	****	< 0.0001	F-H
HCRA1Y1117A_10 vs. HCRA2_10	0.5767	-17.39 to 18.54	No	ns	> 0.9999	F-I
HCRA1Y1117A_10 vs. HCRA2F1117A_250	-99.51	-117.5 to -81.54	Yes	****	< 0.0001	F-J
HCRA1Y1117A_10 vs. HCRA2F1117A_50	-82.74	-100.7 to -64.77	Yes	****	< 0.0001	F-K
HCRA1Y1117A_10 vs. HCRA2F1117A_10	-45.46	-63.43 to -27.50	Yes	****	< 0.0001	F-L
HCRA2_250 vs. HCRA2_50	70.96	53.00 to 88.93	Yes	****	< 0.0001	G-H
HCRA2_250 vs. HCRA2_10	101.6	83.59 to 119.5	Yes	****	< 0.0001	G-I
HCRA2_250 vs. HCRA2F1117A_250	1.465	-16.50 to 19.43	No	ns	> 0.9999	G-J
HCRA2_250 vs. HCRA2F1117A_50	18.24	0.2686 to 36.20	Yes	*	0.0432	G-K

HCRA2_250 vs. HCRA2F1117A_10	55.51	37.55 to 73.48	Yes	****	< 0.0001	G-L
HCRA2_50 vs. HCRA2_10	30.59	12.62 to 48.55	Yes	****	< 0.0001	H-I
HCRA2_50 vs. HCRA2F1117A_250	-69.5	-87.47 to -51.53	Yes	****	< 0.0001	H-J
HCRA2_50 vs. HCRA2F1117A_50	-52.73	-70.70 to -34.76	Yes	****	< 0.0001	H-K
HCRA2_50 vs. HCRA2F1117A_10	-15.45	-33.42 to 2.515	No	ns	0.169	H-L
HCRA2_10 vs. HCRA2F1117A_250	-100.1	-118.1 to -82.12	Yes	****	< 0.0001	I-J
HCRA2_10 vs. HCRA2F1117A_50	-83.32	-101.3 to -65.35	Yes	****	< 0.0001	I-K
HCRA2_10 vs. HCRA2F1117A_10	-46.04	-64.01 to -28.07	Yes	****	< 0.0001	I-L
HCRA2F1117A_250 vs. HCRA2F1117A_50	16.77	-1.196 to 34.74	No	ns	0.0924	J-K
HCRA2F1117A_250 vs. HCRA2F1117A_10	54.05	36.08 to 72.01	Yes	****	< 0.0001	J-L
HCRA2F1117A_50 vs. HCRA2F1117A_10	37.28	19.31 to 55.24	Yes	****	< 0.0001	K-L

However, the differences in uptake could be negated by incubation of cells with high concentrations (1 μM) of both proteins (**data not shown**). Binding to neurons was dose dependent for all HCRs and HCR variants tested. When compared to parental HCRs, HCR/A1^{Y1117A} and HCR/A2^{F1117A} were able bind and enter neurons with higher efficiency, consistent with the *in vitro* binding assay (**Figure 21** and statistical analysis on **Table 7**. HCR/A2^{F1117A} was able to bind and enter cells more efficiently than all other proteins tested including HCR/A1, and HCR/A2. At increased doses however, the efficiency of entry is similar.

3.5 Discussion and Future directions

3.5.1 Discussion

Accumulating evidence suggests BoNT/A2 is more is more toxic and has higher relative activity than BoNT/A1. One reason for the higher toxicity of BoNT/A2 may be the higher efficiency of entry. BoNT/A2 has been shown to bind and enter both human and rodent derived neuronal cells with higher efficiency than BoNT/A1. Although highly conserved, BoNT/A1 and BoNT/A2 may not interact with the Sia5 sugar in the same manner. Stevens *et al* reported a structural discrepancy between the position of BoNT/A1^{Y1117} in the apostructure of BoNT/A1 and the BoNT/A1 HCR co-crystal with GT1b

oligosaccharide. In HCR co-crystal, Y1117 was rotated 25º and shifted 1.7 Å in order to demonstrate ganglioside coordination with Sia5 as predicted in the apostructure. This work suggests BoNT/A1^{Y1117} and the equivalent residue, BoNT/A2^{F1117} are inhibitory to ganglioside binding and do not directly interact with the Sia5 sugar. Replacing the phenylalanine rings may allow the GA1 core to pack tighter against the conserved residues increasing affinity for ganglioside GT1b (**Figure 20**). However, when HCR/A1^{Y1117A} and HCR/A2^{F1117A} were tested for relative affinity for GM1a, no binding was seen indicating suggesting Sia5 was still required.

Improving our understanding of the mechanism of BoNT/A1 and BoNT/A2 binding will enhance our overall understanding of the CNT entry and intoxication process. In addition, increased use of CNTs as therapeutics has caused development of antibody resistance. Development of a class of BoNTs with increased toxicity would lower the EC_{50} and decrease the chance of antibody mediated immune response.

3.5.2 Future directions: Development of a heterologous reporter assay to assess the effects of point mutations on toxicity

BoNTs are categorized as Tier 1 Category "A" Select Agents by the CDC. As a result, the production and use of recombinant, catalytically active toxin is highly regulated. It is therefore not practical to assess the effects of individual point mutations on toxicity in a catalytically active background. Therefore, we decided to take advantage of the exclusion from Select Agent regulation of BoNT/A which contains three point mutations within the light chain that prevent zinc coordination, rendering the protein non-toxic [157]. Recently, βlac-TeNT(RY), a catalytic inactive variant of TeNT modified with an N-terminal β-lactamase reporter domain was utilized to measure LC translocation by detecting β-lactamase dependent cleavage of the FRET reporter substrate CCF2-AM [41]. Using catalytically inactive forms of BoNT/A1 and A2, β-lactamase reporter proteins (TEM-Bla_BoNT/A) were generated to test whether mutations which increase cellular uptake result in increased toxicity. After purification of recombinant toxins, an *in vitro* assay was carried out to verify the activity of β-lactamase utilizing the chromogenic cephalosporin nitrocefin (Sigma). The enzyme was found to be highly active, indicating expression and purification did not inhibit β-lactamase function (**Figure 22)**

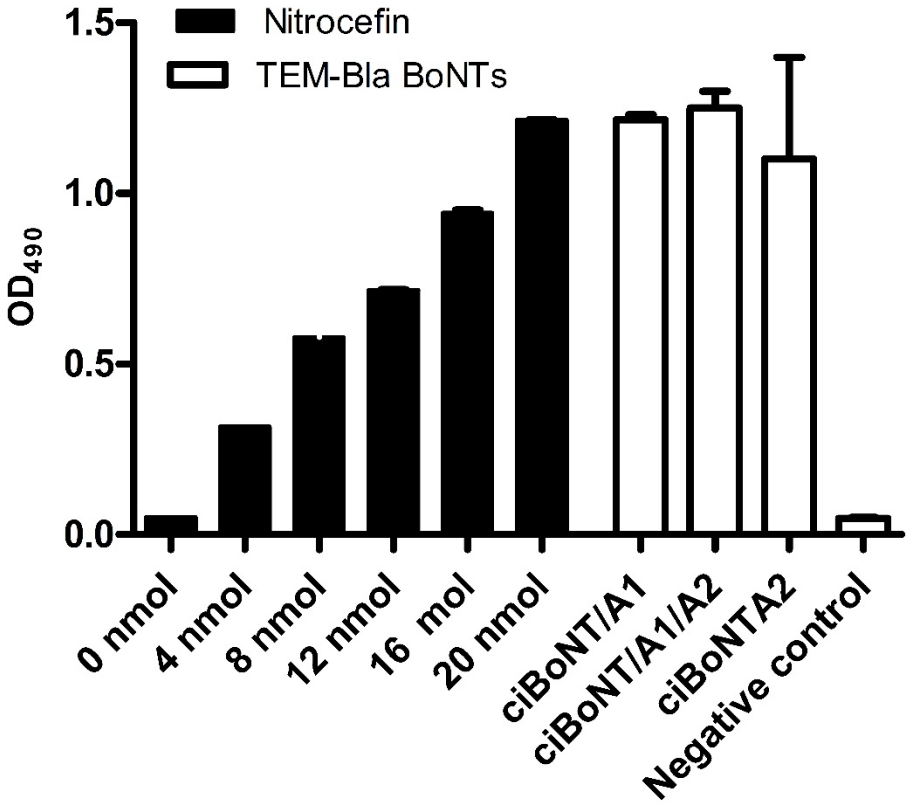

Figure 22. Validation of TEM_BLA reporter. An *in vitro* assay utilizing the chromogenic cephalosporin substrate nitrocefin. and 10 nm TEM BLA ciBoNT fusions showed high activity compared to nitrocefin controls and TEM BLA ciBoNT catalytic null. Data represents. Values represent the arithmetic mean± SD of 2 independent experiments.

To assess TEM-Bla_BoNT/A1 and A2 function in cells, rat cortical neurons were incubated toxins for 3 hours to allow uptake and translocation, and then loaded with CCF4-AM. Cells were subsequently analyzed by flow cytometry to determine the ratio of green to blue cells. In theory, delivery of the lactamase into the neuronal cytosol will result in cleavage of CCF4, causing the cell to change color from green to blue.

Regrettably, under numerous experimental conditions, we have not yet been able to generate a population of cells with detectable translocated lactamase. We have consistently observed a pattern of green cells (75-80%) with a small population of double positive cells (4-10%) (**Figure 23**). We have generated and increased a percentage of double positive cells, but as yet, have not detected a significant population of blue cells. It is unclear at this time whether the double positive cell population represents "noise", or cells in which only a small percentage of the CCF4 substrate has been cleaved. While we are not currently able to explain why the assay is not working, one possible explanation might be linked to the localization of the BoNT/A LC within neurons.

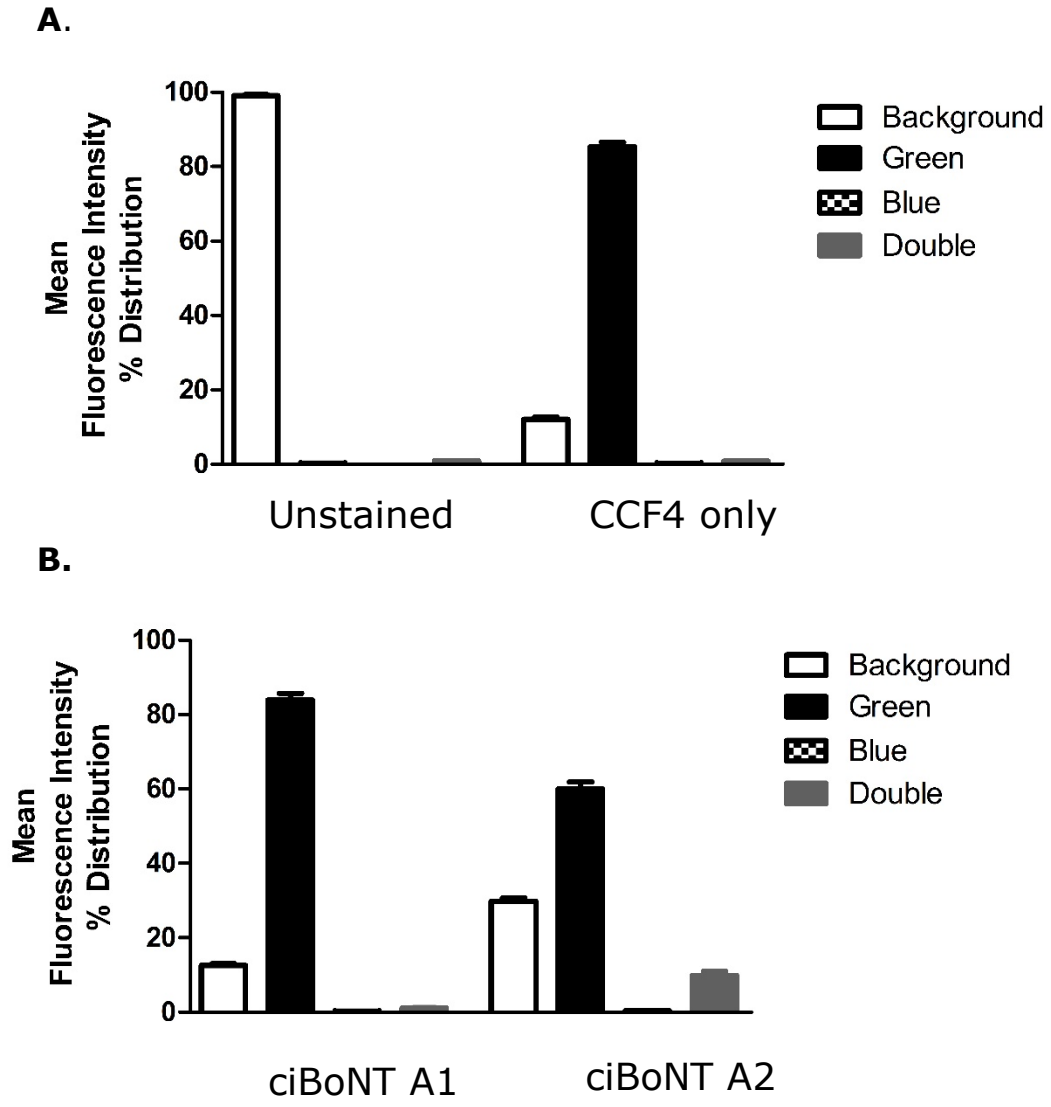

Figure 23. Heterologous LC Translocation Assay. (A) Untreated neurons or neurons exposed to CCF4-AM only. (B) Neurons treated with TEM-BLA A1 or TEM BLA A2 and exposed to CCF4 AM substrate were excited at 405 nm. Emission was taken at 455 nm and at 525 nm and 100,000 cells were counted. n=2 biological repeats. % distribution is shown.

Previous work by Fernández-Salas and colleagues demonstrated that the LC of BoNT/A, but not BoNT/B or BoNT/E, is specifically localized to the plasma membrane [77, 158]. A subsequent study confirmed and extended these observations by showing that the LC of Tetanus toxin is also cytoplasmic [76]. Moreover, they demonstrated that removal of the first 8-17 N-terminal amino acids in LC/A resulted in loss of plasma membrane binding. The observation that Tetanus LC localizes to the cytoplasm while BoNT/A LC localizes to the membrane suggests this could alter the function of the lactamase. To test this possibility a construct lacking the first 10 amino acids was generated (TEM-Bla_BoNT/A$^{\Delta 1\text{-}10}$). However, upon purification little or no full length product was isolated, suggesting the deletion may have destabilized the protein. An alternative to the Δ1-10 deletion construct is to mutate two lysine residues (K6 and K11) previously shown to be involved in membrane binding [76]. Given that the mutated LC/A protein has been previously expressed and purified from *E. coli*, we do not anticipate problems in the expression and purification of the mutated TEM-Bla_BoNT/A protein. If additional problems in expression and purification do arise and are not able to be resolved, the proteins could be expressed and purified from *Bacillus megaterium,* an alternative expression system used in the lab to express large proteins (>150 kDa) more effectively than *E. coli*. In the event that we are

unable to generate a functional reporter assay, catalytically active forms of the toxin will be assessed in the laboratory of Dr. Eric Johnson, University of Wisconsin, under Select Agent regulation.

CHAPTER 4: TETANUS NEUROTOXIN UTILIZES TWO SEQUENTIAL MEMBRANE INTERACTIONS FOR CHANNEL FORMATION

As found in: Joshua R Burns and Michael Baldwin. Tetanus Neurotoxin Utilizes Two Sequential Membrane Interactions for Channel Formation. *The Journal of Biological Chemistry*. 2014;289(32):22450-22458.

4.1 Abstract

Tetanus neurotoxin (TeNT) causes neuroparalytic disease by entering the neuronal soma to block the release of neurotransmitters. Yet, the mechanism by which TeNT translocates its enzymatic domain (light chain, LC) across endosomal membranes remains unclear. We found that TeNT - and a truncated protein devoid of the receptor binding domain (TeNT-LH_N) - associated with membranes enriched in acidic phospholipids in a pH-dependent manner. Thus, in contrast to diphtheria toxin the formation of a membrane-competent state of TeNT requires the membrane interface and is modulated by the bilayer composition. Channel formation is further enhanced by tethering of TeNT to the membrane through ganglioside co-receptors prior to acidification. Thus, TeNT channel formation can be resolved into two sequential steps: (1) interaction of the receptor binding domain (HCR) with ganglioside co-

receptors to orient the translocation domain (HCT) as the lumen of the endosome is acidified and (2) low pH, in conjunction with acidic lipids within the membrane drives the conformational changes in TeNT necessary for channel formation.

4.2 Introduction

Numerous bacterial pathogens produce toxins which enter into the cytosol of mammalian cells and disrupt normal cellular function. Many of these toxins are referred to as A-B toxins because of their structural and functional organization [159]. The B (binding) moiety, composed of one or more subunits, binds to a cell surface receptor and facilitates delivery of the A (active) moiety into the cytosol where it enzymatically modifies a cellular target. In a subset of A-B toxins, the B domain has the ability to undergo a series of structural changes that allows integration into lipid membranes and formation of a protein conducting channel through which the A domain may be delivered. What drives the structural changes within the B moiety and how polypeptides are translocated across membranes are fundamental questions yet to be fully resolved for any A-B toxin.

The clostridial neurotoxins (CNTs) are a family of bacterial A-B toxins which are among the most lethal natural agents known to humans [9, 160]. Nine CNTs have been described to date: tetanus

neurotoxin (TeNT) produced by *Clostridium tetani*, and eight botulinum neurotoxins (BoNTs, serotypes A-H) produced by strains of *Clostridium botulinum*, *C. butyricum*, and *C. baratii* [13, 136, 161, 162]. CNTs are synthesized as single chain polypeptides with a molecular mass of ~150 kDa. The precursor is subsequently proteolytically cleaved into an ~50-kDa light chain (LC, A subunit) and an ~100 kDa heavy chain (HC, B subunit) linked by an essential interchain disulfide bond [26]. HC contains an ~50 kDa N-terminal translocation domain (HCT) and an ~50 kDa C-terminal receptor binding domain (HCR) [163]. The HCT facilitates translocation of the LC into the neuronal cytosol while the HCR binds neuronal co-receptors [54-56, 103, 153, 164-168].

How CNTs are able to convert from fully folded water-soluble proteins into membrane integrated protein translocating channels remains unclear. Traditionally low pH was proposed to trigger the translocation process, presumably by promoting structural changes facilitating the insertion of the HCT domain into the membrane bilayer. However, the recent demonstration that the isolated HCT domain of BoNT/A can form ion conducting channels in the absence of a transmembrane pH gradient brings this model into question [35, 60]. Rather, it appears that low pH serves to: (i) relieve the inhibition of the translocation process mediated by the HCR domain and (ii) facilitate the partial unfolding of the LC into a conformation necessary for passage through

the translocation channel [169, 170]. The presence of reductant and neutral pH in the cytosol promotes release of the LC from the HC after completion of translocation. While our understanding of the translocation process has grown in recent years, the precise molecular mechanisms driving the conversion of the water-soluble form into the membrane integrated form of TeNT remain to be determined.

In the present study, we investigated mechanisms leading to formation of membrane channels using a combination of full-length TeNT and variants defective in the ability to bind ganglioside co-receptors. Here we demonstrate that ganglioside binding enhances the rate of channel formation, presumably by tethering TeNT close to the target membrane. Furthermore, we demonstrate that membrane association is moderated by the presence of acidic phospholipids, suggesting the transition from a water-soluble protein into a translocase channel occurs close to the membrane interface. Based on our observations, we propose a sequential two-step model for TeNT channel formation that differs from the mechanisms employed by diphtheria and anthrax toxins, the current paradigms for cell entry of bacterial toxins.

4.3 Experimental procedures

4.3.1 Reagents

Molecular biology grade reagents were purchased from either Fisher Scientific (Houston, TX) or Sigma-Aldrich Company (St. Louis, MO). *Escherichia coli* optimized DNA encoding TeNT residues 1-1315 was synthesized by EZBiolab (Carmel, IN). Gangliosides, cholesterol and the following phospholipids were purchased from Avanti Polar Lipids (Alabaster, AL): 1-palmitoyl-2-oleoyl-*sn*-glycero-3-phosphocholine (POPC), 1-palmitoyl-2-oleoyl-*sn*-glycero-3-phosphoethanolamine (POPE), L-α-phosphatidylserine (Porcine brain), and L-α-phosphatidylcholine soy 20% (asolectin).

4.3.2 Tetanus neurotoxin expression and purification

DNA encoding TeNT was cloned into the pET28a expression vector (Merck KGaA, Darmstadt, Germany) using appropriate restriction endonuclease sites resulting in an N-terminal His-tag fusion protein. To generate a catalytically inactive form of TeNT, two point mutations within the light chain (R372A and Y375F) were generated using the Quikchange II site-directed mutagenesis kit (Agilent). Proteins were expressed in *E. coli* BL-21 AI cells and purified as previously described [47, 111]. Peak fractions from the Sephacryl S-200 column were concentrated using an Amicon filtration device (YM-100 type filter), dialyzed into 10 mM HEPES-NaOH, 250 mM NaCl, pH

7.4 and stored at -80ºC until use. A typical preparation yielded 3-5 mg of purified toxin / liter of batch culture.

4.3.3 Cloning and expression of TeNT LH_N construct

DNA encoding TeNT amino acids 1-864 was amplified by PCR and cloned into the pET-28a expression vector using appropriate restriction endonuclease sites to generate an N-terminal His-tag fusion protein. Protein was expressed in *E. coli* BL-21 AI cells and purified as described for TeNT.

4.3.4 Trypsinization of TeNT proteins

Trypsin agarose (500 µl) was washed three times in phosphate buffered saline (PBS) prior to incubation with 2 mg TeNT or TeNT variants for 60 min at 4ºC. Proteins were separated from agarose beads by gentle centrifugation and a sample resolved by SDS-PAGE. SDS-PAGE analysis of trypsinized proteins in the presence or absence of reducing agent confirmed the proteins were converted to di-chain molecules of the anticipated sizes (data not shown).

4.3.5 Intoxication of rat cortical neurons with TeNT

Rat E18 cortical neurons (Brainbits, LLC, Springfield, Il) were cultured on poly-d-lysine coated glass coverslips in Neurobasal

medium supplemented with 0.5 mM Glutamax, Primocin, and B27 supplement for 10−14 days prior to use. Cells were treated with TeNT or TeNT variants at the indicated concentrations for 24 hours at 37ºC. In some experiments, cells were pre-treated for 1 hour with either 100 nM Bafilomycin A1 or solvent (DMSO) prior to addition of the toxins. Following treatment, cells were washed three times in Hanks balanced salt solution (HBSS), lysed with RIPA (radio immunoprecipitation assay) buffer at 4°C for 30 min and clarified by centrifugation at 20,000×*g*. Lysates were boiled in SDS-PAGE sample buffer, resolved on 13.5% w/v SDS-PAGE gels, transferred to Immobilon PVDF membranes, and subjected to Western blotting using antibodies against VAMP2 (1:5000, clone 69.1, Synaptic Systems, Germany), beta-actin (1:1000, mAbcam 8226, Abcam, Cambridge, MA) and goat anti-mouse HRP (1:100,000, Pierce). The membranes were washed, incubated with SuperSignal Dura (Pierce), and visualized using a CCD imaging system.

4.3.6 Circular dichroism

An AVIV model 202 far UV spectrometer was used to collect spectra (196 nm to 265 nm) of TeNT or TeNT variants (2 μM) obtained at pH 7.4 (10 mM HEPES-NaOH, 15 mM NaCl, 0.1 mM EDTA) and pH 4.0 (10 mM sodium acetate-acetic acid, 15 mM NaCl, 0.1 mM EDTA) at

42ºC using 1 mm pathlength quartz cuvettes. Gangliosides were added to a final concentration of 30 μM unless otherwise indicated and samples were re-scanned. A spectrum of buffer alone or buffer + gangliosides were subtracted from the appropriate data sets. Data analysis was carried out using CDPro software [171].

4.3.7 Triton X-114 partitioning

Triton X-114 partitioning assays were performed as described previously [172]. For pH 7.4 samples, buffer containing 10 mM HEPES-NaOH, 150 mM NaCl and 1 mM EDTA was used (hereafter referred to as neutral buffer). For samples at pH 6.5, 6.0, and 5.5, HEPES was replaced with 10 mM MES-NaOH and for pH 5.0 and 4.0, HEPES was replaced with 10 mM sodium acetate-acetic acid. Final concentrations were 600 nM for TeNT or TeNT variants and 113 μM ganglioside. After partitioning, the aqueous and detergent phases of each sample were collected and resolved on 8% w/v SDS-PAGE gels, visualized by silver staining and quantified by densitometry.

4.3.8 Liposome preparation

Liposomes were freshly prepared by the freeze-thaw and extrusion method as described previously [173]. Briefly, lipids (40 μmol total) dissolved in chloroform were mixed in the indicated ratios

(within Figure legends), dried under a gentle stream of nitrogen, and placed under vacuum overnight to remove residual solvent. The dried lipid cake was hydrated in potassium buffer (10 mM HEPES-KOH, 150 mM KCl, 1 mM EDTA, pH 7.4) to a final concentration of 40 mM by brief sonication at 55ºC. The rehydrated lipid was then subjected to three cycles of rapid freeze-thaw, followed by extrusion through a 200 nm pore membrane (Nucleopore) using a mini-extruder apparatus (Avanti Polar Lipids). Immediately prior to use, liposomes were exchanged into neutral buffer by passage over a pre-equilibrated column of G-25 sephadex.

4.3.9 Association and proteoliposome isolation

Liposomes (100 µl) were combined with 10 µg TeNT or TeNT variants in 500 µl neutral buffer or low pH buffer (10 mM sodium acetate-acetic acid, 150 mM NaCl, 1 mM EDTA, pH 4.0). Liposomes were isolated by centrifugation at 100,000 ×*g* for 30 minutes at 4ºC. Supernatants containing unbound proteins were recovered and held on ice for further analysis. Liposomes were suspended in 500 µl fresh neutral or low pH buffer and recovered by centrifugation as above. Supernatants (Wash fractions) were collected, and along with those from the first centrifugation step, concentrated to ~50 µl using Microcon centrifugal filter devices. Liposomes were suspended in 50 µl

neutral buffer and all fractions mixed with an equal volume of SDS-PAGE buffer. Volume equivalents of each fraction were resolved on SDS-PAGE gels and visualized by staining with Coomassie Blue dye.

4.3.10 K^+ Release assay

Liposomes (100 µl) were diluted into 5 ml neutral- or low pH-buffer with constant stirring and allowed to equilibrate for 1-5 minutes. TeNT or TeNT variants (2.5 nmol) were then added to the solution and potassium ion release monitored using a potassium selective electrode (Orion, ThermoFisher Scientific, Houston, TX). After 5 min 0.01 M KCl was added to the solution to ensure the electrode was functioning as expected. Specific K^+ release was determined by subtraction of basal release values obtained from liposomes incubated in buffer alone.

4.3.11 Statistical analysis

Densitometric analysis was performed using Protein Simple AlphaView 3.0 software (Santa Clara, CA). Data were analyzed using GraphPad Prism, version 6.0 (La Jolla, CA). One-way ANOVA with Student-Newman-Keuls post-test was performed to determine the difference between means after treatment. Two-way ANOVA with Bonferroni post-test was used to determine the difference between pH

and treatments and the possible interactions of each. Differences were considered significant at $p < 0.05$.

4.4 Results

4.4.1 Functional Entry of Recombinant Tetanus Toxin and Protein Variants into Cortical Neurons

The mechanism by which the LC protease of tetanus neurotoxin (TeNT) is translocated across the endosomal membrane is currently unresolved. To investigate this mechanism further, a series of TeNT variants were constructed (**Figure 24A**) and validated by monitoring their ability to enter primary cortical neurons. Exposure of neurons to recombinant TeNT resulted in efficient cleavage of the physiologic substrate VAMP2 after 24 hours as determined by Western blotting (**Figure 24B**). To determine whether the receptor binding domain of TeNT is essential for intoxication, a protein variant composed only of the LC and HCT domains was generated (**Figure 24A**).

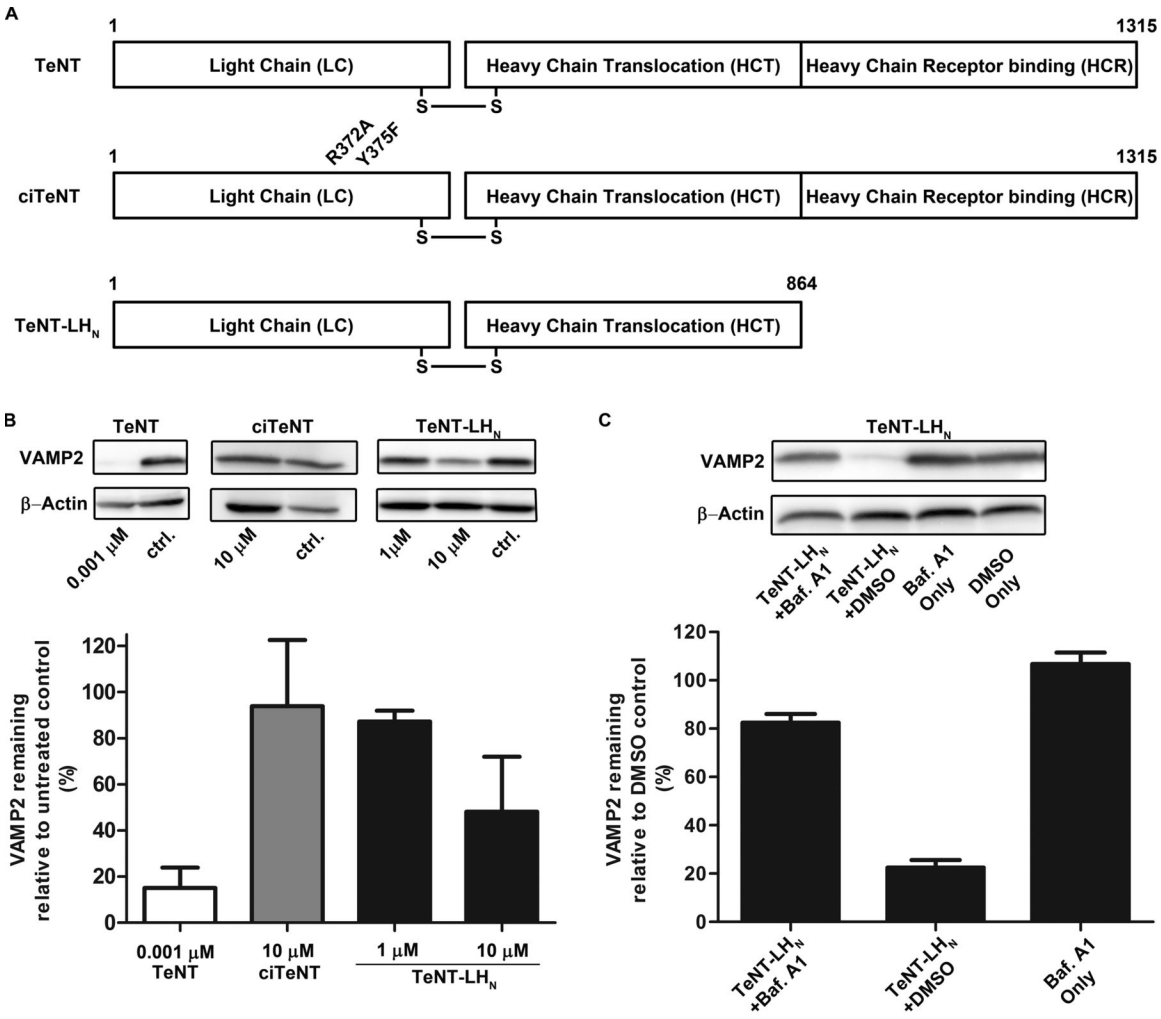

Figure 24. TeNT cleavage of VAMP2 in rat cortical neurons. *A*, schematic representation of TeNT, ciTeNT, and TeNT-LH_N showing domain organization. The disulfide bond between the LC and the HC in the mature toxin is indicated by *S-S. B*, rat cortical neurons (10–14 days *in vitro*) were incubated for 24 h with the indicated concentrations of TeNT (*white bar*), ciTeNT (*gray bar*), or TeNT-LH_N (*black bar*). VAMP2 cleavage was visualized by Western blotting using a mouse α-VAMP2 antibody, which recognizes only uncleaved VAMP2. VAMP2 levels were normalized to β-actin controls and then expressed as a percentage relative to untreated control cells ± S.E. (*error bars*) (≥3 individual experiments). *C*, rat cortical neurons were incubated for 1 h with either bafilomycin A1 or solvent (DMSO) prior to the addition of TeNT-LH_N. VAMP2 cleavage was visualized and quantified as described above.

When applied to cells this variant, hereafter named TeNT-LH_N, was able to enter cells and cleave VAMP2; however, a significantly higher concentration was needed relative to the full length toxin. Thus, similar to other A-B type toxins the receptor binding domain of TeNT is not essential for toxicity. Finally, a recombinant, full-length tetanus toxin was engineered with two point mutations within the light chain (R372A and Y375F). Arg372 and Tyr375 are conserved across all CNT family members and are known to contribute to catalysis by facilitating correct alignment of conserved histidine and glutamate residues for the Zn coordination sphere [78, 174, 175]. Treatment of cells with a 10,000-fold higher concentration of the catalytic inactive form of toxin (termed ciTeNT) also failed to cleave VAMP2 (**Figure 24B**). This is consistent with the recent study of Blum *et al* [176] which showed that mice injected with 5 µg of a protein containing the same two mutations (R372A, Y375F, equivalent to ~125,000 lethal doses) did not develop any signs of disease. Thus, ciTeNT was substituted for wild type protein in the remaining assays to maximize safety. To further validate the use of TeNT-LH_N as a tool to study translocation, the requirement for passage through an acidified compartment was investigated. In agreement with previous studies, the activity of recombinant TeNT was inhibited by the vacuolar proton pump inhibitor Bafilomycin A1 [177]. TeNT-LH_N was also inhibited by Bafilomycin A1,

indicating that translocation of the light chain by TeNT-LH_N was still dependent on exposure to an acidified environment (**Figure 24C**).

4.4.2 TeNT Undergoes Secondary Structural Changes in the Presence of Polysialogangliosides at Low pH

Recent studies demonstrated that interaction of ganglioside GT1b with BoNT/B and BoNT/E triggers conformational changes within the two proteins that facilitates transformation into hydrophobic proteins at low pH [178, 179]. To test whether gangliosides trigger a similar conformational change in TeNT, CD spectroscopy was performed at neutral and acidic pH in the absence and presence of GT1b. At neutral pH, the far-UV CD spectra (196-265 nm) of TeNT with or without the addition of GT1b overlapped extensively and the helical content was estimated at 18.4% and 19.6% respectively (**Figure 25A** and **Table 8**). Reducing the pH to 4.0 had little effect on the CD spectrum of TeNT, indicating the protein secondary structure remains largely unchanged. By comparison, addition of GT1b at low pH caused a dramatic shift in the CD spectrum, with a reduction in helical content to 7.8% and a marked increase in beta-strand content to 40.8%. The binding of several CNTs to gangliosides is mediated by a conserved binding pocket located within the receptor binding (HCR)

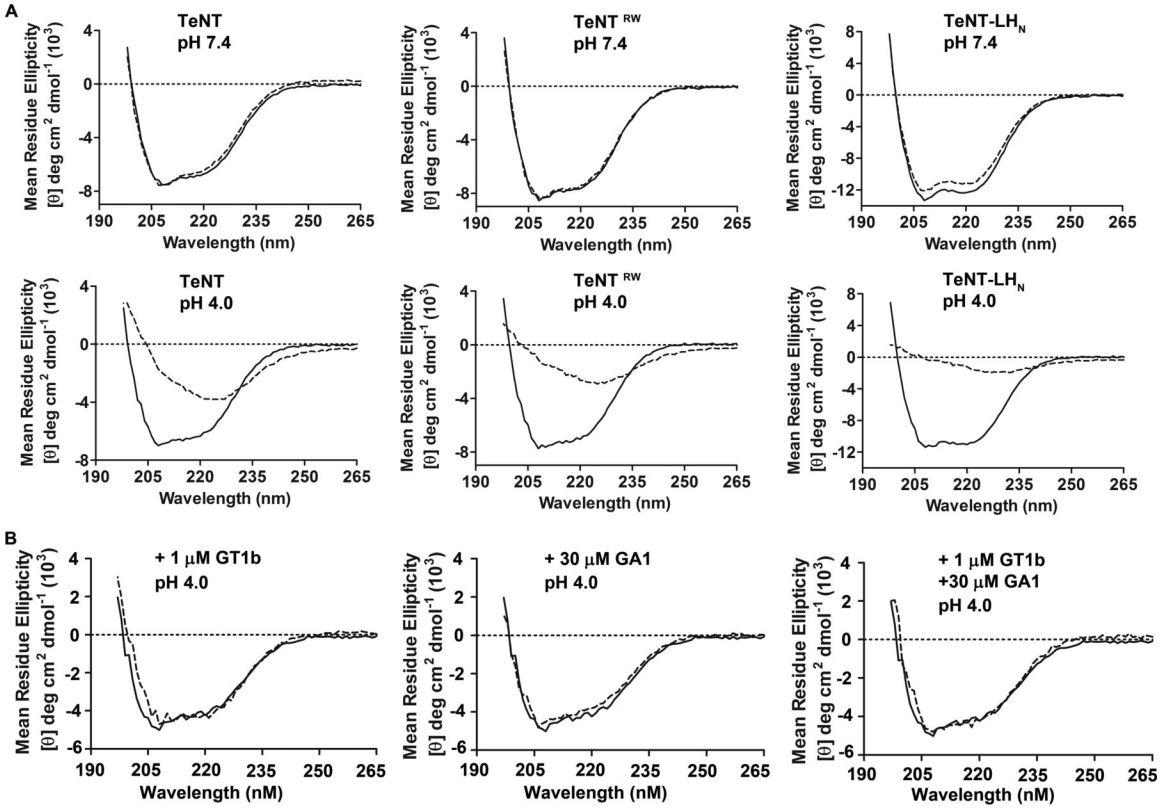

Figure 25. Polysialogangliosides induce changes in TeNT secondary structure at low pH. A, far-UV CD spectra of TeNT, TeNT^{RW}, and TeNT-LH$_N$ at pH 7.4 and 4.0 in the absence (solid lines) and presence (dashed lines) of 30 μm GT1b. B, far-UV CD spectra of TeNT at pH 4.0 in the absence (solid lines) or presence (dashed lines) of 1 μm GT1b, 30 μm GA1, or both.

Table 8. Far UV spectra values

	Secondary Structure			
	pH 7.4		pH 4.0	
Toxin	**Buffer only**	**Buffer + GT1b**	**Buffer only**	**Buffer + GT1b**
	%	%	%	%
TeNT	α = 19.6	α = 18.4	α = 17.9	α = 7.8
	β = 27.8	β = 27.9	β = 28.1	β = 40.8
$TeNT^{RW}$	α = 21.6	α = 21.1	α = 19.5	α = 6.5
	β = 25.6	β = 26.6	β = 27.9	β = 42.6
$TeNT\text{-}LH_N$	α = 36.9	α = 34.3	α = 32	α = 5
	β = 13.8	β = 14.5	β = 16.3	β = 45.7

Secondary structure analysis of far UV CD spectra as determined by CD-PRO software for TeNT and TeNT variants at pH 7.4 and 4.0

.

domain [47]. It was therefore anticipated that TeNT-LH_N, which lacks the HCR domain, would not undergo secondary structural changes at low pH in the presence of ganglioside. However, similar to full length TeNT, TeNT-LH_N shifted to a largely beta-strand dominated structure at low pH in the presence of ganglioside (**Figure 25A and Table 8**). It is therefore assumed that the conformational changes occurring in the LC and HCT domains of both proteins are largely the same. Finally, the CD spectra of a mutated TeNT protein deficient in the ability to bind gangliosides (previously termed $TeNT^{RW}$) [103, 111] were acquired. The CD spectra of $TeNT^{RW}$ at both neutral and acidic pH are similar to those obtained with the wild-type protein (**Figure 25 and Table 9**). This is consistent with data indicating that mutations at R1226 and W1289 have little effect on the tertiary structure of the HCR domain [102]. Only by addition of GT1b at low pH could a change in the secondary structure of $TeNT^{RW}$ be observed (Figure 23A). Furthermore, pH-triggered conformational changes in TeNT could also be observed by addition of alternative polysialogangliosides - GD3, GM1a, GD1a and GD1b - previously demonstrated to bind TeNT in a HCR-dependent manner (data not shown, [111]). These data strongly argue against a role for the HCR domain in detecting the presence of gangliosides at low pH. Next, the assay was performed using GT1b at concentrations below the reported critical micelle concentration (CMC $\sim 1 \times 10^{-5}$M,

[180]). Under these conditions, addition of GT1b did not promote a shift in the CD spectrum of TeNT (**Figure 25B**). This implied that. structural changes in TeNT might simply be a function of ganglioside micelle formation If this assertion was correct, then it follows that micelles formed from asialo-GM1a (GA1) should also stimulate a change in TeNT secondary structure, However, as shown in **Figure 25B**, addition of GA1 alone or as mixed micelles composed of GA1 and GT1b (30:1 molar ratio) did not result in secondary structure changes (**Figure 25B**). These observations suggest that both micelle formation and the presence of sialic acid(s) is necessary to drive conformational changes in TeNT at low pH.

4.4.3 TeNT Partitions into the Detergent Phase in Triton X-114 Partitioning Assays in the Presence of GT1b at Low pH

Triton X-114 phase partitioning is routinely exploited as a means of separating hydrophilic proteins from GPI-anchored-, acylated- and integral-membrane proteins [172]. Using this approach, the distribution of TeNT and TeNT-LH_N between the aqueous and detergent phases in the presence or absence of ganglioside at pH values ranging from 4.0 to 7.4 was investigated. In the absence of GT1b, TeNT was largely recovered in the aqueous phase. However, the addition of

ganglioside caused TeNT to transition from the aqueous to detergent phase only as the pH decreased below ~6.5 (**Figure 26A**). In comparison, the partitioning of TeNT-LH_N into the detergent phase was dependent on the addition of GT1b, but unaffected by the pH of the system (**Figure 26B**). This observation suggests the HCR domain may function in part to mask hydrophobic membrane binding regions until the toxin is exposed to a low pH environment.

4.4.4 TeNT Associates with Liposomal Membranes Enriched in Acidic Lipids

The ability of TeNT to bind to liposomal membranes as a function of pH was determined. Consistent with the reported binding data, treatment of base liposomes (zwitterionic) with TeNT or $TeNT^{RW}$ at either neutral or low pH resulted in a minor release of total K^+ content (**Figure 27B and 27C**). A similar level of release was also observed when base liposomes + PS (10 mol %) were exposed to TeNT or $TeNT^{RW}$ at neutral pH (**Figure 27B**). Initial experiments employing liposomes composed of zwitterionic lipids (base liposomes, PC: PE: Cholesterol, 45:45:10, mol %) did not result in detectable binding at either neutral or low pH (data not shown).

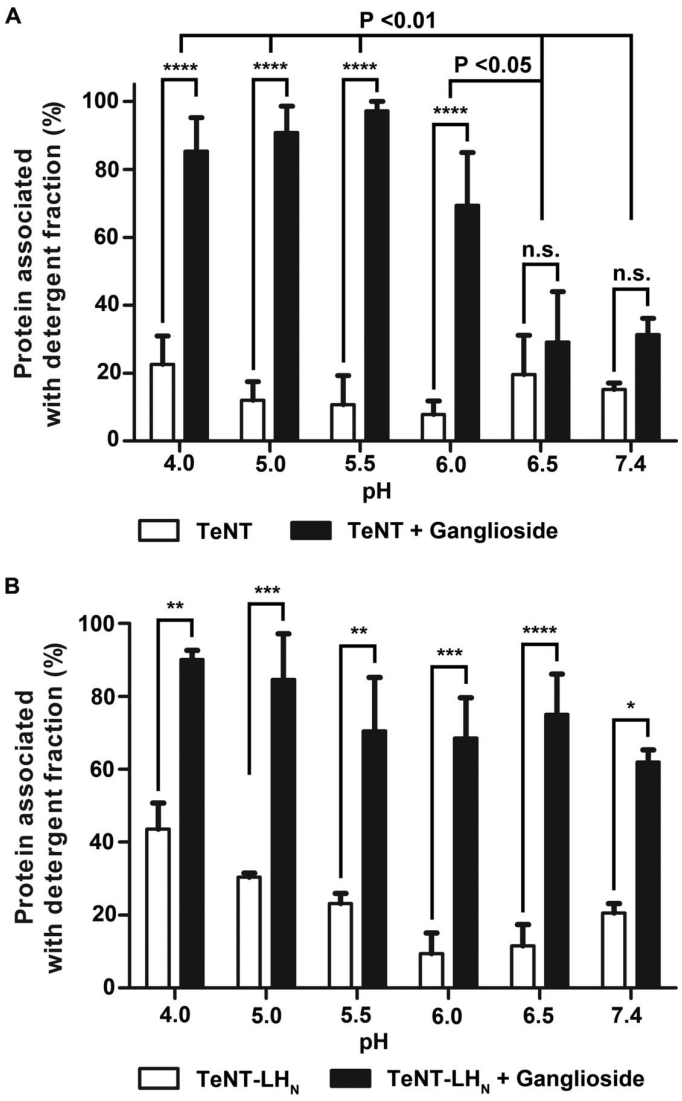

Figure 26. Gangliosides facilitate transformation of TeNT into a hydrophobic protein at low pH. Triton X-114 partitioning assays were performed at various pH values in the absence or presence of ganglioside. TeNT (*A*) and TeNT-LH$_N$ (*B*) were detected by silver staining, and the percentage distribution in the detergent phase was determined by densitometry. Mean values ± S.E. (*error bars*) for at least three independent experiments are shown. *, $p < 0.05$; **, $p < 0.01$; ***, $p < 0.001$; ****, $p < 0.0001$, two-way analysis of variance with Bonferroni post-test. *n.s.*, not significant.

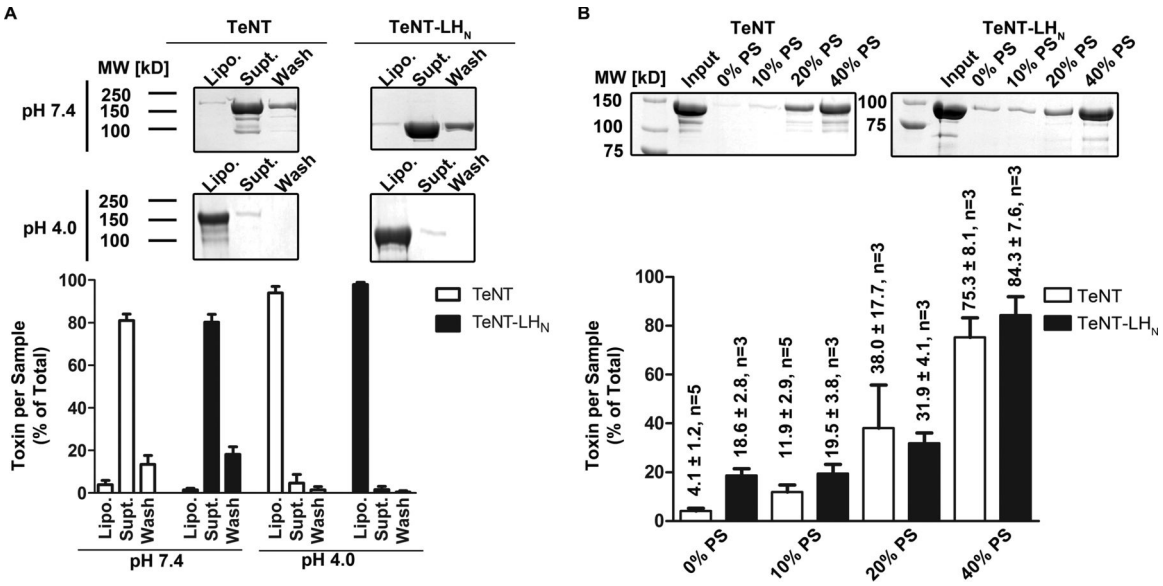

Figure 27 TeNT associates with liposomal membranes. *A*, *top*, ~70 pmol of TeNT or TeNT-LH$_N$ was mixed with 4 µmol of asolectin liposomes in buffer at either pH 7.4 or pH 4.0. Proteoliposomes (*Lipo*.) were isolated by centrifugation, washed with buffer, and recovered by a second centrifugation step. Supernatants (*Supt*.) from the initial centrifugation step and wash fractions (*Wash*) were analyzed along with the proteoliposomes by SDS-PAGE. A representative example of TeNT and TeNT-LH$_N$ association with asolectin liposomes at pH 7.4 and pH 4.0 is shown. *Bottom*, the relative distribution of TeNT (*white bars*) and TeNT-LH$_N$ (*black bars*) ± S.E. (*error bars*) from three independent experiments was determined by densitometry. *B*, ~70 pmol of TeNT or TeNT-LH$_N$ was mixed with 4 µmol of base liposomes (45% phosphatidylcholine, 45% phosphatidylethanolamine, 10% cholesterol, mol %) containing increasing amounts of phosphatidylserine (0–40 mol%) in buffer at pH 4.0. Proteoliposomes were isolated as above and resolved by SDS-PAGE, followed by staining with Coomassie Blue. The image is representative of at least three independent determinations. The relative distribution of TeNT (*white bars*) and TeNT-LHN (*black bars*) ± S.E. from the indicated number of independent experiments was determined by densitometry.

However, in agreement with previous studies [181, 182], pH dependent binding of both TeNT and TeNT-LH_N to asolectin liposomes was observed (**Figure 27A**). Based on these opposing observations, it was postulated that the increased anionic charge present in asolectin liposomes might facilitate toxin binding. To directly examine this possibility, base liposomes containing increasing amounts of the acidic phospholipid, phosphatidylserine (PS) were prepared. As shown in **Figure 27B**, binding of TeNT to liposomes (base liposomes + PS) at low pH showed a clear dependence on PS through 40 mol %. This supports a role for acidic lipids in triggering membrane association of TeNT. While binding of TeNT-LH_N to liposomes also showed a clear dependence on PS, association with base liposomes (no PS) was also increased relative to TeNT (**Figure 27B**). The reason for this difference is not yet clear, but may reflect exposure of hydrophobic surfaces by removal of the HCR domain.

4.4.5 Acidic Lipids Enhance TeNT Mediated Release of K^+ from Liposomes

To further characterize the role of acidic lipids in the action of TeNT, channel formation was assayed by measuring K^+ release from liposomes at neutral and low pH using an ion specific electrode.

Addition of toxins to asolectin liposomes at low pH resulted in a rapid, dose dependent release of K^+ content (**Figure 28A**). Treatment of liposomes with identical concentrations of toxins at neutral pH resulted in a small amount of K^+ release (<5% of total K^+ content, data not shown). Thus, it appears that a basal level of channel formation occurs in a manner largely independent of lipid composition. By comparison, when base liposomes + PS were exposed to TeNT or $TeNT^{RW}$ at low pH, a significant increase in the level of K^+ release was observed, consistent with the model that membrane binding/ channel formation is enhanced by the presence of acidic lipids (**Figure 28C**). Given the observed increase in binding of TeNT-LH_N to base liposomes (Figure 25B) it was anticipated that this would also lead to increased K^+ release at low pH. However, the K^+ release evoked by TeNT-LH_N was similar to that of TeNT and $TeNT^{RW}$ under the tested conditions (**Figure 28B and 28C**). Thus, at this time we are not able to explain the increased K^+ release caused by TeNT-LH_N from base liposomes containing 10 mol % PS versus base liposomes alone (**Figure 28C**).

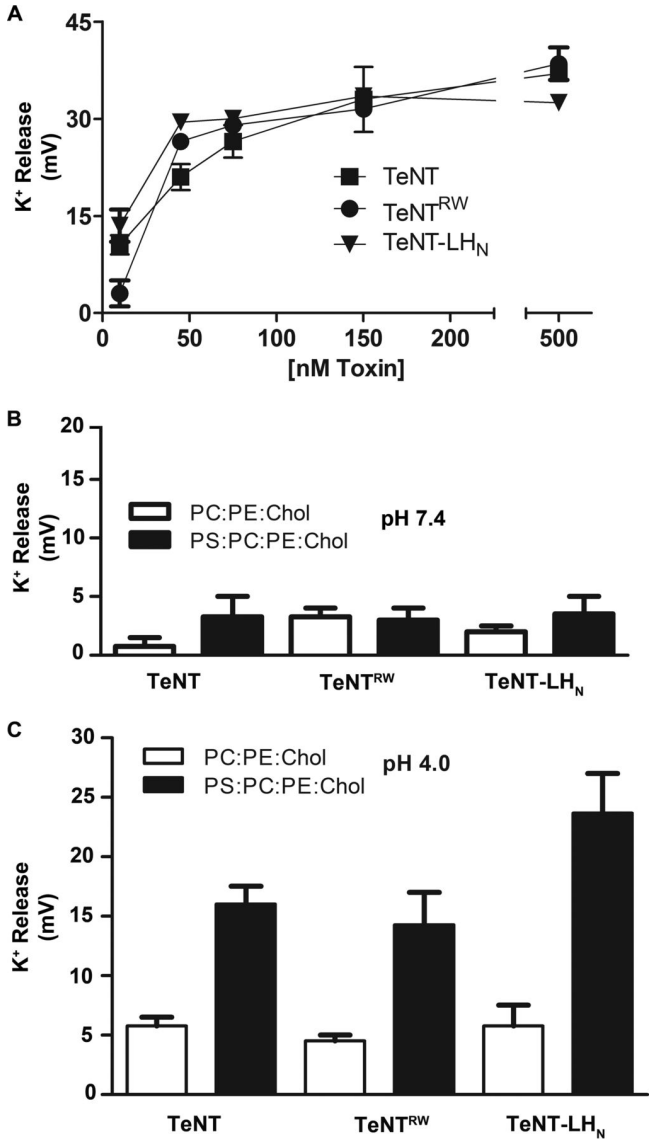

Figure 28. Acidic phospholipids enhance K^+ release from liposomes. *A*, asolectin liposomes (4 µmol) were diluted into buffer at pH 4.0 and incubated with the indicated proteins (2.5 nmol) for 5 min at 24 °C, and K^+ release was recorded using an ion-specific electrode. K^+ release values (mV) are the mean ± S.E. (*error bars*) of three independent experiments. Base liposomes (*white bars*) or base liposomes + PS (10% PS, mol %; *black bars*) were diluted into pH 7.4 (*B*) or pH 4.0 buffer (*C*) and incubated with the indicated proteins for 5 min at 24 °C, and K^+ release was recorded. K^+ release values (mV) are the mean ± S.E. of three independent experiments. *PC*, phosphatidylcholine; *PE*, phosphatidylethanolamine.

4.4.6 Binding of TeNT to Liposomes Through Ganglioside Receptors Mediates Efficient Channel Formation

To determine what effect cellular receptors may play in the translocation process, base liposomes + PS were doped with gangliosides to facilitate direct binding of TeNT to the membrane. Initial experiments were conducted using liposomes containing 2 mol % GT1b and 10 mol % PS. Under these conditions the rate of K^+ release was too rapid to allow for the contribution of GT1b to be assessed (data not shown). Therefore, the concentrations of PS and TeNT were reduced to the minimum levels necessary to detect K^+ release as compared to base liposomes. Under these conditions (base liposomes + 2 mol % GT1b and 5 mol % PS) binding of TeNT - but not $TeNT^{RW}$ or TeNT-LH_N was observed at both neutral and low pH (**Figure 29A**). This demonstrates that binding of TeNT to liposomes containing gangliosides is mediated through HCR-ganglioside interactions, and not through electrostatic interactions between the toxin and the charged membrane environment. Coupling of the toxin to the liposomal membrane resulted in significantly enhanced release of K^+ content when compared with base liposomes containing PS only.

.

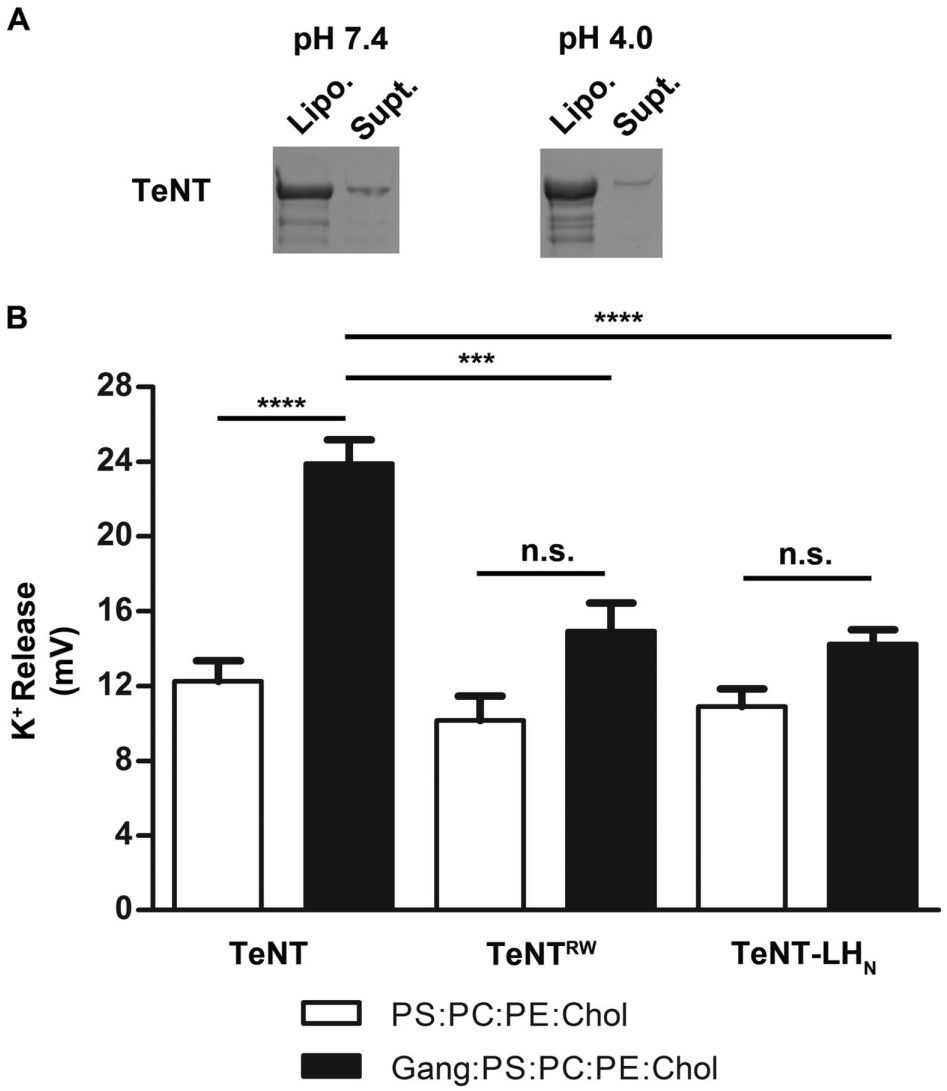

Figure 29 Ganglioside incorporation enhances K^+ release from liposomes at low pH. *A*, ~70 pmol of TeNT was mixed with 4 µmol of base liposomes + PS and gangliosides (5% PS, 2% mixed gangliosides, mol %) in buffer at either pH 7.4 or pH 4.0. Proteoliposomes were isolated by centrifugation, washed with buffer, and analyzed by SDS-PAGE followed by staining with Coomassie Blue. A representative example of TeNT association with liposomes at pH 7.4 and 4.0 is shown. *B*, base liposomes + PS (5% PS, mol %; *white bars*) or base liposomes + PS and gangliosides were diluted into buffer at pH 4.0 and incubated with the indicated proteins (1 nmol) for 5 min at 24 °C, and K^+ release was recorded using an ion-specific electrode. K^+ release values (mV) are the mean ± S.E. of six independent experiments. Base liposomes + PS and gangliosides were $p < 0.001$ (***) or $p < 0.0001$ (****) (one-way ANOVA with Student-Newman-Keuls post-test) compared with base liposomes + PS only. *PC*, phosphatidylcholine; *PE*, phosphatidylethanolamine; *n.s.*, not significant.

However, no such effect was observed when base liposomes + PS and gangliosides were incubated with either $TeNT^{RW}$ or TeNT-LH_N (**Figure 29B**).

4.5 Discussion

Clostridial neurotoxins (CNTs) cause neuroparalytic diseases by preventing the release of neurotransmitters at nerve terminals In recent years our understanding of their structure- function relationships (e.g. catalytic light chain (LC), translocation (HCT), and receptor binding (HCR) domains), enzymatic mode of action, and identification of neuronal cell surface receptors have all rapidly evolved [163]. By comparison, the mechanism by which low pH drives the conversion of CNTs from water-soluble molecules into protein translocase channels remains elusive. Here we investigated the mechanism of channel formation by TeNT to gain new insights into this enigmatic step in the intoxication process. Our data are summarized in **Figure 30**, where we propose a novel two-step model for TeNT channel formation. Initially the HCR domain binds to ganglioside co-receptors present in the neuronal plasma membrane (Step 1) [103, 111].

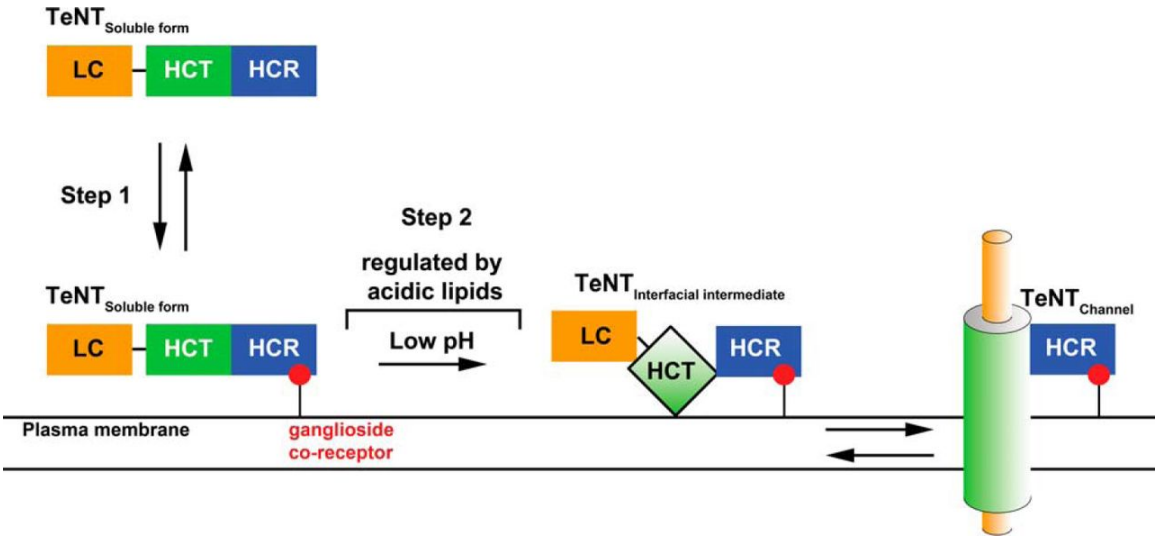

Figure 30. Model for the pH-triggered membrane insertion pathway of tetanus neurotoxin. Initially TeNT exists as a fully folded, water-soluble protein freely able to diffuse within the extracellular milieu ($TeNT_{soluble\ form}$). Binding of TeNT to the plasma membrane is mediated by interaction of the HCR with ganglioside co-receptors (Step 1). Ganglioside binding brings TeNT into close proximity to the target membrane and orients the catalytic LC and HCT domains for optimal channel formation and protein translocation. This interaction alone is not sufficient to initiate membrane insertion. Following endocytic uptake, protonation results in the formation of a membrane-competent state (indicated by the *outlined diamond*) at the membrane interface ($TeNT_{interfacial\ intermediate}$), which is regulated by lipid composition (Step 2). The intermediate state then rapidly transforms into the channel state able to mediate translocation of the enzymatic domain across the membrane.

This interaction presumably promotes partitioning into the bilayer by tethering the HCT domain close to the membrane, such that its orientation relative to the bilayer is optimal for subsequent channel formation. The interaction of HCR with ganglioside is independent of pH ranging from 4.0-7.4 (data not shown), suggesting the toxin remains bound to the membrane within the acidified endosome. Intriguingly, the interaction of BoNT/B with synaptotagmin II was also reported to be independent of pH, potentially signifying a shared mechanism among the CNTs [113]. The need to orient the HCT domain relative to the membrane may be related to the large α-helices of the domain which likely insert into the bilayer. By comparison, the interaction of diphtheria toxin with its cellular receptors is sensitive to pH, and consequently formation of membrane channels occurs independently of receptor [183]. Furthermore, CNTs do not undergo changes in secondary structure response to low pH alone (Figure 23),as has been reported for diphtheria toxin [184]. Thus, the initial interaction of TeNT with the membrane does not appear to require the formation of a membrane-competent state in solution. In step 2, low pH triggers the formation of an interfacial intermediate state that is regulated by the presence of acidic lipids within the membrane. The molecular basis of this regulation is currently unknown and will be the subject of future investigations. The requirement for acidic lipids

further distinguishes TeNT from the interaction of diphtheria toxin with the bilayer which is largely unaltered by the physicochemical nature of the membrane. Once the toxin has formed the interfacial intermediate state, we posit a rapid and possibly irreversible transformation into the channel state occurs (**Figure 30**). Recent studies have demonstrated that BoNT/B and BoNT/E undergo pH-triggered conformational changes and transformation into oligomeric membrane proteins in the presence of ganglioside GT1b. We observed similar conformational changes in TeNT, a ganglioside-binding deficient form of TeNT ($TeNT^{RW}$), and a truncated protein lacking the entire receptor binding domain (TeNT-LH_N) at low pH in the presence of GT1b (**Figure 25A**). These data indicate that the observed structural changes in response to GT1b are not dependent on the HCR domain. Future studies are planned to determine if the HCR domains of BoNT/B and BoNT/E are necessary for the reported effects of ganglioside on secondary structure and oligomerization. How therefore is GT1b able to stimulate the observed changes in TeNT secondary structure? Based on the data presented in **Figure 25** we hypothesize that the observed changes in secondary structure result from insertion of the HCT domain into the hydrophobic core of the ganglioside micelle. Moreover, given that addition of GA1 alone or GA1 in combination with a low amount of GT1b did not stimulate a change in secondary structure, the negative

charge of the sialic acids also appears to play an important role in the interaction. Thus it is posited that polysialoganglioside micelles mimic an acidic membrane environment necessary to drive the formation of the interfacial intermediate state as proposed in **Figure 30**.

Low pH within the lumen of endosomal compartments has long been postulated as the trigger for translocase channel formation. This is in agreement with previous studies demonstrating single-channel activity of BoNTs in planar bilayers and membrane patches excised from neuroendocrine cell lines. Therefore what role if any, does lipid composition play in channel formation by BoNTs? Interestingly, channel formation in planar bilayer systems employed either asolectin or defined lipid mixtures containing both phosphatidylserine and ganglioside GT1b [42, 60]. Thus, the requirement for acidic lipids in regulating the formation of the TeNT interfacial intermediate state may be a shared property among the CNTs. Indeed, Fischer *et al*., previously noted that translocation activity of BoNT/A devoid of the receptor binding domain could not be observed in non-neuronal cell lines and speculated that membrane lipid composition might contribute to this effect [60].

In summary, the data presented provide new insights into the mechanism by which the HCT domain is able to form a channel capable of translocating the LC moiety across the endosomal

membrane. Moreover, they suggest a new mechanism for A-B toxin translocation which differs significantly from the current paradigms of diphtheria and anthrax toxin.

CHAPTER 5: GENERAL DISCUSSION

Scientists and physicians have documented their study of botulism and tetanus since Hippocrates wrote of tetanus in the 5th century. With all that we have learned, we do not fully understand why BoNT is primarily retained in α-motor neurons and why TeNT is sorted into a retrograde axonal transport pathway. These studies focused on the contribution of the heavy chain receptor binding domain (HCR) to better understand mechanisms of ganglioside binding and receptor interactions required for toxicity, to better understand the difference between BoNT and TeNT. In addition, an investigation into the role of receptor binding and CNT translocation was carried out to better understand universal mechanisms of CNT pathogenesis.

One of the long term goals in CNT research has been to explain the unique ability of TeNT to interact with, or to associate with, detergent rich membranes (DRM) on the neuronal surface. GM1a was previously identified as a DRM marker, and has been shown to contribute to retrograde trafficking in cholera toxin and the *E. coli* heat labile toxins. To test the ability of TeNT to undergo retrograde axonal trafficking, a variant of HCR/T (HCR/T^{MO}) required to bind Sia5 and unable to bind the DRM marker GM1a was developed. We propose the unique ability of TeNT to bind ganglioside GM1a allows TeNT to

undergo retrograde axonal trafficking. CNTs other than TeNT are able to bind multiple gangliosides. Analogous to TeNT, two ganglioside binding pockets have been identified in BoNT/C. However, structure based sequence alignments and the crystal structure of HCR/C demonstrate the mechanism of binding between HCR/C and TeNT are quite different. The Sia1 one site, composed of a distal loop and several non-connected peptides has high affinity for GT1b and low affinity for GM1a [185]. A second site, referred to as ganglioside binding pocket 2 (GBP2) has affinity for dia-sia sugars of b series gangliosides [168]. The ability to bind multiple gangliosides is not the only factor in retrograde trafficking.

As we did not test HCR/T^{MO} in a direct retrograde trafficking assay, we cannot rule out a role for GM1 in retrograde axonal trafficking. In addition, we don't know that HCR/T^{MO} cannot be optimized. Identification of the determinant of TeNT retrograde trafficking, either a membrane raft domain or protein domain that directs TeNT entry into a retrograde pathway would be a significant finding and is worth continued effort.

Many variations in sequence and structure do not alter the function of the CNTs. Previous results suggest, as do prior data with HCR/T and HCR/T^{MO}, the importance of characterizing individual CNT variants and subtypes. However, increasing data suggest seemingly

innocuous mutations may change serotype and subtype affinity for substrate or receptor. Thorough analysis of CNT serotypes and subtypes are required to better understand these mechanisms. For example, our lab previously published data demonstrating interactions between HCR/F and the Sia5 sugar are required for sufficient ganglioside binding and entry. Similar interactions are predicted to exist in HCR/A, but had not been tested biochemically.

A second study of receptor binding was undertaken utilizing ciBoNT/A1 and ciBoNT/A2. BoNT/A subtypes are 90% identical as determined by protein based sequence alignment. However, BoNT/A2 was determined to be more toxic than BoNT/A1, and binding and entry more efficient as determined through biochemical and *in vivo* assays. Point mutations designed to test interactions between the Sia5 sugar and HCRs A1 and A2 indicated hydrogen bonds may not be present as indicated in the crystal structure of HCR/A1 and GT1b oligosaccharide. Mutation of F/Y-1117 to alanine increased affinity to ganglioside, suggesting a novel binding mechanism exists in BoNTs A1 and A2 that utilizes a conserved phenylalanine ring shared between HCR/A1 and A2. The presence of the phenylalanine ring may create torsion on GA1 core sugars, preventing high affinity binding to core GBM residues. But, an interaction with Sia5 is still present as the toxin was unable to bind GM1a. Increased affinity for ganglioside in the absence of the

phenylalanine ring increased entry efficiency in cortical neurons and proteins had a higher ratio of colocalization with synaptophysin positive synaptic vesicles. A toxicity assay is currently under development in order to determine relative toxicity of induced mutations.

Discovery of a novel, shared entry mechanism, utilized by multiple BoNT serotypes opens the door to exciting therapeutic possibilities. Current BoNT treatments may have a limited treatment duration due to development of toxin antibodies. Developing BoNT/A2 will improve our basic understanding of CNT binding and entry mechanisms which in turn will lead to development of improved treatment options and vaccine design.

The CNT intoxication process is a stepwise process that begins with binding and internalization at the neuronal membrane, followed by exposure to low pH, formation of a channel and LC translocation. CNT LC translocation is perhaps the least understood step of the intoxication process. LC translocation is shared between BoNTs and TeNT and is pH dependent. The CNTs are believed to form channels (via the HCT domain) in the vesicle membrane and cross from the low pH environment of the vesicle lumen into the neutral pH of the neuronal cytosol. One function of the low pH environment may be to regulate translocation. LC was shown to partially unfold at low pH,

prior to transiting the HCT channel. In addition to low pH, a new mechanism for HCT channel formation dependent on the presence of acidic lipids has been described [63]. In addition, the role for receptor binding in CNT channel formation, has been clarified. The presence of ganglioside in liposome membranes created a greater propensity for the toxin to insert and form ion selective channels.

The HCR domain may perform additional functions outside of receptor binding. It may serve as a pH sensor, preventing channel formation at neutral pH. In support of this idea, BoNT/A-HCT, lacking LC and HCR formed channels in a pH independent manner [186]. Similar to TeNT, ciBoNT was able to bind to acidic lipids at low pH suggesting a universal mechanism for interacting with acidic lipids at low pH although the mechanisms behind the process is not clear.

Full characterization of HCT/HCR interactions are required to understand the mechanism of CNT binding, entry, and channel formation leading to productive LC translocation. At best, we have an incomplete picture of the intoxication process. In order to better understand how the HCR contributes to channel formation, we need more complete understanding of how the structure is oriented on membrane and how it can therefore move. Static crystal structures are helpful, but do not provide all required information about fluid

membrane/protein interactions in order to understand how structural change occurs relative to membrane positioning.

This research has focused on mechanisms between toxin and host required for CNT toxicity in partial fulfillment of the Ph.D. requirements for the University of Missouri.

CHAPTER 6: APPENDIX

Appendix 6.1

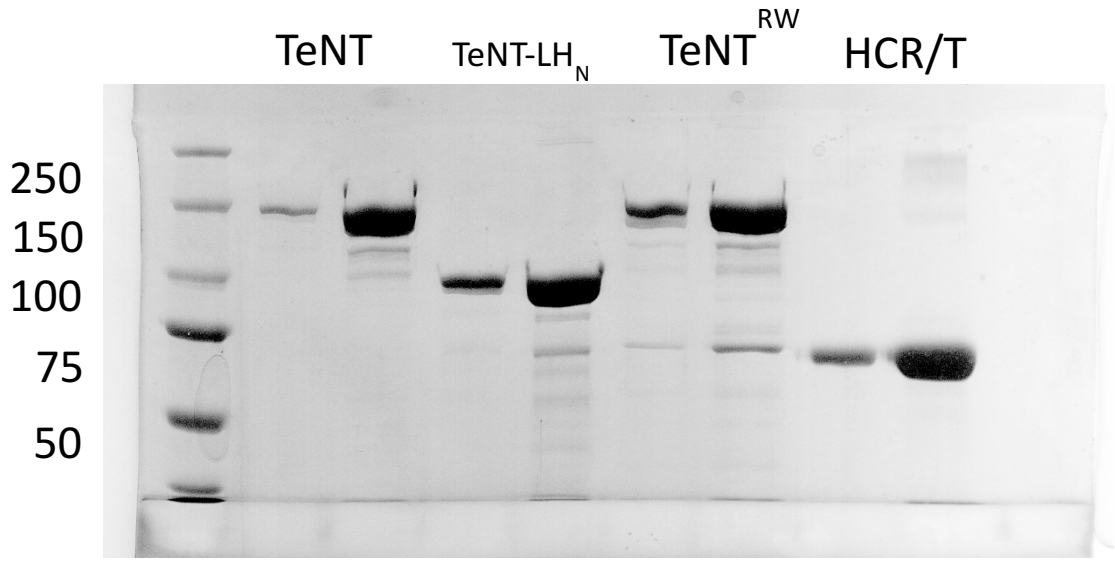

Figure S1. Relative purity of TeNT and TeNT variants. 1 and 5 μg of TeNT and TeNT variants were analysed by SDS-PAGE and stained by Coomassie Blue.

Appendix 6.2 Chapter 2 primers

HCR/T W1289A:
Fwd:
GATATTCTGATTGCGAGCAACGCGTATTTTAACCATCTGAAAGAT
Rev:
ATCTTTCAGATGGTTAAAATACGCGTTGCTCGCAATCAGAATATC

R1226L
Fwd:
C AACCTGGATCGTATTCTGCTGCGTGTGGGCTATAACGCG
Rev:
CGCGTTATAGCCCACACGCAGCAGAATACGATCCAGGTT G

HCR/T A1134L
Fwd:
GAATATTATCTGATTCCGGTGCTGAGCAGCAGCAAAGATGTGCAG
Reverse:
CTGCACATCTTTGCTGCTGCTCAGCACCGGAATCAGATAATATTC

T1270F/H1271N
Fwd:
CGAGCCTGGGCCTGGTGGGCTTCAACAACGGCCAGATTGGCAACG
Rev:
CGTTGCCAATCTGGCCGTTGTTGAAGCCCACCAGGCCCAGGCTCG

T1270F/H1271A
Fwd:
CG AGCCTGGGCCTGGTGGGCTTCGCGAACGGCCAGATTGGCAAC G
Rev:
CGTTGCCAATCTGGCCGTTCGCGAAGCCCACCAGGCCCAGGCTCG

N1219S, R1226L
Fwd:
CCGAAAGATGGCAACGCGTTTAGCAACCTGGATCGTATTCTGCTG
Rev:
CAGCAGAATACGATCCAGGTTGCTAAACGCGTTGCCATCTTTCGG

N1219V, R1226L
Fwd:
CCGAAAGATGGCAACGCGTTTGTGAACCTGGATCGTATTCTGCTG
Rev:
CAGCAGAATACGATCCAGGTTCACAAACGCGTTGCCATCTTTCGG

D1222E, R1226L
Fwd:
GGCAACGCGTTTAACAACCTGGAACGTATTCTGCTGGTGGGCTAT
Rev:
ATAGCCCACCAGCAGAATACGTTCCAGGTTGTTAAACGCGTTGCC

D1222A/E, R1226L
Fwd:
GGCAACGCGTTTGCGAACCTGGAACGTATTCTGCTGGTGGGCTAT
Rev:
ATAGCCCACCAGCAGAATACGTTCCAGGTTCGCAAACGCGTTGCC

T-MO: W/A
Fwd:
GATATTCTGATTGCGAGCAACGCGTATTTTAACCAGATCGAACGT
Rev:
ACGTTCGATCTGGTTAAAATACGCGTTGCTCGCAATCAGAATATC

HCR/T-MO: R1299S
Fwd:
AACCAGATCGAACGTTCTTCTTCTACCCTGGGCTGCGATTGGTAT
Rev:
ATACCAATCGCAGCCCAGGGTAGAAGAAGAACGTTCGATCTGGTT

D1222N
Fwd:
GGCAACGCGTTTAACAACCTGAACCGTATTCTGCGTGTGGGCTAT
Rev:
ATAGCCCACACGCAGAATACGGTTCAGGTTGTTAAACGCGTTGCC

D1222A
Fwd:
GGCAACGCGTTTAACAACCTGGCGCGTATTCTGCGTGTGGGCTAT
Rev:
ATAGCCCACACGCAGAATACGCGCCAGGTTGTTAAACGCGTTGCC

G1300F
Fwd*:*
CCATCTGAAAGATAAAATTCTGTTTTGCGATTGGTATTTTGTGCCGACCG
Rev:
CGGTCGGCACAAAATACCAATCGCAAAACAGAATTTTATCTTTCAGATGG

G1300Y:
Fwd:
CCATCTGAAAGATAAAATTCTGTATTGCGATTGGTATTTTGTGCCGACCG
Rev:
CGGTCGGCACAAAATACCAATCGCAATACAGAATTTTATCTTTCAGATGG

R1226L/H1271A
Fwd:
CG AGCCTGGGCCTGGTGGGCACCGCGAACGGCCAGATTGGCAAC G
Rev:
CGTTGCCAATCTGGCCGTTCGCGGTGCCCACCAGGCCCAGGCTCG

ARTS F-Loop/S1287A
Fwd:
CGTGATATTCTGATTGCGGCGAACTGGTATTTTAACAACATC
Rev:
GATGTTGTTAAAATACCAGTTCGCCGCAATCAGAATATCACG

NART/H1271K
Fwd:
AGCCTGGGCCTGGTGGGCTTCAAAAACGGCCAGATTGGCAACGAT
Rev:
ATCGTTGCCAATCTGGCCGTTTTTGAAGCCCACCAGGCCCAGGCT

R1226L/N1219A/H1271K
Fwd:
AGCCTGGGCCTGGTGGGCACCAAAAACGGCCAGATTGGCAACGAT
Rev:
ATCGTTGCCAATCTGGCCGTTTTTGGTGCCCACCAGGCCCAGGCT

TeNT-BoNT/A Loop
Fwd:
CAGATCGAACGTTCTTCTCGTACCCTGGGCTGCGATTGGTATTTTGTG
Rev:
CAGGGTACGAGAAGAACGTTCGATCTGGTTAAAATACCAGTTGCTCGC

TeNT-BoNT/E Loop
Fwd:
CATATGCGTGATAACACCAACAGCAACGGCTGCGATTGGTATTTTGTGCCG
ACC
Rev:
GCCGTTGCTGTTGGTGTTATCACGCATATGGTTAAAATACCAGTTGCTCGCA
ATCAG

TeNT-BoNT/F Loop
Fwd:
AACATCCGTAAAAACACCTCTTCTAACGGCTGCGATTGGTATTTTGTG
Rev:
GTTAGAAGAGGTGTTTTTACGGATGTTGTTAAAATACCAGTTGCT

6.3 HCR/TMO Manders Analysis

Run 1 - Mar 2016						
Image	Pearson's Coefficient	Manders Overlap Coefficient	Ngreen / Nred	Manders' coefficient_green	Manders' coefficient_red	Ntotal
HCR/T_CTxB_37_1	0.739	0.869	0.924	0.998	0.972	970967
HCR/T_CTxB_37_2	0.782	0.875	0.946	0.998	0.883	964651
HCR/T_CTxB_37_3	0.751	0.872	0.938	0.993	0.981	952751
HCR/T_CTxB_37_4	0.805	0.894	0.939	0.998	0.934	963450
HCR/T_CTxB_37_5	794	0.888	0.969	0.996	0.902	964605
HCR/T_CTxB_37_6	0.806	0.894	0.94	0.996	0.984	963445
HCR/T_CTxB_37_7	0.758	0.874	0.942	0.994	0.976	974993
HCR/T_CTxB_37_8	0.767	0.876	0.963	0.993	0.977	962732
HCR/T_CTxB_37_9	0.789	0.834	0.947	0.989	0.976	943788
HCR/T_CTxB_37_10	0.731	0.809	0.959	0.994	0.977	962458
HCR/T_CTxB_37_11	0.759	0.858	0.962	0.994	0.974	964590

HCR/T_CTxB_37_12	0.782	0.869	0.981	0.994	0.976	960135
HCR/T_CTxB_37_13	0.8	0.912	0.977	0.993	0.982	969600
HCR/T_CTxB_37_14	0.799	0.871	0.965	0.996	0.978	970686
HCR/T_CTxB_37_15	0.736	0.794	0.979	0.995	0.982	962263
Image	Pearson's Coefficient	Overlap Coefficient	Ngreen / Nred	Manders' coefficient_green	Manders' coefficient_red	Ntotal
HCR/T-MO_CTxB_37_1	0.556	0.754	0.906	0.999	0.767	975315
HCR/T-MO_CTxB_37_2	0.581	0.698	0.925	0.997	0.712	968215
HCR/T-MO_CTxB_37_3	0.421	0.588	0.967	0.989	0.653	971289
HCR/T-MO_CTxB_37_4	0.567	0.764	0.918	0.994	0.702	969349
HCR/T-MO_CTxB_37_5	0.46	0.612	0.968	0.989	0.688	961192
HCR/T-MO_CTxB_37_6	0.57	0.772	0.954	0.992	0.699	962604
HCR/T-MO_CTxB_37_7	0.57	0.776	0.968	0.989	0.705	968018
HCR/T-MO_CTxB_37_8	0.458	0.597	0.936	0.986	0.68	965442
HCR/T-MO_CTxB_37_9	0.506	0.712	0.967	0.99	0.718	961932

HCR/T-MO_CTxB_37_10	0.438	0.593	0.994	0.988	0.628	960438
HCR/T-MO_CTxB_37_11	0.477	0.635	0.961	0.992	0.667	968878
HCR/T-MO_CTxB_37_12	0.552	0.658	0.985	0.992	0.678	964721
HCR/T-MO_CTxB_37_13	0.493	0.606	0.936	0.986	0.715	968122
HCR/T-MO_CTxB_37_14	0.507	0.632	0.923	0.994	0.725	968404
HCR/T-MO_CTxB_37_15	0.517	0.628	0.949	0.989	0.713	969054
Run 2 - Apr 2016						
Image	Pearson's Coefficient	Overlap Coefficient	Ngreen / Nred	Manders' coefficient_green	Manders' coefficient_red	Ntotal
HCR/T_CTxB_37_1	0.807	0.91	0.908	0.994	0.857	899240
HCR/T_CTxB_37_2	0.722	0.814	0.935	0.996	0.972	904976
HCR/T_CTxB_37_3	0.812	0.915	0.981	0.994	0.942	900199
HCR/T_CTxB_37_4	0.75	0.845	0.963	0.984	0.926	904751

HCR/T_CTxB_37_5	0.681	0.768	0.924	0.992	0.907	890711
HCR/T_CTxB_37_6	0.736	0.829	0.975	0.993	0.956	896605
HCR/T_CTxB_37_7	0.814	0.917	0.883	0.993	0.847	911852
HCR/T_CTxB_37_8	0.71	0.8	0.903	0.982	0.818	824047
HCR/T_CTxB_37_9	0.749	0.844	0.915	0.989	0.832	909320
HCR/T_CTxB_37_10						
Image	Pearson's Coefficient	Overlap Coefficient	Ngreen / Nred	Manders' coefficient_green	Manders' coefficient_red	Ntotal
HCR/T-MO_CTxB_37_1	0.611	0.786	0.903	0.983	0.723	889886
HCR/T-MO_CTxB_37_2	0.578	0.744	0.937	0.993	0.68	891605
HCR/T-MO_CTxB_37_3	0.503	0.647	0.918	0.985	0.741	911903
HCR/T-MO_CTxB_37_4	0.516	0.664	0.937	0.988	0.689	900383
HCR/T-MO_CTxB_37_5	0.621	0.799	0.936	0.995	0.688	890364
HCR/T-MO_CTxB_37_6	0.46	0.591	0.93	0.997	0.672	894270
HCR/T-MO_CTxB_37_7	0.448	0.577	0.915	0.996	0.707	892152
HCR/T-MO_CTxB_37_8	0.505	0.65	0.888	0.991	0.689	907389

HCR/T-MO_CTxB_37_9	0.561	0.721	0.904	0.989	0.649	896999
HCR/T-MO_CTxB_37_10	0.475	0.611	0.955	0.987	0.666	891520
Image	Pearson's Coefficient	Overlap Coefficient	Ngreen / Nred	Manders' coefficient_green	Manders' coefficient_red	Ntotal
HCR/T_CTxB_4_1	0.833	0.914	0.979	0.986	0.967	983368
HCR/T_CTxB_4_2	0.731	0.802	0.956	0.997	0.929	1034110
HCR/T_CTxB_4_3	0.809	0.888	0.923	0.989	0.974	1064327
HCR/T_CTxB_4_4	0.744	0.816	0.925	0.998	0.935	1063226
HCR/T_CTxB_4_5	0.847	0.929	0.965	0.998	0.935	1064800
HCR/T_CTxB_4_6	0.802	0.88	0.97	0.991	0.949	983457
HCR/T_CTxB_4_7	0.818	0.897	0.938	0.999	0.972	1083111
HCR/T_CTxB_4_8	0.812	0.89	0.949	0.982	0.982	1018486
HCR/T_CTxB_4_9	0.743	0.816	0.975	0.995	0.969	1029077
HCR/T_CTxB_4_10	765	0.839	0.986	0.984	0.946	971387

Image	Pearson's Coefficient	Overlap Coefficient	Ngreen / Nred	Manders' coefficient_green	Manders' coefficient_red	Ntotal
HCR/T-MO_CTxB_4_1	0.801	0.879	0.956	0.991	0.944	1026557
HCR/T-MO_CTxB_4_2	0.787	0.863	0.977	0.983	0.978	1048108
HCR/T-MO_CTxB_4_3	0.808	0.886	0.956	0.99	0.934	1078813
HCR/T-MO_CTxB_4_4	0.785	0.862	0.943	0.998	0.963	1082185
HCR/T-MO_CTxB_4_5	0.846	0.928	0.983	0.991	0.977	1089488
HCR/T-MO_CTxB_4_6	0.765	0.839	0.95	0.983	0.927	1012152
HCR/T-MO_CTxB_4_7	0.75	0.823	0.928	0.984	0.983	901799
HCR/T-MO_CTxB_4_8	0.825	0.905	0.971	0.988	0.959	967397
HCR/T-MO_CTxB_4_9	0.786	0.844	0.983	0.922	0.951	952932
HCR/T-MO_CTxB_4_10	0.739	0.862	0.977	0.986	0.94	1070255

Chapter 7: Literature Cited

1. Popoff, M.R. and P. Bouvet, *Clostridial toxins.* Future Microbiol, 2009. **4**(8): p. 1021-64.
2. Popoff, M.R. and P. Bouvet, *Genetic characteristics of toxigenic Clostridia and toxin gene evolution.* Toxicon, 2013. **75**: p. 63-89.
3. Verherstraeten, S., et al., *Perfringolysin O: The Underrated Clostridium perfringens Toxin?* Toxins (Basel), 2015. **7**(5): p. 1702-21.
4. Popoff, M.R., *Clostridial pore-forming toxins: powerful virulence factors.* Anaerobe, 2014. **30**: p. 220-38.
5. Pruitt, R.N. and D.B. Lacy, *Toward a structural understanding of Clostridium difficile toxins A and B.* Front Cell Infect Microbiol, 2012. **2**: p. 28.
6. Carle, A.R., G. , *Studio esperimentale sull'eziologia del tetano[Experimental studies of the etiology of tetanus].* Giorn. Accad. Med.Torino, 1884 **32**: p. 174-179.
7. Gill, D.M., *Bacterial toxins: a table of lethal amounts.* Microbiol Rev, 1982. **46**(1): p. 86-94.
8. Montal, M., *Botulinum neurotoxin: a marvel of protein design.* Annu Rev Biochem, 2010. **79**: p. 591-617.
9. Schiavo, G., M. Matteoli, and C. Montecucco, *Neurotoxins affecting neuroexocytosis.* Physiol Rev, 2000. **80**(2): p. 717-66.
10. Erbguth, F.J., *Historical notes on botulism, Clostridium botulinum, botulinum toxin, and the idea of the therapeutic use of the toxin.* Mov Disord, 2004. **19 Suppl 8**: p. S2-6.
11. Hatheway, C.L., *Toxigenic clostridia.* Clin Microbiol Rev, 1990. **3**(1): p. 66-98.
12. McCroskey, L.M., et al., *Characterization of an organism that produces type E botulinal toxin but which resembles Clostridium butyricum from the feces of an infant with type E botulism.* J Clin Microbiol, 1986. **23**(1): p. 201-2.
13. McCroskey, L.M., et al., *Type F botulism due to neurotoxigenic Clostridium baratii from an unknown source in an adult.* J Clin Microbiol, 1991. **29**(11): p. 2618-20.
14. Altwegg, M. and C.L. Hatheway, *Multilocus enzyme electrophoresis of Clostridium argentinense (Clostridium botulinum toxin type G) and phenotypically similar asaccharolytic clostridia.* J Clin Microbiol, 1988. **26**(11): p. 2447-9.
15. Hill, K.K. and T.J. Smith, *Genetic diversity within Clostridium botulinum serotypes, botulinum neurotoxin gene clusters and toxin subtypes.* Curr Top Microbiol Immunol, 2013. **364**: p. 1-20.
16. Arnon, S.S., et al., *Botulinum toxin as a biological weapon: medical and public health management.* Jama, 2001. **285**(8): p. 1059-70.
17. Bruggemann, H., et al., *Genomics of Clostridium tetani.* Res Microbiol, 2015. **166**(4): p. 326-31.
18. McCallum, N., et al., *Genomic Epidemiology of Clostridium botulinum Isolates from Temporally Related Cases of Infant Botulism in New South Wales, Australia.* J Clin Microbiol, 2015. **53**(9): p. 2846-53.

19. Fenicia, L. and F. Anniballi, *Infant botulism.* Ann Ist Super Sanita, 2009. **45**(2): p. 134-46.
20. Ahsan, C.R., et al., *Visualization of binding and transcytosis of botulinum toxin by human intestinal epithelial cells.* J Pharmacol Exp Ther, 2005. **315**(3): p. 1028-35.
21. Maksymowych, A.B. and L.L. Simpson, *Binding and transcytosis of botulinum neurotoxin by polarized human colon carcinoma cells.* J Biol Chem, 1998. **273**(34): p. 21950-7.
22. Park, J.B. and L.L. Simpson, *Inhalational poisoning by botulinum toxin and inhalation vaccination with its heavy-chain component.* Infect Immun, 2003. **71**(3): p. 1147-54.
23. Al-Saleem, F.H., et al., *Analysis of the mechanisms that underlie absorption of botulinum toxin by the inhalation route.* Infect Immun, 2012. **80**(12): p. 4133-42.
24. Montecucco, C. and G. Schiavo, *Structure and function of tetanus and botulinum neurotoxins.* Q Rev Biophys, 1995. **28**(4): p. 423-72.
25. Montecucco, C., G. Schiavo, and O. Rossetto, *The mechanism of action of tetanus and botulinum neurotoxins.* Arch Toxicol Suppl, 1996. **18**: p. 342-54.
26. Lacy, D.B. and R.C. Stevens, *Sequence homology and structural analysis of the clostridial neurotoxins.* J Mol Biol, 1999. **291**(5): p. 1091-104.
27. Lacy, D.B., et al., *Crystal structure of botulinum neurotoxin type A and implications for toxicity.* Nat Struct Biol, 1998. **5**(10): p. 898-902.
28. Vaidyanathan, V.V., et al., *Proteolysis of SNAP-25 isoforms by botulinum neurotoxin types A, C, and E: domains and amino acid residues controlling the formation of enzyme-substrate complexes and cleavage.* J Neurochem, 1999. **72**(1): p. 327-37.
29. Foran, P., C.C. Shone, and J.O. Dolly, *Differences in the protease activities of tetanus and botulinum B toxins revealed by the cleavage of vesicle-associated membrane protein and various sized fragments.* Biochemistry, 1994. **33**(51): p. 15365-74.
30. Kroken, A.R., et al., *Unique ganglioside binding by botulinum neurotoxins C and D-SA.* Febs j, 2011. **278**(23): p. 4486-96.
31. Strotmeier, J., et al., *Botulinum neurotoxin serotype D attacks neurons via two carbohydrate-binding sites in a ganglioside-dependent manner.* Biochem J, 2010. **431**(2): p. 207-16.
32. Benecke, R., et al., *Tetanus toxin induced actions on spinal Renshaw cells and Ia-inhibitory interneurones during development of local tetanus in the cat.* Exp Brain Res, 1977. **27**(3-4): p. 271-86.
33. Deinhardt, K., et al., *Rab5 and Rab7 control endocytic sorting along the axonal retrograde transport pathway.* Neuron, 2006. **52**(2): p. 293-305.
34. Koriazova, L.K. and M. Montal, *Translocation of botulinum neurotoxin light chain protease through the heavy chain channel.* Nat Struct Biol, 2003. **10**(1): p. 13-8.
35. Fischer, A., et al., *Beltless translocation domain of botulinum neurotoxin A embodies a minimum ion-conductive channel.* J Biol Chem, 2012. **287**(3): p. 1657-61.

36. Pirazzini, M., et al., *The thioredoxin reductase--Thioredoxin redox system cleaves the interchain disulphide bond of botulinum neurotoxins on the cytosolic surface of synaptic vesicles.* Toxicon, 2015. **107**(Pt A): p. 32-6.
37. Kurazono, H., et al., *Minimal essential domains specifying toxicity of the light chains of tetanus toxin and botulinum neurotoxin type A.* J Biol Chem, 1992. **267**(21): p. 14721-9.
38. Kumaran, D., et al., *Domain organization in Clostridium botulinum neurotoxin type E is unique: its implication in faster translocation.* J Mol Biol, 2009. **386**(1): p. 233-45.
39. Swaminathan, S. and S. Eswaramoorthy, *Structural analysis of the catalytic and binding sites of Clostridium botulinum neurotoxin B.* Nat Struct Biol, 2000. **7**(8): p. 693-9.
40. Schiavo, G., et al., *An intact interchain disulfide bond is required for the neurotoxicity of tetanus toxin.* Infect Immun, 1990. **58**(12): p. 4136-41.
41. Zuverink, M., et al., *A Heterologous Reporter Defines the Role of the Tetanus Toxin Interchain Disulfide in Light-Chain Translocation.* Infect Immun, 2015. **83**(7): p. 2714-24.
42. Hoch, D.H., et al., *Channels formed by botulinum, tetanus, and diphtheria toxins in planar lipid bilayers: relevance to translocation of proteins across membranes.* Proc Natl Acad Sci U S A, 1985. **82**(6): p. 1692-6.
43. Brunger, A.T., et al., *Botulinum neurotoxin heavy chain belt as an intramolecular chaperone for the light chain.* PLoS Pathog, 2007. **3**(9): p. 1191-4.
44. Gul, N., L.A. Smith, and S.A. Ahmed, *Light chain separated from the rest of the type a botulinum neurotoxin molecule is the most catalytically active form.* PLoS One, 2010. **5**(9): p. e12872.
45. Breidenbach, M.A. and A.T. Brunger, *Substrate recognition strategy for botulinum neurotoxin serotype A.* Nature, 2004. **432**(7019): p. 925-9.
46. Fischer, A., et al., *Molecular architecture of botulinum neurotoxin E revealed by single particle electron microscopy.* J Biol Chem, 2008. **283**(7): p. 3997-4003.
47. Benson, M.A., et al., *Unique ganglioside recognition strategies for clostridial neurotoxins.* J Biol Chem, 2011. **286**(39): p. 34015-22.
48. Agarwal, R., et al., *Structural analysis of botulinum neurotoxin type E catalytic domain and its mutant Glu212-->Gln reveals the pivotal role of the Glu212 carboxylate in the catalytic pathway.* Biochemistry, 2004. **43**(21): p. 6637-44.
49. Arndt, J.W., et al., *Crystal structure of botulinum neurotoxin type G light chain: serotype divergence in substrate recognition.* Biochemistry, 2005. **44**(28): p. 9574-80.
50. Arndt, J.W., et al., *Structure of botulinum neurotoxin type D light chain at 1.65 A resolution: repercussions for VAMP-2 substrate specificity.* Biochemistry, 2006. **45**(10): p. 3255-62.
51. Fotinou, C., et al., *The crystal structure of tetanus toxin Hc fragment complexed with a synthetic GT1b analogue suggests cross-linking between ganglioside receptors and the toxin.* J Biol Chem, 2001. **276**(34): p. 32274-81.
52. Montecucco, C., *How do tetanus and botulinum toxins bind to neuronal membranes?* Trends in Biochemical Sciences, 1986. **11**(8): p. 314-317.

53. Karlsson, K.A., *On the character and functions of sphingolipids.* Acta Biochim Pol, 1998. **45**(2): p. 429-38.
54. Fu, Z., et al., *Glycosylated SV2 and gangliosides as dual receptors for botulinum neurotoxin serotype F.* Biochemistry, 2009. **48**(24): p. 5631-41.
55. Dong, M., et al., *Glycosylated SV2A and SV2B mediate the entry of botulinum neurotoxin E into neurons.* Mol Biol Cell, 2008. **19**(12): p. 5226-37.
56. Dong, M., et al., *SV2 is the protein receptor for botulinum neurotoxin A.* Science, 2006. **312**(5773): p. 592-6.
57. Rummel, A., et al., *Identification of the protein receptor binding site of botulinum neurotoxins B and G proves the double-receptor concept.* Proc Natl Acad Sci U S A, 2007. **104**(1): p. 359-64.
58. Chai, Q., et al., *Structural basis of cell surface receptor recognition by botulinum neurotoxin B.* Nature, 2006. **444**(7122): p. 1096-100.
59. Schmitt, J., et al., *Structural analysis of botulinum neurotoxin type G receptor binding.* Biochemistry, 2010. **49**(25): p. 5200-5.
60. Fischer, A., et al., *Botulinum neurotoxin devoid of receptor binding domain translocates active protease.* PLoS Pathog, 2008. **4**(12): p. e1000245.
61. Fischer, A. and M. Montal, *Crucial role of the disulfide bridge between botulinum neurotoxin light and heavy chains in protease translocation across membranes.* J Biol Chem, 2007. **282**(40): p. 29604-11.
62. Parikh, S. and B.R. Singh, *Comparative membrane channel size and activity of botulinum neurotoxins A and E.* Protein J, 2007. **26**(1): p. 19-28.
63. Burns, J.R. and M.R. Baldwin, *Tetanus neurotoxin utilizes two sequential membrane interactions for channel formation.* J Biol Chem, 2014. **289**(32): p. 22450-8.
64. Mushrush, D.J., et al., *Studies of the mechanistic details of the pH-dependent association of botulinum neurotoxin with membranes.* J Biol Chem, 2011. **286**(30): p. 27011-8.
65. Montecucco, C. and G. Schiavo, *Mechanism of action of tetanus and botulinum neurotoxins.* Mol Microbiol, 1994. **13**(1): p. 1-8.
66. Schiavo, G., et al., *Tetanus and botulinum-B neurotoxins block neurotransmitter release by proteolytic cleavage of synaptobrevin.* Nature, 1992. **359**(6398): p. 832-5.
67. Schiavo, G., et al., *Botulinum neurotoxin type C cleaves a single Lys-Ala bond within the carboxyl-terminal region of syntaxins.* J Biol Chem, 1995. **270**(18): p. 10566-70.
68. Yamasaki, S., et al., *Botulinum neurotoxin type G proteolyses the Ala81-Ala82 bond of rat synaptobrevin 2.* Biochem Biophys Res Commun, 1994. **200**(2): p. 829-35.
69. Binz, T., et al., *Proteolysis of SNAP-25 by types E and A botulinal neurotoxins.* J Biol Chem, 1994. **269**(3): p. 1617-20.
70. Yamasaki, S., et al., *Synaptobrevin/vesicle-associated membrane protein (VAMP) of Aplysia californica: structure and proteolysis by tetanus toxin and botulinal neurotoxins type D and F.* Proc Natl Acad Sci U S A, 1994. **91**(11): p. 4688-92.
71. Schiavo, G., et al., *Botulinum neurotoxin serotype F is a zinc endopeptidase specific for VAMP/synaptobrevin.* J Biol Chem, 1993. **268**(16): p. 11516-9.

72. Schiavo, G., et al., *Botulinum neurotoxins serotypes A and E cleave SNAP-25 at distinct COOH-terminal peptide bonds.* FEBS Lett, 1993. **335**(1): p. 99-103.
73. Schiavo, G., et al., *Identification of the nerve terminal targets of botulinum neurotoxin serotypes A, D, and E.* J Biol Chem, 1993. **268**(32): p. 23784-7.
74. Foran, P., et al., *Botulinum neurotoxin C1 cleaves both syntaxin and SNAP-25 in intact and permeabilized chromaffin cells: correlation with its blockade of catecholamine release.* Biochemistry, 1996. **35**(8): p. 2630-6.
75. Guo, J. and S. Chen, *Unique substrate recognition mechanism of the botulinum neurotoxin D light chain.* J Biol Chem, 2013. **288**(39): p. 27881-7.
76. Chen, S. and J.T. Barbieri, *Association of botulinum neurotoxin serotype A light chain with plasma membrane-bound SNAP-25.* J Biol Chem, 2011. **286**(17): p. 15067-72.
77. Fernandez-Salas, E., et al., *Plasma membrane localization signals in the light chain of botulinum neurotoxin.* Proc Natl Acad Sci U S A, 2004. **101**(9): p. 3208-13.
78. Fu, Z., et al., *Light chain of botulinum neurotoxin serotype A: structural resolution of a catalytic intermediate.* Biochemistry, 2006. **45**(29): p. 8903-11.
79. Chen, S. and J.T. Barbieri, *Unique substrate recognition by botulinum neurotoxins serotypes A and E.* J Biol Chem, 2006. **281**(16): p. 10906-11.
80. Chen, S., C. Hall, and J.T. Barbieri, *Substrate recognition of VAMP-2 by botulinum neurotoxin B and tetanus neurotoxin.* J Biol Chem, 2008. **283**(30): p. 21153-9.
81. Chen, S. and J.T. Barbieri, *Engineering botulinum neurotoxin to extend therapeutic intervention.* Proc Natl Acad Sci U S A, 2009. **106**(23): p. 9180-4.
82. Keller, J.E., et al., *Persistence of botulinum neurotoxin action in cultured spinal cord cells.* FEBS Lett, 1999. **456**(1): p. 137-42.
83. Davletov, B., M. Bajohrs, and T. Binz, *Beyond BOTOX: advantages and limitations of individual botulinum neurotoxins.* Trends Neurosci, 2005. **28**(8): p. 446-52.
84. Eleopra, R., et al., *Different time courses of recovery after poisoning with botulinum neurotoxin serotypes A and E in humans.* Neurosci Lett, 1998. **256**(3): p. 135-8.
85. Sobel, J., *Botulism.* Clinical Infectious Diseases, 2005. **41**(8): p. 1167-1173.
86. Chang, G.Y. and G. Ganguly, *Early antitoxin treatment in wound botulism results in better outcome.* Eur Neurol, 2003. **49**(3): p. 151-3.
87. Stiehm, E.R., *Standard and special human immune serum globulins as therapeutic agents.* Pediatrics, 1979. **63**(2): p. 301-19.
88. Chalya, P.L., et al., *Ten-year experiences with Tetanus at a Tertiary hospital in Northwestern Tanzania: A retrospective review of 102 cases.* World J Emerg Surg, 2011. **6**: p. 20.
89. Collins, S., et al., *The importance of tetanus risk assessment during wound management.* IDCases, 2015. **2**(1): p. 3-5.
90. Lisboa, T., et al., *Guidelines for the management of accidental tetanus in adult patients.* Rev Bras Ter Intensiva, 2011. **23**(4): p. 394-409.
91. CDC. *Epidemiology and Prevention of Vaccine-Preventable Diseases 13th edition*. 2015.

92. Nigg, C., G.A. Hottle, and et al., *Studies on botulinum toxoid, types A and P; production of alum precipitated toxoids.* J Immunol, 1947. **55**(3): p. 245-54.
93. Hottle, G.A., C. Nigg, and J.A. Lichty, *Studies on botulinum toxoid, types A and B; methods for determining antigenicity in animals.* J Immunol, 1947. **55**(3): p. 255-62.
94. Reames, H.R., P.J. Kadull, and et al., *Studies on botulinum toxoids, types A and B; immunization of man.* J Immunol, 1947. **55**(4): p. 309-24.
95. Smith, L.A. and J.M. Rusnak, *Botulinum neurotoxin vaccines: past, present, and future.* Crit Rev Immunol, 2007. **27**(4): p. 303-18.
96. Webb, R.P. and L.A. Smith, *What next for botulism vaccine development?* Expert Rev Vaccines, 2013. **12**(5): p. 481-92.
97. Webb, R.P., et al., *Production of catalytically inactive BoNT/A1 holoprotein and comparison with BoNT/A1 subunit vaccines against toxin subtypes A1, A2, and A3.* Vaccine, 2009. **27**(33): p. 4490-7.
98. Przedpelski, A., et al., *Enhancing the protective immune response against botulism.* Infect Immun, 2013. **81**(7): p. 2638-44.
99. Liu, B., et al., *Characterization and immunological activity of different forms of recombinant secreted Hc of botulinum neurotoxin serotype B products expressed in yeast.* Sci Rep, 2015. **5**: p. 7678.
100. Van Heyningen, W.E. and P.A. Miller, *The fixation of tetanus toxin by ganglioside.* J Gen Microbiol, 1961. **24**: p. 107-19.
101. Van Heyningen, W.E., *The relation between the fixation and inactivation of tetanus toxin by ganglioside.* Br J Exp Pathol, 1961. **42**: p. 397-8.
102. Rummel, A., et al., *Two carbohydrate binding sites in the H(CC)-domain of tetanus neurotoxin are required for toxicity.* J Mol Biol, 2003. **326**(3): p. 835-47.
103. Chen, C., et al., *Gangliosides as high affinity receptors for tetanus neurotoxin.* J Biol Chem, 2009. **284**(39): p. 26569-77.
104. Mocchetti, I., *Exogenous gangliosides, neuronal plasticity and repair, and the neurotrophins.* Cell Mol Life Sci, 2005. **62**(19-20): p. 2283-94.
105. Svennerholm, L., *Designation and schematic structure of gangliosides and allied glycosphingolipids.* Prog Brain Res, 1994. **101**: p. Xi-xiv.
106. Kolter, T., R.L. Proia, and K. Sandhoff, *Combinatorial ganglioside biosynthesis.* J Biol Chem, 2002. **277**(29): p. 25859-62.
107. Kozaki, S., et al., *Ganglioside GT1b as a complementary receptor component for Clostridium botulinum neurotoxins.* Microb Pathog, 1998. **25**(2): p. 91-9.
108. Singh, A.K., S.H. Harrison, and J.S. Schoeniger, *Gangliosides as receptors for biological toxins: development of sensitive fluoroimmunoassays using ganglioside-bearing liposomes.* Anal Chem, 2000. **72**(24): p. 6019-24.
109. Yowler, B.C., R.D. Kensinger, and C.L. Schengrund, *Botulinum neurotoxin A activity is dependent upon the presence of specific gangliosides in neuroblastoma cells expressing synaptotagmin I.* J Biol Chem, 2002. **277**(36): p. 32815-9.
110. Kitamura, M., et al., *Different response of the knockout mice lacking b-series gangliosides against botulinum and tetanus toxins.* Biochim Biophys Acta, 2005. **1741**(1-2): p. 1-3.
111. Chen, C., M.R. Baldwin, and J.T. Barbieri, *Molecular basis for tetanus toxin coreceptor interactions.* Biochemistry, 2008. **47**(27): p. 7179-86.

112. Stenmark, P., et al., *Crystal Structure of Botulinum Neurotoxin Type A in Complex with the Cell Surface Co-Receptor GT1b—Insight into the Toxin–Neuron Interaction.* PLoS Pathog, 2008. **4**(8).
113. Jin, R., et al., *Botulinum neurotoxin B recognizes its protein receptor with high affinity and specificity.* Nature, 2006. **444**(7122): p. 1092-5.
114. Sutton, J.M., et al., *Tyrosine-1290 of tetanus neurotoxin plays a key role in its binding to gangliosides and functional binding to neurones.* FEBS Lett, 2001. **493**(1): p. 45-9.
115. Yeh, F.L., et al., *SV2 mediates entry of tetanus neurotoxin into central neurons.* PLoS Pathog, 2010. **6**(11): p. e1001207.
116. Bercsenyi, K., et al., *Tetanus toxin entry. Nidogens are therapeutic targets for the prevention of tetanus.* Science, 2014. **346**(6213): p. 1118-23.
117. Bohnert, S. and G. Schiavo, *Tetanus toxin is transported in a novel neuronal compartment characterized by a specialized pH regulation.* J Biol Chem, 2005. **280**(51): p. 42336-44.
118. Deinhardt, K., et al., *Tetanus toxin is internalized by a sequential clathrin-dependent mechanism initiated within lipid microdomains and independent of epsin1.* J Cell Biol, 2006. **174**(3): p. 459-71.
119. Gil, C., et al., *HC fragment (C-terminal portion of the heavy chain) of tetanus toxin activates protein kinase C isoforms and phosphoproteins involved in signal transduction.* Biochem J, 2001. **356**(Pt 1): p. 97-103.
120. Oda, M., et al., *Clostridium perfringens alpha-toxin recognizes the GM1a-TrkA complex.* J Biol Chem, 2012. **287**(39): p. 33070-9.
121. Fukuta, S., et al., *Comparison of the carbohydrate-binding specificities of cholera toxin and Escherichia coli heat-labile enterotoxins LTh-I, LT-IIa, and LT-IIb.* Infect Immun, 1988. **56**(7): p. 1748-53.
122. Fujinaga, Y., et al., *Gangliosides That Associate with Lipid Rafts Mediate Transport of Cholera and Related Toxins from the Plasma Membrane to Endoplasmic Reticulm.* Mol Biol Cell, 2003. **14**(12): p. 4783-93.
123. Chinnapen, D.J.F., et al., *Lipid-sorting by ceramide structure from plasma membrane to ER for the cholera toxin receptor ganglioside GM1.* Dev Cell, 2012. **23**(3): p. 573-86.
124. Chen, C., et al., *Heat-Labile Enterotoxin IIa, a Platform To Deliver Heterologous Proteins into Neurons.* mBio, 2015. **6**(4).
125. Baldwin, M.R. and J.T. Barbieri, *Association of botulinum neurotoxin serotypes a and B with synaptic vesicle protein complexes.* Biochemistry, 2007. **46**(11): p. 3200-10.
126. Minor, W., D. Tomchick, and Z. Otwinowski, *Strategies for macromolecular synchrotron crystallography.* Structure, 2000. **8**(5): p. R105-10.
127. Dodson, E.J., M. Winn, and A. Ralph, *Collaborative Computational Project, number 4: providing programs for protein crystallography.* Methods Enzymol, 1997. **277**: p. 620-33.
128. Brunger, A.T., *Version 1.2 of the Crystallography and NMR system.* Nat Protoc, 2007. **2**(11): p. 2728-33.
129. Jayaraman, S., et al., *Common binding site for disialyllactose and tri-peptide in C-fragment of tetanus neurotoxin.* Proteins, 2005. **61**(2): p. 288-95.

130. Restani, L., et al., *Botulinum neurotoxins A and E undergo retrograde axonal transport in primary motor neurons.* PLoS Pathog, 2012. **8**(12): p. e1003087.
131. Wang, J., et al., *Novel chimeras of botulinum and tetanus neurotoxins yield insights into their distinct sites of neuroparalysis.* Faseb j, 2012. **26**(12): p. 5035-48.
132. Manders, E.M.M., F.J. Verbeek, and J.A. Aten, *Measurement of co-localization of objects in dual-colour confocal images.* Journal of Microscopy, 1993. **169**(3): p. 375-382.
133. Blum, F.C., et al., *Entry of a recombinant, full-length, atoxic tetanus neurotoxin into Neuro-2a cells.* Infect Immun, 2014. **82**(2): p. 873-81.
134. Hill, K.K., et al., *Genetic diversity among Botulinum Neurotoxin-producing clostridial strains.* J Bacteriol, 2007. **189**(3): p. 818-32.
135. Hill, K.K., et al., *Genetic diversity within the botulinum neurotoxin-producing bacteria and their neurotoxins.* Toxicon, 2015. **107**(Pt A): p. 2-8.
136. Smith, T.J., et al., *Sequence variation within botulinum neurotoxin serotypes impacts antibody binding and neutralization.* Infect Immun, 2005. **73**(9): p. 5450-7.
137. Lin, G., et al., *Expression of the Clostridium botulinum A2 Neurotoxin Gene Cluster Proteins and Characterization of the A2 Complex.* Applied and Environmental Microbiology, 2010. **76**(1): p. 40-47.
138. Sakaguchi, G., et al., *Distinct characters of Clostridium botulinum type A strains and their toxin associated with infant botulism in Japan.* Int J Food Microbiol, 1990. **11**(3-4): p. 231-41.
139. Horowitz, B.Z., *The ripe olive scare and hotel Loch Maree tragedy: Botulism under glass in the 1920's.* Clin Toxicol (Phila), 2011. **49**(4): p. 345-7.
140. Tepp, W.H., G. Lin, and E.A. Johnson, *Purification and Characterization of a Novel Subtype A3 Botulinum Neurotoxin.* Applied and Environmental Microbiology, 2012. **78**(9): p. 3108-3113.
141. Bradshaw, M., et al., *Holotoxin Activity of Botulinum Neurotoxin Subtype A4 Originating from a Nontoxigenic Clostridium botulinum Expression System.* Appl Environ Microbiol, 2014. **80**(23): p. 7415-22.
142. Jacobson, M.J., et al., *Purification, modeling, and analysis of botulinum neurotoxin subtype A5 (BoNT/A5) from Clostridium botulinum strain A661222.* Appl Environ Microbiol, 2011. **77**(12): p. 4217-22.
143. Luquez, C., B.H. Raphael, and S.E. Maslanka, *Neurotoxin gene clusters in Clostridium botulinum type Ab strains.* Appl Environ Microbiol, 2009. **75**(19): p. 6094-101.
144. Mazuet, C., et al., *Toxin detection in patients' sera by mass spectrometry during two outbreaks of type A Botulism in France.* J Clin Microbiol, 2012. **50**(12): p. 4091-4.
145. Kull, S., et al., *Isolation and functional characterization of the novel Clostridium botulinum neurotoxin A8 subtype.* PLoS One, 2015. **10**(2): p. e0116381.
146. Henkel, J.S., et al., *Subunit vaccine efficacy against Botulinum neurotoxin subtypes.* Vaccine, 2011. **29**(44): p. 7688-95.
147. Pearce, L.B., et al., *Measurement of botulinum toxin activity: evaluation of the lethality assay.* Toxicol Appl Pharmacol, 1994. **128**(1): p. 69-77.

148. Whitemarsh, R.C.M., et al., *Characterization of Botulinum Neurotoxin A Subtypes 1 Through 5 by Investigation of Activities in Mice, in Neuronal Cell Cultures, and In Vitro.* Infection and Immunity, 2013. **81**(10): p. 3894-3902.
149. Pier, C.L., et al., *Botulinum neurotoxin subtype A2 enters neuronal cells faster than subtype A1.* FEBS Lett, 2011. **585**(1): p. 199-206.
150. Torii, Y., et al., *Comparison of effects of botulinum toxin subtype A1 and A2 using twitch tension assay and rat grip strength test.* Toxicon, 2011. **57**(1): p. 93-9.
151. Arndt, J.W., et al., *A structural perspective of the sequence variability within botulinum neurotoxin subtypes A1-A4.* J Mol Biol, 2006. **362**(4): p. 733-42.
152. Henkel, J.S., et al., *Catalytic Properties of Botulinum Neurotoxins Subtypes A3 and A4.* Biochemistry, 2009. **48**(11): p. 2522-2528.
153. Rummel, A., et al., *The HCC-domain of botulinum neurotoxins A and B exhibits a singular ganglioside binding site displaying serotype specific carbohydrate interaction.* Mol Microbiol, 2004. **51**(3): p. 631-43.
154. Schneider, C.A., W.S. Rasband, and K.W. Eliceiri, *NIH Image to ImageJ: 25 years of image analysis.* Nat Methods, 2012. **9**(7): p. 671-5.
155. Li, Q., et al., *A syntaxin 1, Galpha(o), and N-type calcium channel complex at a presynaptic nerve terminal: analysis by quantitative immunocolocalization.* J Neurosci, 2004. **24**(16): p. 4070-81.
156. Biasini, M., et al., *SWISS-MODEL: modelling protein tertiary and quaternary structure using evolutionary information.* Nucleic Acids Res, 2014. **42**(Web Server issue): p. W252-8.
157. Rossetto, O., et al., *Active-site mutagenesis of tetanus neurotoxin implicates TYR-375 and GLU-271 in metalloproteolytic activity.* Toxicon, 2001. **39**(8): p. 1151-9.
158. Fernandez-Salas, E., et al., *Is the light chain subcellular localization an important factor in botulinum toxin duration of action?* Mov Disord, 2004. **19 Suppl 8**: p. S23-34.
159. Lemichez, E. and J.T. Barbieri, *General aspects and recent advances on bacterial protein toxins.* Cold Spring Harb Perspect Med, 2013. **3**(2): p. a013573.
160. Maksymowych, A.B., et al., *Pure botulinum neurotoxin is absorbed from the stomach and small intestine and produces peripheral neuromuscular blockade.* Infect Immun, 1999. **67**(9): p. 4708-12.
161. Barash, J.R. and S.S. Arnon, *A Novel Strain of Clostridium botulinum That Produces Type B and Type H Botulinum Toxins.* J Infect Dis, 2014. **209**(2): p. 183-91.
162. Poulet, S., et al., *Sequences of the botulinal neurotoxin E derived from Clostridium botulinum type E (strain Beluga) and Clostridium butyricum (strains ATCC 43181 and ATCC 43755).* Biochem Biophys Res Commun, 1992. **183**(1): p. 107-13.
163. Binz, T. and A. Rummel, *Cell entry strategy of clostridial neurotoxins.* J Neurochem, 2009. **109**(6): p. 1584-95.
164. Pirazzini, M., et al., *Double anchorage to the membrane and intact inter-chain disulfide bond are required for the low pH induced entry of tetanus and botulinum neurotoxins into neurons.* Cell Microbiol, 2011. **13**(11): p. 1731-43.
165. Dong, M., et al., *Synaptotagmins I and II mediate entry of botulinum neurotoxin B into cells.* J Cell Biol, 2003. **162**(7): p. 1293-303.

166. Peng, L., et al., *Botulinum neurotoxin D-C uses synaptotagmin I and II as receptors, and human synaptotagmin II is not an effective receptor for type B, D-C and G toxins.* J Cell Sci, 2012. **125**(Pt 13): p. 3233-42.
167. Rummel, A., et al., *Botulinum neurotoxins C, E and F bind gangliosides via a conserved binding site prior to stimulation-dependent uptake with botulinum neurotoxin F utilising the three isoforms of SV2 as second receptor.* J Neurochem, 2009. **110**(6): p. 1942-54.
168. Karalewitz, A.P., et al., *Botulinum neurotoxin serotype C associates with dual ganglioside receptors to facilitate cell entry.* J Biol Chem, 2012. **287**(48): p. 40806-16.
169. Cai, S., et al., *Botulinum neurotoxin light chain refolds at endosomal pH for its translocation.* Protein J, 2006. **25**(7-8): p. 455-62.
170. Fu, F.N., D.D. Busath, and B.R. Singh, *Spectroscopic analysis of low pH and lipid-induced structural changes in type A botulinum neurotoxin relevant to membrane channel formation and translocation.* Biophys Chem, 2002. **99**(1): p. 17-29.
171. Sreerama, N. and R.W. Woody, *On the analysis of membrane protein circular dichroism spectra.* Protein Sci, 2004. **13**(1): p. 100-12.
172. Bordier, C., *Phase separation of integral membrane proteins in Triton X-114 solution.* J Biol Chem, 1981. **256**(4): p. 1604-7.
173. Sun, J., et al., *Insertion of anthrax protective antigen into liposomal membranes: effects of a receptor.* J Biol Chem, 2007. **282**(2): p. 1059-65.
174. Agarwal, R., T. Binz, and S. Swaminathan, *Analysis of active site residues of botulinum neurotoxin E by mutational, functional, and structural studies: Glu335Gln is an apoenzyme.* Biochemistry, 2005. **44**(23): p. 8291-302.
175. Binz, T., et al., *Arg(362) and Tyr(365) of the botulinum neurotoxin type a light chain are involved in transition state stabilization.* Biochemistry, 2002. **41**(6): p. 1717-23.
176. Blum, F.C., et al., *Entry of a recombinant full-length, atoxic tetanus neurotoxin into Neuro-2a cells.* Infect Immun, 2013.
177. Simpson, L.L., J.A. Coffield, and N. Bakry, *Inhibition of vacuolar adenosine triphosphatase antagonizes the effects of clostridial neurotoxins but not phospholipase A2 neurotoxins.* J Pharmacol Exp Ther, 1994. **269**(1): p. 256-62.
178. Sun, S., et al., *Receptor binding enables botulinum neurotoxin B to sense low pH for translocation channel assembly.* Cell Host Microbe, 2011. **10**(3): p. 237-47.
179. Sun, S., et al., *Botulinum neurotoxins B and E translocate at different rates and exhibit divergent responses to GT1b and low pH.* Biochemistry, 2012. **51**(28): p. 5655-62.
180. Ulrich-Bott, B. and H. Wiegandt, *Micellar properties of glycosphingolipids in aqueous media.* J Lipid Res, 1984. **25**(11): p. 1233-45.
181. Schiavo, G., et al., *Membrane interactions of tetanus and botulinum neurotoxins: a photolabelling study with photoactivatable phospholipids.* J Physiol (Paris), 1990. **84**(2): p. 180-7.
182. Boquet, P. and E. Duflot, *Tetanus toxin fragment forms channels in lipid vesicles at low pH.* Proc Natl Acad Sci U S A, 1982. **79**(24): p. 7614-8.

183. Petosa, C., et al., *Crystal structure of the anthrax toxin protective antigen.* Nature, 1997. **385**(6619): p. 833-8.
184. Kyrychenko, A., et al., *Kinetic intermediate reveals staggered pH-dependent transitions along the membrane insertion pathway of the diphtheria toxin T-domain.* Biochemistry, 2009. **48**(32): p. 7584-94.
185. Strotmeier, J., et al., *The biological activity of botulinum neurotoxin type C is dependent upon novel types of ganglioside binding sites.* Mol Microbiol, 2011. **81**(1): p. 143-56.
186. Fischer, A. and M. Montal, *Molecular dissection of botulinum neurotoxin reveals interdomain chaperone function.* Toxicon, 2013. **75**: p. 101-7.

VITA

Josh was born in Sandusky, Ohio in 1979. Josh then moved to Mansfield, Ohio where he lived for 18 years. In 1998 he moved to Missouri. Soon thereafter, he started taking college classes at a local community college. In 2002 he was hired on full time at St. John's Mercy Medical Center as a patient care technician. By 2003, he transferred into the Microbiology Dept. During this same time, Josh began taking classes full time at Lindenwood University and worked towards completing a BS in Chemistry with an emphasis in Biochemistry. In May of 2010, Josh completed his BS in Chemistry and quickly started the graduate program at the University of Missouri in the laboratory of Michael Baldwin. After completing his graduate degree, Josh will begin a post-graduate fellowship in the lab of Rod Tweten at the University of Oklahoma Health Science Center.